

Université du Québec
Institut national de la recherche scientifique
Centre Énergie Matériaux Télécommunications

Near Infrared-Emitting Quantum Dots: Synthesis, Characterization and Biological Applications

Par

Fuqiang Ren

Thèse présentée pour l'obtention du grade de Philosophiæ Doctor (Ph.D.) en Sciences de
l'énergie et des matériaux

Jury d'évaluation

Président du jury et examineur interne	Aycan Yurtsever INRS-EMT
Examineur externe	Xiaoxia Zhu Université de Montréal
Examineur externe	Jean-François Morin Université Laval
Directeur de recherche	Dongling Ma INRS-EMT, Université du Québec
Codirecteur de recherche	Fiorenzo Vetrone INRS-EMT, Université du Québec

ABSTRACT

Quantum dots (QDs) have attracted significant attention in many applications due to their unique features, such as size-dependent optical absorption and emission, arising from the quantum confinement effect, which the bulk material does not possess. Among diverse QDs, near infrared (NIR) emitting QDs, such as lead-based QDs, which can be tuned to emit from below 1000 nanometer to several thousand nanometers are particularly interesting. Both their excitation and emission can be easily adjusted to lie within the biological windows, highly desirable for some demanding biological applications. Although the synthesis of NIR QDs with a uniform and narrow size distribution is well known today, achieving QDs with high quantum efficiency and excellent stability is still a big challenge.

QDs are tiny crystalline particles with typical dimensions in the range of 1-100 nm. Their surface-to-volume ratio is very large, therefore the properties of QDs become extremely sensitive to surface characteristics. In order to improve the optical properties of these QDs, great efforts have been made in the past few decades on the surface engineering of QDs. A passivation shell is normally grown over the QDs to form a core/shell structure, which in turn improves the optical properties and stability. In the first part of this thesis, the synthesis and optical properties of PbS/CdS core/shell QDs are presented and discussed. We firstly synthesized a series of differently sized PbS QDs by using the traditional hot injection method, then these PbS QDs were coated with a thin CdS shell to form a PbS/CdS core/shell structure by the cation exchange approach, finally the optical properties of these core/shell QDs

were studied.

In Section I of Part I, we report the development of a reproducible and controllable microwave-assisted cation exchange approach, for the first time, to quickly synthesize high-quality, NIR emitting PbS/CdS core/shell QDs. These monodisperse QDs, emitting in the range of 1300-1600 nm, show a quantum yield (QY) as high as 57% that is ~1.4 times higher than that of QDs achieved by conventional heating in oil bath. Meanwhile, the reaction was successfully scaled up by several times by increasing the starting PbS concentration or by amplifying the reaction volume and the as-synthesized core/shell QDs show similarly high QY.

We then report anomalous size-dependent photoluminescence (PL) intensity variation of PbS QDs with the formation of a thin CdS shell via the same microwave-assisted cation exchange approach. We found previously that thin shell formation is an effective strategy for increasing the PL intensity of large sized PbS QDs. Nonetheless, herein we observed an unusual PL decrease in ultrasmall QDs upon shell formation. We attempted to understand this abnormal phenomenon from the perspective of trap density variation and the probability of electrons and holes reaching surface defects. To this end, QY and PL lifetime (on the ns- μ s time scale) of pristine PbS QDs and PbS/CdS core/shell QDs were measured and radiative and non-radiative recombination rates were derived and compared. Moreover, transient absorption (TA) analysis (on the fs-ns time scale) was performed to better understand exciton dynamics on ultrafast time scales. These experimental results along with theoretical calculations of electron and hole wave functions provide a complete

picture of the photophysics governing the core/shell system. Ultimately, a model was constructed to show the energy levels and trap states for various sizes.

Part II focuses on the photostability and colloidal stability of water dispersible PbS/CdS/ZnS core/shell/shell QDs and their potential bio-applications. We report for the first time detailed investigations of the synthesis of NIR, water dispersible, strongly luminescent and highly stable PbS/CdS/ZnS core/shell/shell QDs, their properties in different buffers, their cytotoxicity and further their applications in tumor imaging. In particular, we focus on the QDs emitting at 930 and 1220 nm, within the first and second biological windows, respectively. These QDs were synthesized via our recently developed microwave-assisted approach to grow a ZnS shell and to simultaneously exchange initial ligand with mercaptopropyl acid on the PbS/CdS core/shell QDs dispersed in an organic phase. These QDs were extremely stable in commonly used biological buffers and remarkably, they could keep their initial morphology, dispersion status and PL in phosphate buffered saline buffer (PBS) for as long as 14 months, which was the longest time we investigated with both transmission electron microscopy and PL spectroscopy herein. PL images taken on the 930 nm emitting PbS/CdS/ZnS core/shell/shell QDs revealed that they could still emit strongly after 30-month storage in PBS. Such long term stability of water dispersible QDs is rarely reported in the literature. Their colloidal stability was further investigated by keeping them in high ionic concentration conditions. Their PL intensity did not show any change for at least 3 weeks at high NaCl concentration up to 400 mM. The QDs also showed excellent photostability and could keep about 80%

of their initial PL intensity after 1 hour of continuous, strong UV illumination. More interestingly, they showed negligible toxicity to cultured cells even at high QDs concentration (50 nM). Given these outstanding properties, the ultrastable and biocompatible QDs were explored for the first time for in vivo tumor imaging in mice. With one order of magnitude lower QD concentration (0.04 mg/mL), significantly weaker laser intensity (0.04 W/cm^2 vs $\sim 1 \text{ W/cm}^2$) and considerably shorter signal integration time ($\leq 1 \text{ ms}$ vs several hundreds of ms) as compared to the best reported rare earth doped nanoparticles, the QDs showed high emission intensity even at injection depth of $\sim 2.5 \text{ mm}$, hard to achieve with visible QDs and other NIR PL probes.

We developed a QD-based imaging system based on NIR-emitting PbS/CdS/ZnS QDs with minimal noticeable toxicity. Through careful engineering of their emission wavelength, we obtained fluorescence imaging nanoprobe with optimal penetration depths in biological tissue. Additionally, this new platform exhibited multifunctionality beyond their use as pure imaging nanoprobe. The system is capable of acting as a biological nanothermometer, based on the reliable thermal-dependent behavior of the fluorescence signal. The PbS/CdS/ZnS QDs studied here can easily be exploited to obtain thermal mapping of subskin areas in live specimens, an accomplishment of great relevance for early disease detection and also for real-time therapy monitoring. Moreover, as a result of the intense signal provided by the NIR-emitting QDs, we are able to elucidate the real-time biodistribution of the QDs by means of in vivo experiments in live mice. We determined the lack of

detectable chemical toxicity attributed to the QDs based on cell culture assays, as well as the lack of adverse health effects (no significant weight changes or behavior abnormalities were found over 4 weeks) for mice injected with a low concentration of QDs, coupled with the absence of any fluorescence signal detected in the body organs at the end of the experiment. We can therefore ascertain that the ZnS outer shell imparts a great deal of bio-compatibility and stability of the PbS/CdS/ZnS QDs reported here. Also, the intense fluorescent emission of this material allows for low doses to be used, significantly improving the current state of the art. This greatly diminishes the likelihood of causing adverse health effects on the live specimen when used as optical bioimaging probes.

ACKNOWLEDGEMENTS

Foremost I would like to express my deepest gratitude to my supervisor Prof. Dongling Ma for the continuous support of my PhD study and research, for her kindness, patience, enthusiasm, and immense knowledge. I learned lots from her. Her endless effort in improving the quality of my research project by giving me suggestions and some novel ideas is quite appreciable.

Beside my supervisor, I would like to acknowledge with much appreciation my co-supervisor Prof. Fiorenzo Vetrono. He continually and persuasively helped me in all the time of research and gave me precious advice.

My supervisors have created a warm and stimulating research environment allowing me explore a complex and fascinating scientific field. Being able to study under their supervision is one of the most valuable experience in my life.

I thank Prof. Jinzhong Zhang, Prof. François Vidal, Prof. Daniel Jaque, Prof. John Oh and Prof. Xinyu Liu for their important comments during my project research.

I want to acknowledge the contributions to this work made by Dr. Haiguang Zhao, Dr. Antonio Benayas and Dr. Marta Quintanilla, who gave me invaluable help and collaboration. I gratefully acknowledge my collaborators, Dr. Sarah A. Lindley, Dr. Elisa Carrasco, Dr. Vicente Marzal, Dr. Blanca del Rosal, Soyoung An. Thanks to all the group members for their help throughout the work. I am grateful to have been part of such supportive, hardworking, and inspiring groups. These people include Belete Atomsa Gonfa, Long Tan, Fan Yang, Zhenghe Xu, Mee Rahn Kim and Yanlong Liu. I thank the departmental and technical staff at INRS-EMT.

I would like to thank Jean-Philippe Masse at Ecole Polytechnique for the transmission electron microscopy measurements.

I am eternally grateful to my parents, who have been a constant source of love. I would like to thank my wife, Qian Li, who loves me deeply and supports me selflessly. I want to tell them, I love you. I thank my family and my friends for their continuing love and heartily support.

Finally, I wish to acknowledge the following organizations for their financial support: Fonds de recherche du qu ébec nature et technologies for PhD Program and the Natural Sciences and Engineering Research Council of Canada.

CONTENTS

CHAPTER 1 INTRODUCTION	1
1.1 Quantum dots and their basic properties.....	1
1.2 Near-infrared quantum dots and their applications.....	3
1.3 PbS quantum dots.....	6
1.4 Core shell quantum dots and their advantages.....	8
1.5 Bio-applications of lead based quantum dots.....	12
1.6 Thesis objectives.....	14
1.7 Thesis organization.....	15
CHAPTER 2 EXPERIMENTAL	17
2.1 Materials.....	17
2.2 Reaction setup.....	17
2.3 Synthesis of lead based quantum dots.....	18
2.3.1 Synthesis of PbS and PbS/CdS quantum dots in the organic phase.....	18
2.3.1.1 Synthesis of smaller PbS quantum dots.....	18
2.3.1.2 Synthesis of larger PbS quantum dots.....	19
2.3.1.3 Synthesis of colloidal PbS/CdS quantum dots.....	20
2.3.2 Synthesis of water dispersible PbS/CdS/ZnS quantum dots.....	21
2.4 Characterization.....	22
2.4.1 Structural and optical property characterization.....	22
2.4.1.1 Transmission Electron Microscopy and Energy Dispersive X-ray Spectroscopy.....	22

2.4.1.2 X-ray Powder Diffraction.....	23
2.4.1.3 Inductively coupled plasma optical emission spectroscopy.....	23
2.4.1.4 Property characterization.....	24
2.4.1.5 Estimation of quantum dots concentration, size and shell thickness calculation.....	25
2.4.2 Theoretical calculation of wave functions.....	26
2.4.3 Cytotoxicity study of PbS/CdS/ZnS quantum dots.....	27
2.4.4 In vivo fluorescence imaging in mice.....	27
CHAPTER 3 RESULTS.....	31
3.1 Part I: Quantum dots in organic phase.....	31
Section I Microwave-assisted cation exchange toward synthesis of near-infrared emitting PbS/CdS core/shell quantum dots with significantly improved quantum yields through a uniform growth path.....	33
Section II Towards Understanding Unusual Photoluminescence Intensity Variation of Ultrasmall Colloidal PbS Quantum Dots with the Formation of Thin CdS Shell.....	42
3.2 Part II: Water dispersible quantum dots and their applications.....	64
Section III Development and Investigation of Ultrastable PbS/CdS/ZnS Core/shell/shell Quantum Dots in the First and Second Biological Windows and their Application in Tumor Imaging.....	65
Section IV PbS/CdS/ZnS Quantum Dots: A Multifunctional Platform for In Vivo Near-Infrared Low-Dose Fluorescence Imaging.....	109

CHAPTER 4 CONCLUSIONS AND PERSPECTIVES	132
4.1 Conclusions.....	132
4.2 Perspectives.....	135
REFERENCES	139
RÉSUMÉ	144
Appendix PUBLICATIONS AND CONFERENCE CONTRIBUTIONS	165

LIST OF FIGURES

Figure 1.1 Electronic energy states of a semiconductor in the transition from discrete molecule to nanosized crystals and bulk crystals. Blue shading denotes ground state electron occupation. The schematic illustration is taken from reference [2].

Figure 1.2 Due to quantum confinement effect, an example of size-dependent optical properties. (a): fluorescence image of CdSe QDs as a function of size. (b): absorbance spectrum as a function of size. The graph is taken from: <http://nanocluster.mit.edu/research.php>

Figure 1.3 Absorbance of various tissue and blood components from 200 nm to 10 μm . (Obtained from reference [13]).

Figure 1.4 Optical windows in biological tissues. (Obtained from reference [17]).

Figure 1.5 Composition, size and wavelength ranges of reported NIR-emitting QDs prepared via solution-based methodologies. Emission wavelengths reported for constant size nanocrystals containing different proportions of elements are represented with broken lines rectangle. (Obtained from reference [19]).

Figure 1.6 NIR-II fluorescence imaging of a xenograft tumor with high uptake of Ag_2S QDs. (a–e) Time course of NIR-II fluorescence images of the same mouse injected with Ag_2S QDs. (Obtained from reference [27]).

Figure 1.7 Room-temperature optical characterization of toluene solutions of PbS QDs. a) Absorption spectra spanning the range of tuneable sizes. b) Band-edge absorption and photoluminescence peaks for a sample 6.5 nm in diameter. (Obtained

from reference [49]).

Figure 1.8 (a) TEM image of oleate stabilized PbS or PbSe QDs, (b) pictures of dispersion of PbS/CdS and PbSe QDs in TRIS, buffer and water, respectively. (Obtained from reference [54]).

Figure 1.9 Schematic representation of the four limiting charge carrier localization regimes in core/shell semiconductor QDs. The conduction and valence band edges (i.e., the highest occupied molecular orbital (LUMO) and lowest unoccupied molecular orbital (HOMO) energy levels) are indicated by CB and valence band (VB), respectively. The plus and minus signs represent the charge carriers (hole and electron, respectively). The electron and hole ground-state wave functions are schematically depicted in the lower panel (Type I, Type-I^{1/2} and Type II illustrations obtained from reference [62]).

Figure 1.10 TEM images of the plain CdSe-cores and core/shell nanocrystals obtained under typical reaction conditions: (A) TEM images of CdSe-cores (before injection of Cd²⁺ solution); (B) (A) plus 2 monolayers of CdS; (C)/(E) (B) plus 3.5 monolayers of Zn_{0.5}Cd_{0.5}S; (D)/(F) (C) plus 2 monolayers of ZnS. (Obtained from reference [61]).

Figure 1.11 (a) PL spectra of 5.2 nm diameter PbSe NQDs (higher wavelengths) and corresponding PbSe/CdSe NQDs (lower wavelengths), (b) PL spectra of (~7 nm) PbS and two aliquots during CdS shell formation, showing relative PL enhancement during the process. Arrows indicate progress of reaction during CdS shell formation. (Obtained from reference [67]).

Figure 1.12 II-BW fluorescence images (1100 nm) of a breast cancer tumor 1 h (a) and 48 h (b) after injection of anti-HER2 antibody conjugated PbS QDs. The tumor location in (a) is indicated by the dotted circle. Scale bar: 10 mm. Ex vivo images of the breast cancer tumor using (c) bright field microscopy, (d) fluorescence microscopy at a visible light wavelength (535 nm), and (e) fluorescence microscopy at a II-BW wavelength (1100 nm). Scale bar: 2 mm. (Obtained from reference [76]).

Figure 2.1 Schematic illustration of the setup for the synthesis of PbS, PbS/CdS core shell and PbS/CdS/ZnS core shell shell QDs.

Figure 2.2 Schematic illustration of the synthesis of core shell PbS/CdS QDs by microwave-assisted cation exchange approach.

Figure 2.3 Schematic illustration of the synthesis of core shell shell PbS/CdS/ZnS QDs by microwave-assisted epitaxial growth method.

Figure 2.4 Scheme of the in vivo fluorescence imaging experiments.

LIST OF ABBREVIATIONS AND SYMBOLS

Abbreviations

CB.....	Conduction band
CNTs.....	Single-walled carbon nanotubes
DMEM.....	Dulbecco's modified Eagle's medium
EDX.....	Energy dispersive X-ray spectroscopy
FBS.....	Fetal bovine serum
ICP-OES.....	Inductively Coupled Plasma-Optical Emission Spectrometer
LED.....	Light emitting diode
NC.....	Nanocrystal
NIR.....	Near infrared
NIST.....	National Institute of Standards and Technology
PL.....	Photoluminescence
PBS.....	Phosphate buffered saline
PMT.....	Photomultiplier tube
QD.....	Quantum dot
QY.....	Quantum yield
SILAR.....	Successive ionic layer adsorption and reaction
TEM.....	Transmission electron microscopy
TA.....	Transient absorption
UV.....	Ultraviolet
VB.....	Valence band

Vis..... Visible

XRD.....X-ray powder diffraction

Symbols

AAbsorbance

A_1Normalized amplitudes of the components

A_2Normalized amplitudes of the components

CMolar concentration

dDiameter of a QDs

EBand gap energy

hPlanck constant

IPL intensity

I_0Initial PL intensity

K_{rad}Radiative recombination rate

K_{nr}Non-radiative recombination rate

tTime

τAverage lifetime

τ_1Decay time constant

τ_2Decay time constant

ΦQuantum yield

ηRefractive index

λThe first excitation absorption peak

CHAPTER 1 INTRODUCTION

1.1 Quantum dots and their basic properties

A quantum dot (QD), is a semiconductor nanocrystal (NC), which is normally composed of group II-VI, IV-VI or III-V compounds. Typically, the QDs are smaller than 100 nm in dimension and show novel properties different from their bulk materials, such as size-dependent optical absorption and emission spectra [1]. These unique characteristics arise from the quantum confinement effect which is observed as long as the size of the material is smaller than the Bohr exciton radius, defined as the size of an exciton (the electron-hole pair). The quantum confinement affects the exciton wave function, and induces changes to the density of electronic states and to energy level separation, which are manifested as the increase of the bandgap with decreasing size and the appearance of discrete energy levels near band edges [2, 3]. In fact, the electronic properties of the QDs are intermediate between those of discrete molecules and of bulk semiconductors, displaying discrete electronic transitions [2], as shown in Figure 1. Therefore, the bandgap changes as the size of the QD changes. As a result, the optical properties of QDs become strongly size dependent, making it possible to tune their absorption and photoluminescence (PL) over a wide spectral region by varying their size and shape [3, 4]. For example, lead selenide (PbSe) has a Bohr exciton radius of 46 nm. This means as long as the NCs size is smaller than 46 nm, their optical spectra show size dependent properties. Figure 1.2 displays the quantum confinement effects for CdSe QDs, showing that the wavelengths of fluorescence and absorption can be tuned by nanocrystal size. The Bohr exciton radius of CdSe is 9.6 nm and its emission wavelength can be tuned throughout the visible range by adjusting the QD size from 2 to 8 nm. The size-dependent bandgap and optical properties of QDs have made them potentially a good candidate in a great deal of applications such as bio-imaging [5, 6], light-emitting diodes [7, 8] and solar cells [9, 10].

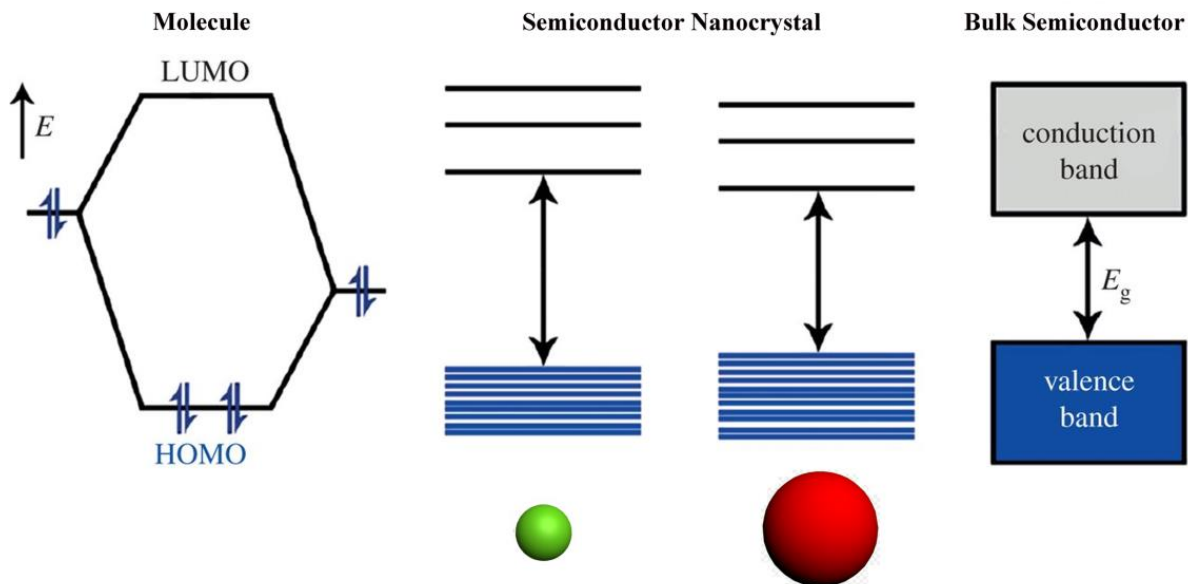


Figure 1.1 Electronic energy states of a semiconductor in the transition from discrete molecules to nanosized crystals and bulk crystals. Blue shading denotes ground state electron occupation. The schematic illustration is taken from reference [2].

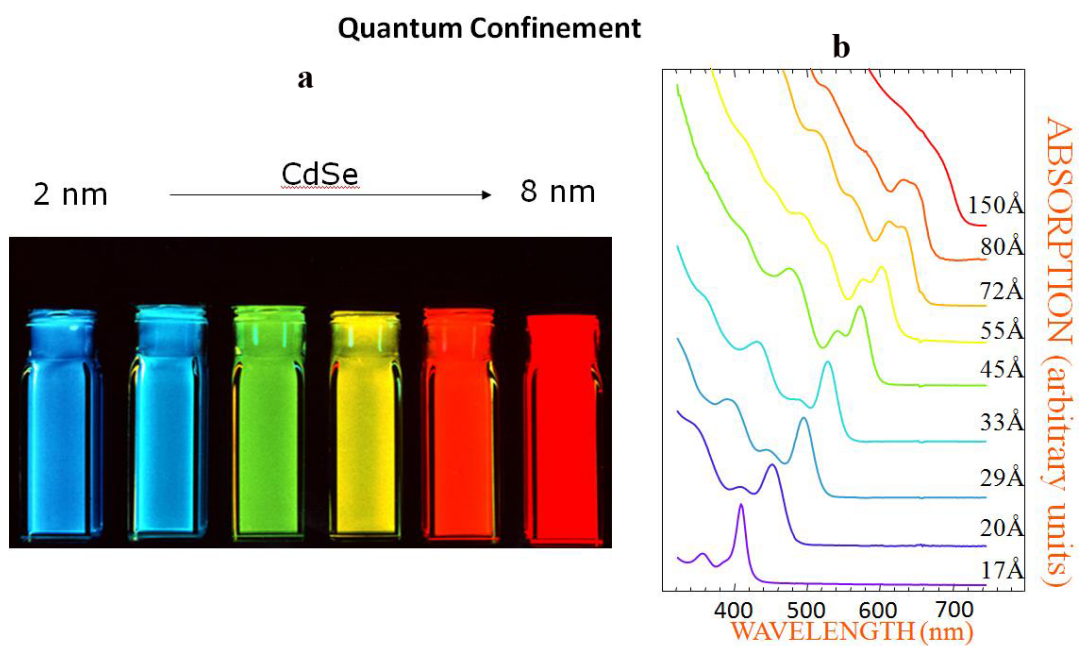


Figure 1.2 An example of size-dependent optical properties due to the quantum confinement effect. (a): fluorescence image of CdSe QDs as a function of size. (b): absorbance spectrum as a function of size.

The graph is taken from: <http://nanocluster.mit.edu/research.php>

1.2 NIR QDs and their applications

Fluorescence-based optical imaging in the visible range (400-700 nm) benefiting from fast feedback has been shown to be useful for both *in vitro* and *in vivo* imaging [11], but it is greatly limited by tissue penetration of approximately 1 mm [12]. In complex biological systems like cells, or especially in living organisms, the fundamental problems for optical imaging are auto-fluorescence, high light reflection, refraction and scattering of the tissue, and strong absorption of the different tissue and blood components: water, haemoglobin (Hb), melanin, protein [13]. Especially in the range of 200 (in the UV range) to 650 nm, the absorbance of blood components are very high, as shown in Figure 1.3. The absorption reduces the transmission of the excitation light and also the emitted fluorescence signal is significantly weakened, or even completely quenched [14]. This is a major barrier for visible optical imaging.

For deep tissue imaging, NIR fluorescence probes, which allow much lower tissue absorption and scattering, lower undesirable infrared autofluorescence and deeper penetration are more desirable [15, 16]. In particular, two wavelength ranges between 650-950 nm and 1000-1350 nm, now known as the first and second biological windows (I-BW and II-BW), respectively, have been identified [17]. Generally speaking, a suitable NIR fluorophore, which can be used for biological application, must fulfil the following requirements [18, 19]: (a) dispersible and stable in relevant buffers, cell culture media or body fluids, (b) high brightness and available in a reproducible quality, (c) no toxicity or interference with cell physiology. However, there are only limited choices of NIR-emitting fluorophores, such as single-walled carbon nanotubes (SWCNTs) [20, 21], Nd³⁺ and Er³⁺ doped nanoparticles [22-25], certain types of QDs [26-28], and a few organic dyes [29, 30]. The relatively low fluorescence quantum yields (QYs) and absorption coefficients, and/or poor biocompatibility of SWCNTs, dyes and rare-earth doped nanoparticles have limited their widespread use for *in vivo* imaging [18, 31]. It has also been reported that carbon nanotubes can impale pulmonary cells like needles [32, 33]. Therefore, it is urgent

to exploit other brightly fluorescent and biocompatible NIR-II fluorescent probes for biological imaging both in vitro and in vivo.

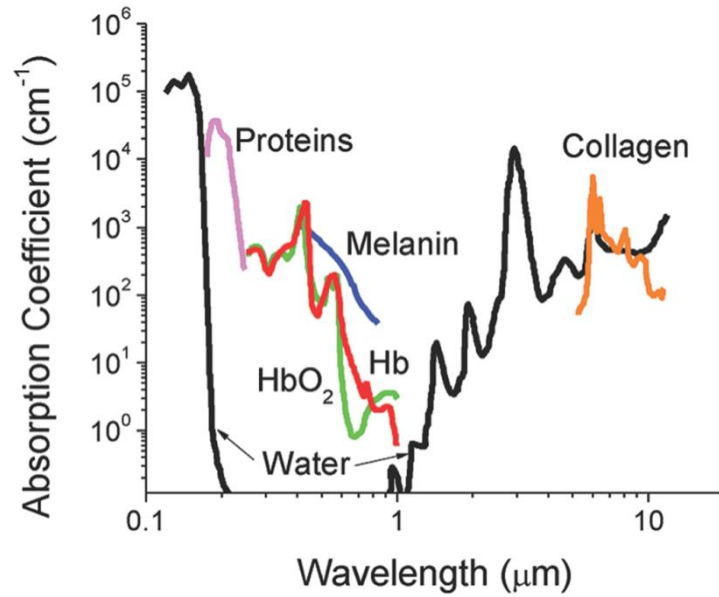


Figure 1.3 Absorbance of various tissue and blood components from 200 nm to 10 μm. (Obtained from reference [13]).

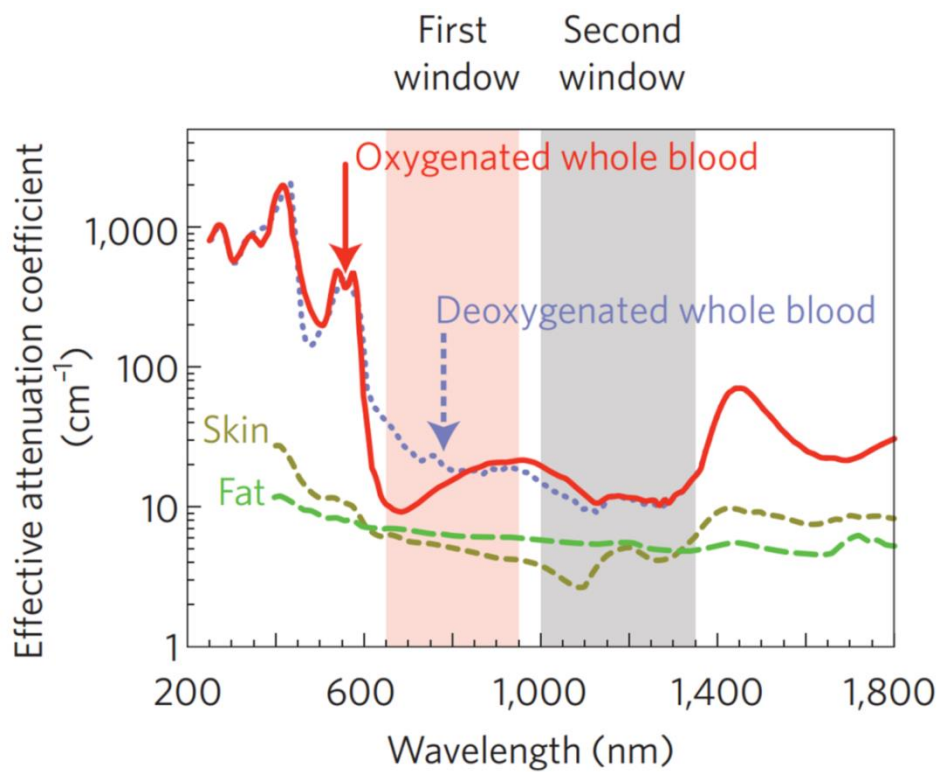


Figure 1.4 Optical windows in biological tissues. (Obtained from reference [17]).

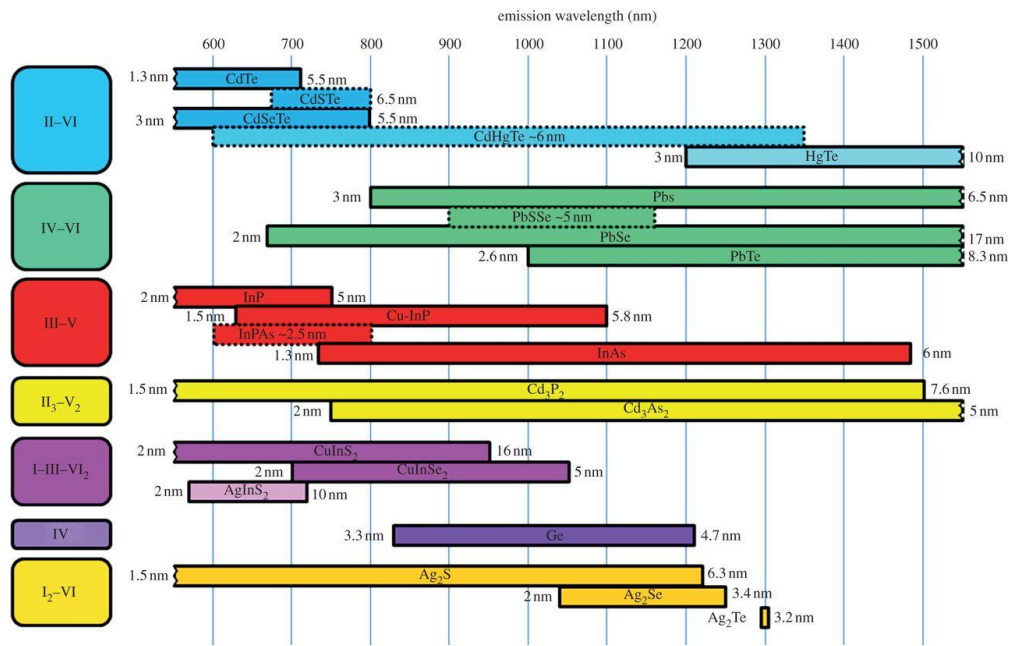


Figure 1.5 Composition, size and wavelength ranges of reported NIR-emitting QDs prepared via solution-based methodologies. Emission wavelengths reported for constant size nanocrystals containing different proportions of elements are represented with broken lines rectangle. (Obtained from reference [19]).

NIR emitting QDs which can be tuned to emit from below 1000 nanometer to several thousand nanometers are particularly interesting [34]. They can absorb photons over a broad wavelength range in the solar spectrum, from ultraviolet (UV)-visible (vis) to NIR. Both the excitation and emission of NIR QDs can be easily tuned to lie within the biological windows, in which tissues do not absorb and scatter the light as much as in the UV-vis regime and thus lower autofluorescence is involved. Bio-imaging with NIR QDs, is more desirable for some demanding biological applications, where deeper tissue penetration and higher signal-to-noise ratios are required [35, 36]. Several types of QDs such as InAs and InP (III-V) [37, 38], PbSe and PbS (IV-VI) [39, 40], Ag₂S and Ag₂Se (I-VI) [26, 41], which can be tuned to emit in the NIR range as shown in Figure 1.5. Among them, Ag₂S QDs with relatively high fluorescence in the second biological window have been used for NIR *in vivo* imaging [42, 43]. Imaging

with these Ag_2S QDs afforded deep inner organ registration, dynamic tumor contrast, and fast tumor detection. However, their low photostability can be a major issue for some applications. It has been reported that their PL intensity decreased by half in the first 200 s under continuous illumination with a 808 nm laser diode [42].

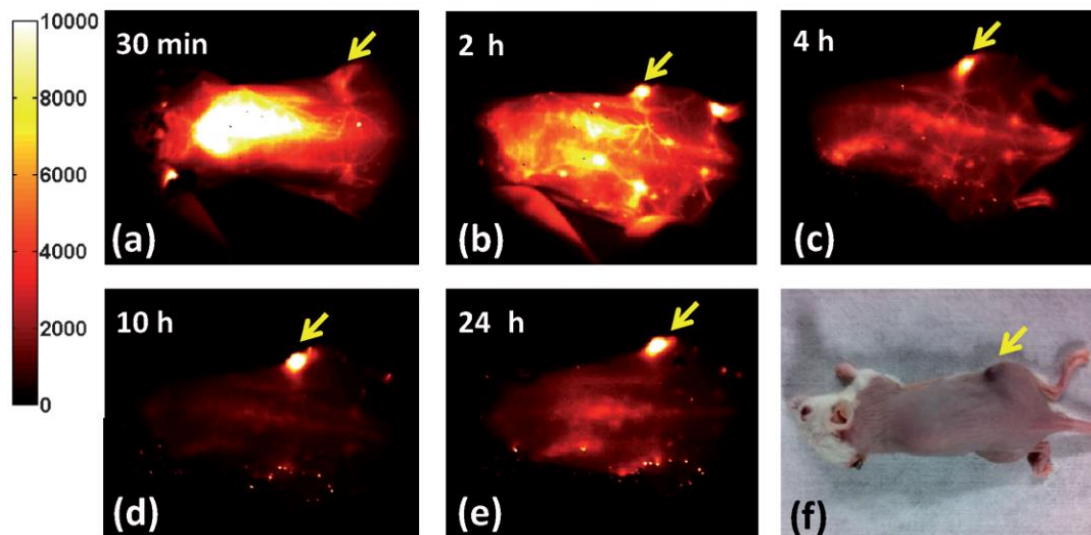


Figure 1.6 NIR-II fluorescence imaging of a xenograft tumor with high uptake of Ag_2S QDs. (a–e) Time course of NIR-II fluorescence images of the same mouse injected with Ag_2S QDs. (Obtained from reference [27]).

1.3 PbS QDs

PbS QDs owing to their unique features, such as narrow bandgaps (0.41 eV at room temperature), large Bohr radii (18 nm) and size-dependent optical absorption and emission spectra (Figure 1.7) have gained considerable attention in the last decade [44]. Due to these unique features, the PbS QDs have shown potential applications in, for instance, solar cells, bioimaging, telecommunications and light emitting diodes (LEDs) [45-47]. Some contents of this chapter were published in a review article by our group in 2016 [48].

The synthesis of colloidal PbS QDs is normally done through the hot injection method, which is performed by injecting the sulfur source to the hot lead organometallic precursors. Since this method can separate the nucleation and growth stages by precisely controlling temperature, it usually yields the

best quality, judged by size and shape distribution as well as optical properties. The seminal work on the synthesis of relatively monodisperse PbS QDs by an organometallic route using hot injection was first reported by Hines and Scholes [49]. The QDs show a narrow size dispersion (15–20%) with a full width at half maximum of PL peak of about 100 meV without any size selection process. However, their synthesis involved the use of the toxic chemical bis(trimethylsilyl)sulfide (TMS) as the sulfur source. Another breakthrough on the PbS QD synthesis was later on achieved by Ozin’s group, who discovered a solventless, heterogeneous, and relatively green route to synthesize PbS QDs via the hot injection method, by replacing TMS with sulfur [50]. The obtained high quality QDs have an even narrower size distribution, with a full width at half maximum of PL peak as low as 52 meV. However, this synthesis was achieved in a highly viscous solution, which may not be easy to operate under certain circumstances. Learned from all these previous studies, we attempted to develop a simple, green and easily reproducible approach to synthesize PbS QDs. We made effort to do the synthesis in a “non-viscous” solventless oleylamine (OLA) system, by using a constant reaction temperature [51].

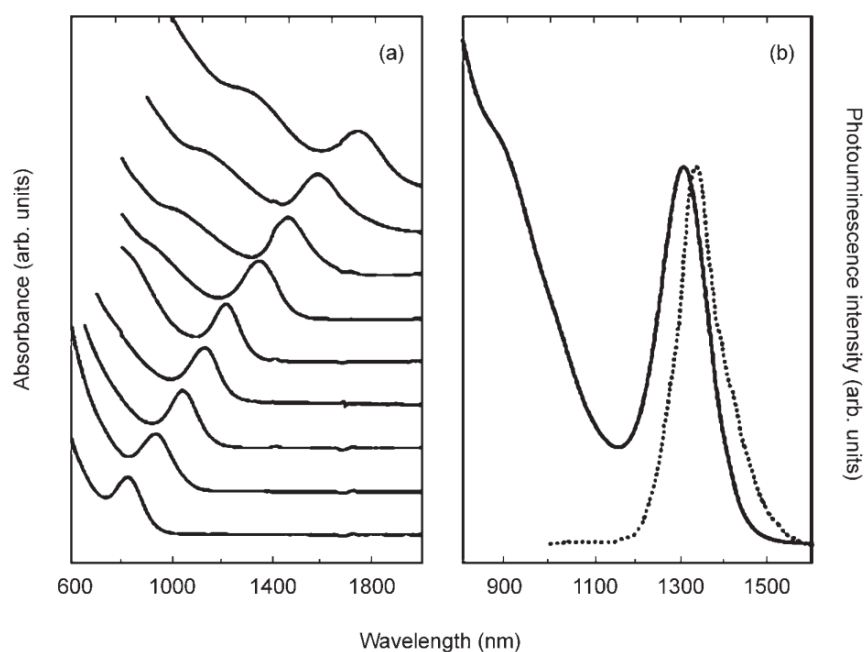


Figure 1.7 Room-temperature optical characterization of toluene solutions of PbS QDs. a) Absorption spectra spanning the range of tuneable sizes. b) Band-edge absorption and photoluminescence peaks for a sample 6.5 nm in diameter. (Obtained from reference [49]).

The hot injection method synthesized PbS QDs are normally dispersed in an organic phase. For biomedical applications, QDs are required to not only be dispersible in water, but also show high QY and good PL stability in buffer. In this case, surface modification of QDs is indispensable, which is usually achieved through ligand exchange, silica coating or intercalation process. One of the earliest reports on surface modification of Pb-based QDs was published by Colvin's group, where 11-mercaptoundecanoic acid was used to replace the oleate ligand on the surface of PbSe QDs [52]. Such prepared water dispersible QDs were found to be stable in water, but not in physiological buffers. Hinds *et al.* subsequently transferred PbS QDs from organic solvent to aqueous solution by replacing the oleate ligand with (1-mercaptoundec-11-yl) tetra (ethylene glycol) [53]. These PbS QDs exhibited improved colloidal stability in buffer for about 5 days. Recently, Veggel's group used a modified polymer approach to functionalize PbS/CdS core/shell QDs and transfer them into water [54], as shown in Figure 1.8. These QDs showed significantly enhanced, excellent long term colloidal stability in buffers, however, no information was provided on the photostability of these QDs under continuous illumination in buffers, which is an important requirement for biomedical applications when long term tracking of biological processes is needed [55].

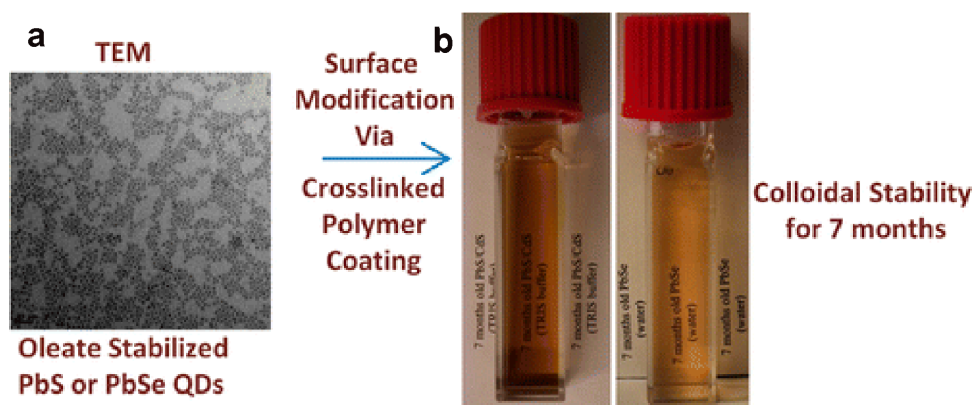


Figure 1.8 (a) TEM image of oleate stabilized PbS or PbSe QDs, (b) pictures of dispersion of PbS/CdS and PbSe QDs in TRIS, buffer and water, respectively. (Obtained from reference [54]).

1.4 Core/Shell QDs and their advantages

As the crystal becomes smaller, the surface-to-volume ratio becomes larger, and therefore the properties

of nanomaterials that only capped by organic ligands become extremely sensitive to surface characteristics. In particular, surface atoms have fewer neighbours than their interior counterparts, it is difficult to simultaneously passivate both anionic and cationic surface sites by organic ligand. Therefore, the surface atoms possess unsatisfied chemical bonds (dangling bonds), which can trap charge carriers and increase the probability of nonradiative decay events [56]. For these reasons, optical properties can be largely affected. It is thus essential to control the surface quality and to eliminate dangling bonds. To this end, researchers have made great efforts in the past few decades on surface engineering of QDs. Better surface passivation has been achieved by overgrowing an inorganic shell of a wider band gap semiconductor to form core/shell structure [57]. As a result, the impact from the surface defect states, trap sites and environmental factors on the QDs will be diminished [2, 58-61].

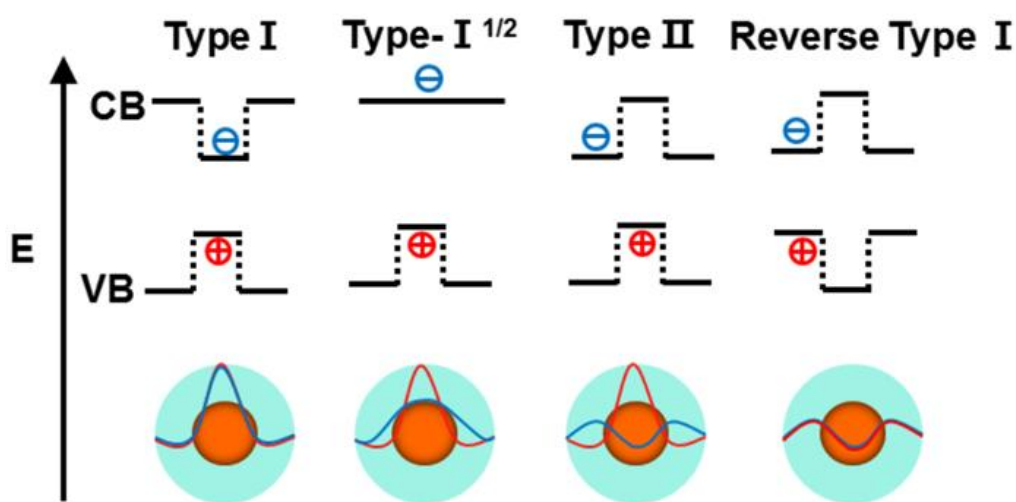


Figure 1.9 Schematic representation of the four limiting charge carrier localization regimes in core/shell semiconductor QDs. The conduction and valence band edges (i.e., the highest occupied molecular orbital (LUMO) and lowest unoccupied molecular orbital (HOMO) energy levels) are indicated by CB and valence band (VB), respectively. The plus and minus signs represent the charge carriers (hole and electron, respectively). The electron and hole ground-state wave functions are schematically depicted in the lower panel (Type I, Type-I^{1/2} and Type II illustrations obtained from reference [62]).

After being coated with an inorganic, robust semiconductor shell, the core QDs can be better

passivated and protected. Therefore, compared to the QDs capped only by organic ligands, the thermal, mechanical and chemical stability of core/shell QDs can all be enhanced. Furthermore, the optical properties of core QDs can be modified or improved via this core/shell strategy through adjusting the energy level alignment in the core/shell structure. This core/shell strategy has been proved to be an effective way to improve the photophysical properties of QDs [61, 63, 64]. Specifically, depending on the relative alignment of CB and VB edges of core and shell semiconductors, the core/shell QDs can be classified as: Type-I, Type-I^{1/2} (also known as “quasi type-II”), Type-II and Reverse Type-I (Figure 1.9). In the Type-I and reverse Type-I core/shell QDs, the VB and CB edges of one semiconductor lies entirely within the bandgap of the other material. Therefore, both electrons and holes are confined primarily in the narrower bandgap material. In type II core/shell QDs, either the VB or CB edge of the core is situated in the bandgap of the shell. As a consequence, the photogenerated electrons and holes are spatially segregated, with one type of charge carriers being preferentially confined in the core and the other in the shell. In the Type-I^{1/2} structure, the energy offset between one type of band edges (VB or CB) of the core and shell is so small that only one type of charge carriers can be confined in one of the components, while the other is delocalized in the entire core/shell structure.

The growth of the shell has been achieved by different approaches, such as precursor co-precipitation and successive ionic layer adsorption and reaction (SILAR) [65]. For example, Bawendi’s group used a two-step method (SILAR) to synthesize monodisperse CdSe/ZnS QDs with CdSe cores ranging in diameter from 2.3 to 5.5 nm as early as 1997 [66]. Recently, R. Xie *et al* used the same method to synthesize highly luminescent CdSe-Core CdS/Zn_{0.5}Cd_{0.5}S/ZnS multishell nanocrystals [61], they gradually changed the shell composition from CdS to ZnS in the radial direction. Due to the stepwise adjustment of the lattice parameters in the radial direction, the resulting nanocrystals show a high crystallinity and are almost perfectly spherical (Figure 1.10). In contrast to the SILAR method, another approach named cation exchange method has been used to synthesize high quality lead chalcogenide core/shell QDs. In this method, a shell grows at the expense of a core crystal by replacing the cations in

the core with newly introduced cations in solution. The synthesis of high quality PbSe/CdSe and PbS/CdS core/shell QDs in a controlled manner via a cation exchange reaction was first reported by Hollingsworth and co-workers [67]. The formation of the core/shell structure was supported by detailed structural characterization as well as PL spectral analysis. Both PbSe/CdSe and PbS/CdS core/shell QDs show gradual blue shift in their PL spectra with the proceeding of the cation exchange reaction, in line with the steady shrinking of the core due to shell growth, as shown in Figure 1.11.

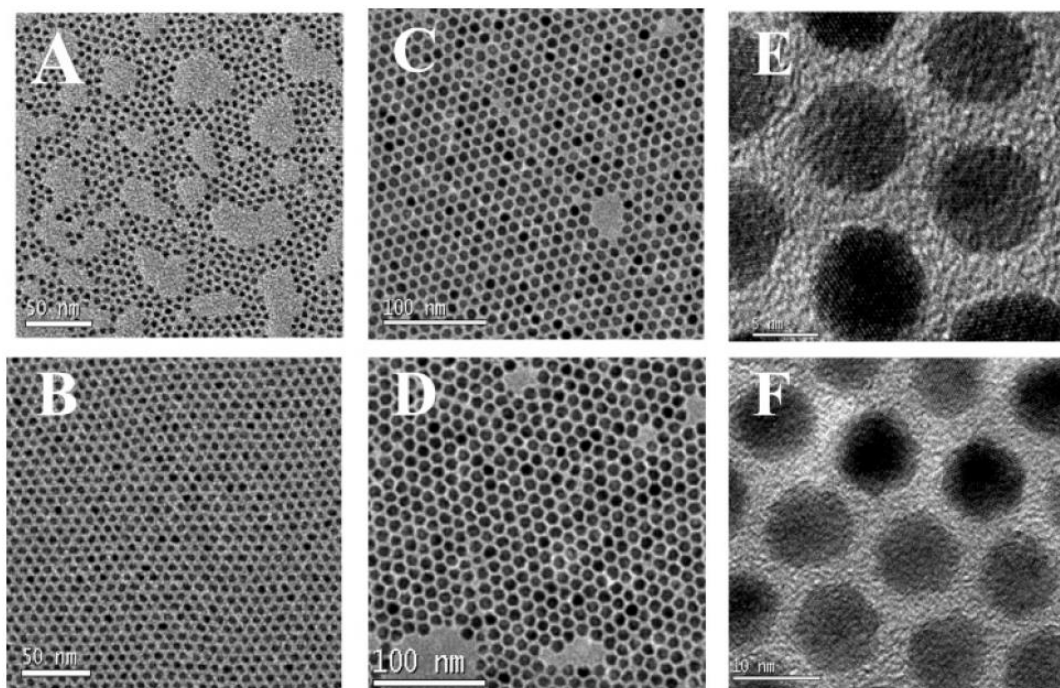


Figure 1.10 TEM images of the plain CdSe-cores and core/shell nanocrystals obtained under typical reaction conditions: (A) TEM images of CdSe-cores (before injection of Cd^{2+} solution); (B) (A) plus 2 monolayers of CdS; (C)/(E) (B) plus 3.5 monolayers of $\text{Zn}_{0.5}\text{Cd}_{0.5}\text{S}$; (D)/(F) (C) plus 2 monolayers of ZnS. (Obtained from reference [61]).

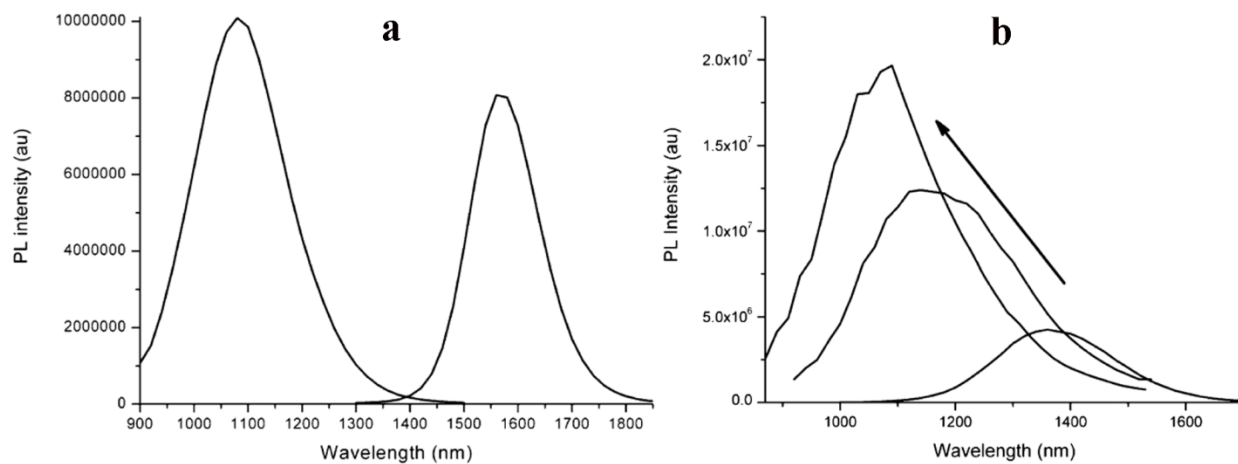


Figure 1.11 (a) PL spectra of 5.2 nm diameter PbSe NQDs (higher wavelengths) and corresponding PbSe/CdSe NQDs (lower wavelengths), (b) PL spectra of (~7 nm) PbS and two aliquots during CdS shell formation, showing relative PL enhancement during the process. Arrows indicate progress of reaction during CdS shell formation. (Obtained from reference [67]).

1.5 Bio-applications of lead based QDs

It is well known that in the first and second biological windows (I-BW and II-BW), the NIR light is minimally absorbed by tissue components and scattered as compared to visible light, resulting in deeper penetration depth [15, 16, 68-74]. The emission of PbS-based chalcogenide QDs with a large Bohr radii can be easily tuned to this spectral range. As such, they have high potential in deep tissue and animal bioimaging. One of the earliest reports on surface modification of Pb-based QDs and their use as NIR fluorophores was published by Colvin's group, where thiol ligands were used to replace the oleic acid ligands on the surface of PbS and PbSe QDs [75]. These water-dispersible lead-based QDs had fluorescence QY of about 10%, as a first example, NIR fluorescence imaging of human colon cancer cells is demonstrated using these fluorophores. Jin's group recently synthesized glutathione (GSH) coated PbS QDs by reacting $\text{Pb}(\text{CH}_3\text{COO})_2$ and Na_2S in the presence of GSH [76]. These QDs were used for non-invasive fluorescence imaging in the second near-infrared biological window (as shown in Figure 1.12). But their QY was too low, which was 6% for 1200 nm emitting PbS QDs.

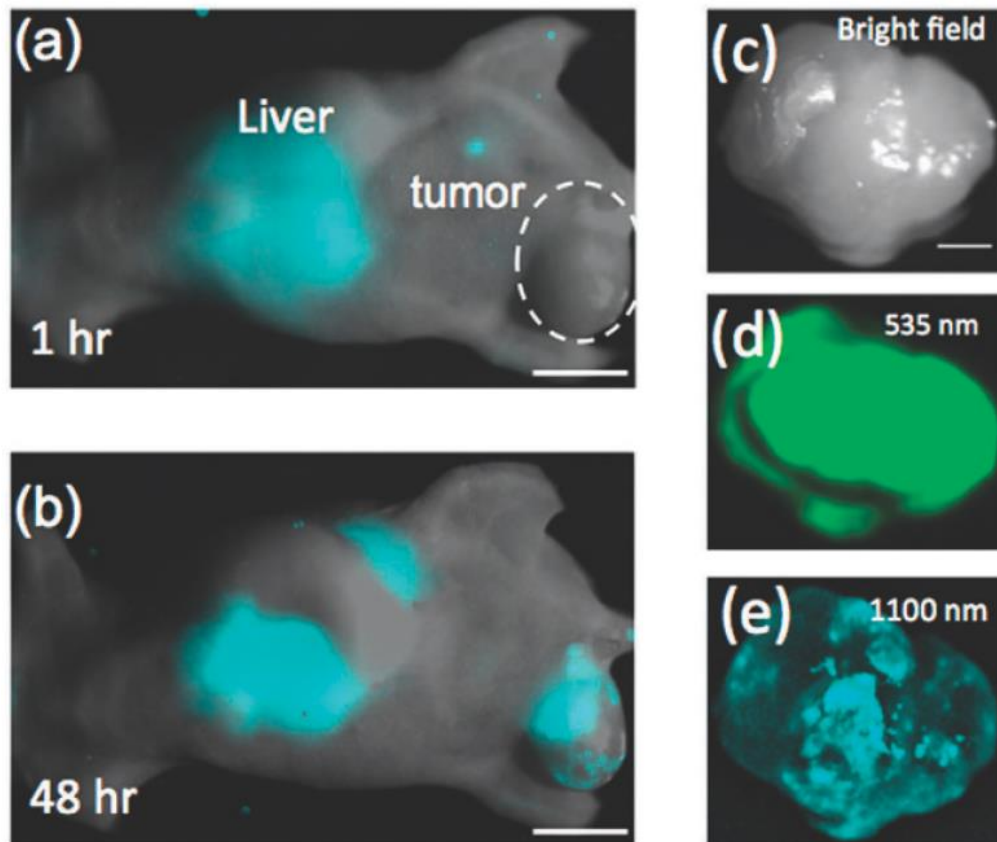


Figure 1.12 II-BW fluorescence images (1100 nm) of a breast cancer tumor 1 h (a) and 48 h (b) after injection of anti-HER2 antibody conjugated PbS QDs. The tumor location in (a) is indicated by the dotted circle. Scale bar: 10 mm. Ex vivo images of the breast cancer tumor using (c) bright field microscopy, (d) fluorescence microscopy at a visible light wavelength (535 nm), and (e) fluorescence microscopy at a II-BW wavelength (1100 nm). Scale bar: 2 mm. (Obtained from reference [76]).

When QDs containing heavy metals of Pb or Cd are used for biological applications, toxicity remains a strong concern. To the best of our knowledge, so far there are no in-depth studies on the toxic effects of Pb-based QDs. However, several reports have demonstrated the toxicity of Cd-based QDs in both cell culture and small animal studies. Derfus *et al.* reported that CdSe QDs dispersed in aqueous solution could release Cd^{2+} ions and the concentration of the Cd^{2+} ions was directly correlated with the level of cytotoxicity [77]. Their research also demonstrated that Cd^{2+} ion release was enhanced by oxidation, either through exposure to air or UV irradiation, but was suppressed by encapsulating the QDs with

appropriate shells, such as ZnS or an additional organic shell. Kirchner *et al.* investigated the cytotoxicity of CdSe and CdSe/ZnS QDs undergoing different surface modifications, such as coating with mercaptopropionic acid, silica and polymer. They claimed that coating of CdSe QDs with a ZnS shell increased the critical concentration, up to which no toxic effects could be observed, by almost a factor of 10, with respect to the CdSe QDs capped only by mercaptopropionic acid [78]. The reason was that a ligand shell of mercaptopropionic acid around the QDs was not very stable and could not prevent the release of Cd²⁺ ions from the QD surface [78]. Ye *et al.* demonstrated that rhesus macaques injected with phospholipid micelle-encapsulated CdSe/CdS/ZnS QDs did not exhibit any evidence of toxicity [5]. Blood and biochemical markers remained within normal ranges following the treatment, and histology of major organs showed no abnormalities after 90 days. Therefore, capping the Pb-based QDs with a biocompatible ZnS shell is an imperative way to use them as fluorescent imaging probes.

1.6 Thesis objectives

This thesis is divided into two parts: the first part is mainly devoted to the study of the PbS/CdS core/shell QDs.

To date, there are several approaches to produce PbS QDs in the organic phase, however, the QY is only between 20%-40% for the larger-sized QDs, whose emission peaks are in the range of 1300-1600 nm [49, 50, 79, 80]. This is because the emission of larger QDs can be easily quenched by localized trap states compared to that of smaller QDs emitting in the region of 1100-1300 nm [81], which typically possess QY between 60%-90% [49, 50, 79, 80]. Therefore, it is highly desirable but also challenging to develop a feasible approach for synthesizing high-quality PbS-based QDs with high QY in the longer wavelength range [82]. The objective for this section is:

1. To develop a reproducible and controllable approach to quickly synthesize high-quality, NIR emitting PbS/CdS core/shell QDs at longer wavelengths (1300-1600 nm).
2. To study the cation exchange mechanism of the forming of PbS/CdS core/shell QDs under different heating source. By understanding the exchange mechanism, further optimizing the reaction parameters

to synthesize high quality and large amounts of core/shell QDs.

3. To synthesize a series of differently sized PbS/CdS core/shell QDs by changing the initial PbS size.
4. To study and understand the PL intensity variation of colloidal PbS QDs with the formation of thin CdS shell from the perspective of trap density variation and the probability of electrons and holes reaching surface defects.

The second part is mainly focused on the photo and colloidal stability of water dispersible PbS/CdS/ZnS core/shell/shell QDs and their potential bio-applications. As mentioned above, the hot injection method synthesized PbS QDs are normally dispersed in an organic phase. For biomedical applications, QDs are required to not only be dispersible in water, but also show high QY and good PL stability in buffer. Although the water dispersible visible emitting QDs have been synthesized through ligand exchange, silica coating or intercalation process, relevant reports on NIR-emitting PbS QDs are still lacking. It is highly desirable but also challenging to develop a feasible approach to synthesize high-quality water- dispersible NIR-emitting PbS-based QDs. Hence, the objective of this section is:

1. To synthesize water dispersible PbS/CdS/ZnS core/shell/shell QDs by growing a biocompatible ZnS shell on the PbS/CdS core/shell QDs surface. By tuning and optimizing the CdS and ZnS shell thickness to synthesize high quality water dispersible QDs.
2. To investigate their photo and colloidal stability as well as their cytotoxicity effects, so as to use these water dispersible QDs to serve as imaging agents.
3. To study their thermal-dependent behavior of the fluorescence signal. The PbS/CdS/ZnS QDs are exploited to obtain thermal mapping of subskin areas in live specimens.

1.7 Thesis organization

This thesis is divided into four chapters and organized as follows:

Chapter 1 Introduction: This chapter is the introduction to the thesis. It also presents the objectives of this thesis.

Chapter 2 Experimental: This chapter presents the experiment details of synthesis processes of

PbS/CdS core/shell and PbS/CdS/ZnS core/shell/shell QDs. The characterization of the core/shell and core/shell/shell QDs and the investigation of the potential biological applications of core/shell/shell QDs are also presented.

Chapter 3 Results:

Part I: Quantum dots in organic phase

Section I: Microwave-assisted cation exchange toward synthesis of near-infrared emitting PbS/CdS core/shell quantum dots with significantly improved QYs through a uniform growth path

Section II: Towards understanding unusual photoluminescence intensity variation of ultrasmall colloidal PbS quantum dots with the formation of thin CdS shell

Part II: Water dispersible quantum dots and their applications

Section III: PbS/CdS/ZnS quantum dots: A multifunctional platform for in vivo near-Infrared low-dose fluorescence imaging

Section IV: Development and investigation of ultrastable PbS/CdS/ZnS core/shell/shell quantum dots in the first and second biological windows and their application in tumor imaging

Chapter 4 Conclusions and Perspectives: In this part the conclusions drawn based on the analysis of the results and future outlook in this area are presented.

CHAPTER 2 EXPERIMENTAL AND CHARACTERIZATION

In this chapter, experiment details for the synthesis and characterization of colloidal PbS, PbS/CdS core/shell and PbS/CdS/ZnS core/shell/shell QDs are described. Firstly, PbS QDs were synthesized by the normally used hot injection method. Then these PbS QDs were coated with a CdS shell via cation exchange approach in an organic phase to form PbS/CdS core/shell structure. Finally, I synthesized water dispersible and biocompatible PbS/CdS/ZnS core/shell/shell QDs by coating another ZnS shell around PbS/CdS QDs and simultaneously replacing hydrophobic oleic acid ligand with mercaptopropyl acid ligand during facile microwave-assisted ZnS shell formation process. After tuning the synthesis parameters to vary separately the shell thickness of CdS and ZnS and performing reaction optimization, I obtained high quality, water dispersible PbS/CdS/ZnS core/shell/shell QDs.

2.1 Materials

Lead chloride (98%), lead acetate trihydrate ($\geq 99.99\%$), bis(trimethylsilyl) sulfide (TMS) (synthesis grade), trioctylphosphine (TOP) (technical grade, 90%), sulfur (100%), oleylamine (OLA) (technical grade, 70%), cadmium oxide (99%), cardiogreen (IR 125), methanol (anhydrous, 99.8%), octadecene (ODE), nitric acid (70%), mercaptopropyl acid (MPA) ($\geq 99.0\%$), 1-methyl-2-pyrrolidinone (NMP) ($\geq 99\%$), butylamine (99.5%), dulbecco's modified Eagle's medium (DMEM), dimethyl sulfoxide (DMSO), 3-(4,5-dimethylthiazol-2-yl)-2,5-diphenyltetrazolium bromide (MTT), phosphorous pentasulfide (99%) and zinc chloride (99.999%) were obtained from Sigma-Aldrich Inc. Hexane, buffer solution pH 9.2 (borate) traceable to National Institute of Standards and Technology (NIST), 10X Tris-EDTA (pH 7.6) solution, phosphate buffered saline (PBS, pH 7.4), oleic acid (OA), toluene, and ethanol were purchased from Fisher Scientific Company. Plasma standard solution (sulfur, lead and zinc) were purchased from Alfa Aesar Company. All chemicals were used as purchased.

2.2 Reaction setup

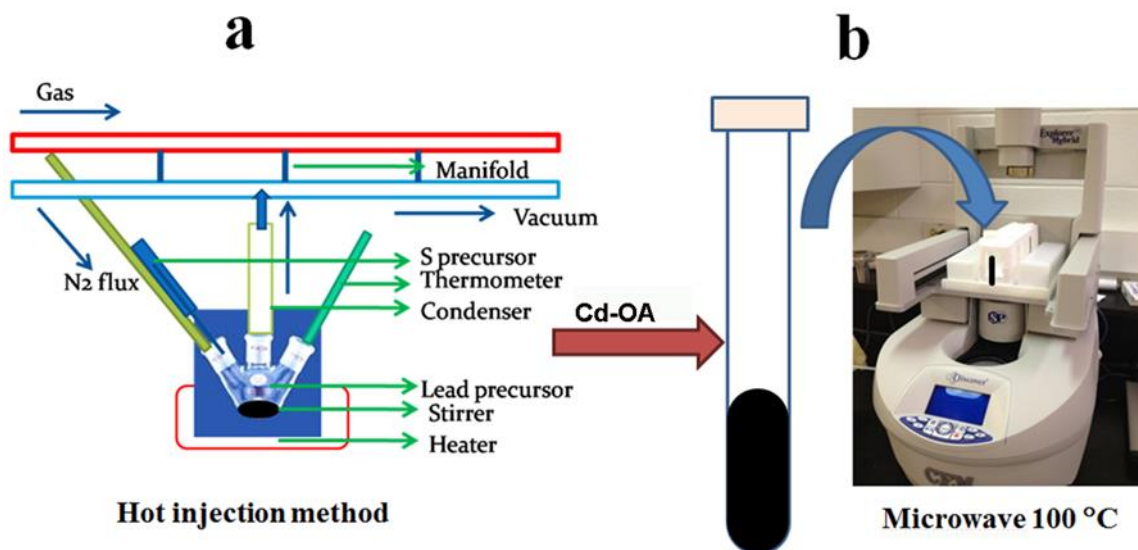


Figure 2.1 Schematic illustration of the setup for the synthesis of (a) PbS and (b) PbS/CdS core/shell and PbS/CdS/ZnS core/shell/shell QDs.

Schematic illustration of the typical reaction setup for the synthesis of PbS, PbS/CdS core/shell and PbS/CdS/ZnS core/shell/shell QDs is shown in Figure 2.1. Both of the smaller sized PbS QDs (less than 3 nm in diameter) and the larger sized PbS QDs (3.4 to 6 nm in diameter) were synthesized by using the reaction setup shown Figure 2.1a. Since the nucleation and growth processes of synthesizing PbS QDs are very sensitive to oxygen, I set up this reaction under the protection of inert N₂. The PbS/CdS core/shell QDs were synthesized by using a microwave-assisted cation exchange approach (Figure 2b). Briefly, the purified PbS QDs were mixed with Cd-OLA solution, after bubbling 10 min of N₂, this mixture was quickly heated to 100 °C by microwave. Depending on the CdS shell thickness, the reaction time can be kept for a few seconds to several min. The same microwave-reaction setup (Figure 2b) was used for synthesizing PbS/CdS/ZnS core/shell/shell QDs. Detailed information can be found in the synthesis part.

2.3 Synthesis of lead based quantum dots

2.3.1 Synthesis of PbS and PbS/CdS quantum dots in the organic phase

2.3.1.1 Synthesis of smaller PbS QDs

The smaller sized PbS QDs (less than 3 nm in diameter) were synthesized following previously reported method [49, 83]. The typical procedures are as follows:

1. Accurately weighed 760 mg of lead acetate trihydrate, 2.4 ml of OA and 15 ml of ODE were added to a 50 ml three neck round bottom flask.
2. The mixture was mixed well and then gradually heated to 150 °C in an oil bath. The mixture was kept at this temperature for at least 1 h under continuous stirring and purging with N₂.
3. After the solution became transparent and homogeneous, the temperature was decreased to 130 °C, the N₂ flow was stopped and then the solution was pumped for 15 min. After that the N₂ flow was restarted.
4. The mixture of TMS and TOP (1:10 ratio by volume; 2 ml in total) was rapidly injected into the flask, the solution was quickly cooled to 100 °C and kept at this temperature for approximately 5 min, and then quenched with cold water.
5. The QDs were precipitated by centrifugation and then re-dispersed in cold hexane. After keeping the QD dispersion at 4 °C for two days, the QD dispersion was centrifuged at 8000 rpm for 30 min and the sediment was discarded. Following methanol addition, it was centrifuged at 3000 rpm for 5 min. After removing the supernatant, the QDs sediment was re-dispersed in toluene. This purification step was repeated one more time.

2.3.1.2 Synthesis of larger PbS QDs

The larger sized PbS QDs (3.4 to 6 nm in diameter) were synthesized by using OLA as capping ligands [40]. The typical procedures are as follows:

1. Accurately weighed 10 g of lead chloride and 24 mL of OLA were loaded into a 50 ml three neck round bottom flask.
2. After mixing well, the solution was heated by oil bath to 160 °C and kept at this temperature for 1 h under the protection of N₂.
3. After the solution became transparent and homogeneous, the solution was cooled to 120 °C and pumped for 30 min.
4. N₂ flux was restored. The PbCl₂-OLA suspension was formed.

5. Accurately weighed 115 mg of sulfur was dissolved in 4 mL of OLA by ultrasonication to form S-OLA precursor.
6. S-OLA precursor was quickly injected into the PbCl_2 -OLA suspension under vigorous stirring. The reaction cell was quenched with cold water after the growth reaction was conducted at 100 °C for 1–30 min to obtain PbS QDs of different sizes (3.4-6 nm).
7. The purification procedure was carried out in air using anhydrous solvents. 20 mL of hexane and 30 mL of ethanol were added to the reaction solution followed by centrifugation to separate QDs. Obtained PbS QDs were redispersed in 20 mL hexane, again precipitated with 40 mL of ethanol and redispersed in toluene.

2.3.1.3 Synthesis of colloidal PbS/CdS QDs.

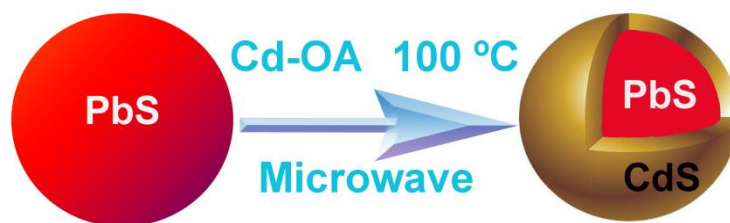


Figure 2.2 Schematic illustration of the synthesis of PbS/CdS core/shell QDs by microwave-assisted cation exchange approach.

The PbS/CdS core/shell QDs were synthesized by microwave-assisted cation exchange approach. The typical procedures are as follows:

1. 3 g of cadmium oxide, 15 mL of OA and 20 mL of ODE were mixed well in a 50 ml three neck round bottom flask.
2. The mixture was heated to 200-250 °C using an oil bath until the solution turned colorless.
3. The solution was cooled to 100 °C and degassed under vacuum for 30 min.
4. The temperature was further decreased to 20 °C and 12 mL of PbS QD dispersion with known concentration was added via syringe to mix with Cd-solution.

- 20 mL of this mixture solution was introduced into a 35 mL reaction tube, and then heated via microwave (Discover; CEM corporation) to 100 °C for different times.
- To purify the PbS/CdS QDs, ethanol was added to precipitate QDs. The precipitate was subsequently redispersed in toluene and again precipitated with ethanol. The redispersion/precipitation procedure was repeated additionally once or twice.

The above recipe was used to synthesize a relatively thick CdS shell (0.3 ~ 0.6 nm). For synthesizing a very thin shell (0.2 ~ 0.4 nm), the precursor concentration was lower, with reaction steps being the same.

2.3.2 Synthesis of water dispersible PbS/CdS/ZnS QDs

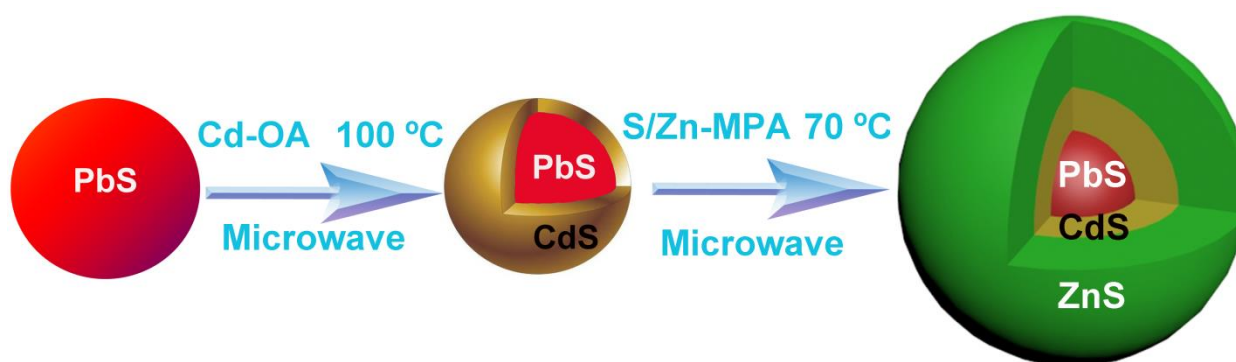


Figure 2.3 Schematic illustration of the synthesis of PbS/CdS/ZnS core/shell/shell QDs by microwave-assisted epitaxial growth method.

The PbS/CdS/ZnS core/shell/shell QDs with MPA as the capping ligand were prepared as follows. Coating the PbS/CdS QDs with a ZnS shell and replacing OLA by MPA were achieved simultaneously.

The typical procedures are as follows:

- 0.02 g of phosphorous pentasulfide, 0.5 g of MPA, 0.3 mL butylamine and 10 ml NMP were mixed well in in a sealed vial then heated to 110 °C and kept at this temperature for 20 min.
- In a separate vial, 0.07 g of zinc chloride, 0.5 g of MPA and 0.3 mL of butylamine were mixed in 10 mL of NMP and heated to dissolve in the same way.

3. 0.007 g of OA-capped PbS/CdS QDs were dispersed in the phosphorous pentasulfide solution after it was cooled down to room temperature, and the QD dispersion was mixed with zinc chloride solution.
4. The mixture solution was heated at 70 °C for 30 min in the microwave oven, yielding the MPA-capped PbS/CdS/ZnS core/shell/shell QDs.
5. The PbS/CdS/ZnS core/shell/shell QDs were purified by solvent extraction four times using hexane. The purified QDs were dried overnight at the room temperature in vacuum and dispersed in water. Water dispersible QDs were purified by ultrafiltration using an Ultracel-15 centrifugal filter (Millipore) three times and re-dispersed in phosphate buffered saline (PBS) solution and the pH of the solution was adjusted to 7.5 by adding NaOH solution.

2.4 Characterization

2.4.1 Structural and optical property characterization

PbS, PbS/CdS and PbS/CdS/ZnS QDs were characterized by various techniques. Briefly, the structure and composition of the QDs were characterized by Transmission Electron Microscopy, Energy Dispersive X-ray Spectroscopy, Powder X-ray Diffraction and Inductively Coupled Plasma-Optical Emission Spectroscopy. The optical property was characterized by a Cary 5000 UV-visible-NIR spectrophotometer and Fluorolog®-3 system. Detailed information is introduced below.

2.4.1.1 Transmission Electron Microscopy and Energy Dispersive X-ray Spectroscopy

Transmission electron microscopy (TEM) provides the direct visualization of nanostructures by using a beam of electrons to transmit through an ultra-thin specimen and an image can be formed from the interaction of the electrons with the specimen. This TEM technique has been a major analysis method for observing the morphology, size and structure of the materials[84]. In my experiments, TEM was used to directly observe the morphology, shape and size of synthesized PbS, PbS/CdS and PbS/CdS/ZnS QDs. Samples for TEM measurements were deposited onto copper TEM grids coated with thin (5-50 nm thickness) carbon films. One drop of solution containing PbS, PbS/CdS or PbS/CdS/ZnS QDs was

deposited onto the grid. The grid was subsequently put in the fume hood with high airflow to let it dry before TEM measurements. Low- and high-resolution TEM images were obtained using a JEOL 2100F microscope. Energy dispersive X-ray spectroscopy (EDX), which is a technique used for determining the elemental composition of a material, was used to confirm the presence of all expected elements (Pb, Cd and S) in the PbS/CdS core/shell QDs and (Pb, Cd, Zn and S) in the PbS/CdS/ZnS core/shell/shell QDs.

2.4.1.2 X-ray Powder Diffraction

X-ray powder diffraction (XRD) is an analytical technique mainly used for identifying the atomic and molecular structure of a crystalline material [85]. XRD study of PbS and PbS/CdS QDs after extensive purification was carried out with a Philips X'pert diffractometer using Cu K α radiation source ($\lambda = 0.15418$ nm). Diffraction patterns were collected in the 2θ range of 20-80 $^\circ$, by using the step of 0.1 $^\circ$ and counting time of 10 s. In order to perform XRD, highly concentrated PbS or PbS/CdS solution was deposited on glass substrate and dried in fume hood to form a film.

2.4.1.3 Inductively coupled plasma optical emission spectroscopy

Inductively Coupled Plasma-Optical Emission Spectrometer (ICP-OES) is an analytical technique used for the determination of trace elements. In ICP-OES, the inductively coupled plasma produces excited atoms and ions that emit electromagnetic radiation at wavelengths characteristic of a particular element. The light emitted by the excited atoms and ions in the plasma is measured to obtain information about the sample [86]. In our experiments, the contents of Pb, Zn and S elements in PbS and PbS/CdS/ZnS QDs were characterized by the ICP-OES (Agilent Technologie, 5100). Basically, the PbS QDs were precipitated with ethanol, centrifuged, and then dried in vacuum. Then, the PbS QD powder was completely dissolved by nitric acid to make aqueous solution for measuring ICP-OES. For the water dispersible PbS/CdS/ZnS QDs, they were dried in vacuum then dissolved by nitric acid. In order to measure ICP-OES, the standard solution of Pb, S and Zn with a series of concentrations: 1, 5, 10, 20, 50, 100 was prepared.

2.4.1.4 Property characterization

Absorption spectra were acquired with a Cary 5000 UV-Vis-NIR spectrophotometer (Varian) with a scan speed of 600 nm/min. Fluorescence spectra were taken with a Fluorolog®-3 system (Horiba Jobin Yvon) using charge coupled device or photomultiplier tube detectors, depending on emission wavelengths. A Xenon lamp was used to excite the QDs. The QY of smaller sized QDs (≤ 2.9 nm) was measured by using dye IR-125 as a reference and the QY of larger sized QDs (≥ 3.4 nm) was measured by using dye IR-26 as a reference, taking their respective sample transmittance η into account [87, 88]:

$$\Phi_x / \Phi_{st} = (Grad_x / Grad_{st}) * (\eta_x^2 / \eta_{st}^2) \quad (2.1)$$

where the subscripts ST and X denote standard and unknown respectively, Φ is the fluorescence QY, $Grad$ is the gradient from the plot of integrated fluorescence intensity *versus* absorbance, and η is the refractive index of the solvents used for the measurements.

The photostability of PbS/CdS/ZnS QDs dispersed in PBS buffer was tested by placing them under continuous illumination of a 4 W UV lamp (115 V, 60 Hz, Model 22-UV, Optical Engineering, UV light Inc.). The NIR luminescence image of 930 nm emitting PbS/CdS/ZnS QDs was obtained under 635 nm excitation with a silicon chip camera (Point Grey) equipped with a 785 long pass filter (Chroma).

The PL lifetimes of PbS and PbS/CdS nanocrystals in toluene were measured using a pulsed laser diode of 2.79 eV, photomultiplier tube detectors, and a fast multichannel scaler mode. PL decay curves were fit with a typical biexponential function [89]:

$$I(t)/I_0 = A_1 \exp(-t/\tau_1) + A_2 \exp(-t/\tau_2) \quad (2.2)$$

In this equation, I represents the PL intensity, t is time and I_0 is the initial PL intensity at $t = 0$. A_1 and A_2 represent the normalized amplitudes of the each components, τ_1 and τ_2 represent the decay time constants.

Average lifetime (τ) was calculated from two lifetime components, τ_1 and τ_2 , by using the following equation:

$$\tau = (B_1 \tau_1^2 + B_2 \tau_2^2) / (B_1 \tau_1 + B_2 \tau_2) \quad (2.3)$$

where B_1 and B_2 represent the relative amplitude of τ_1 and τ_2 , respectively, and were also obtained from the fitting of the biexponential function. The error on τ was obtained through differentiation of the above definition and expressed as a function of the uncertainty on the fitting parameters B_1 , B_2 , τ_1 , and τ_2 . These uncertainties were calculated automatically from the software (DAS6 Fluorescence Decay Analysis).

Transient absorption (TA) spectroscopy was performed with a Quantronix-designed femtosecond transient absorption laser system comprising an Er-doped fiber oscillator, regenerative amplifier, and a diode-pumped, Q-switched, second-harmonic Nd:YLF pump laser (527 nm, 10 W capacity). After amplification, the as-generated fundamental beam (~ 800 nm, 760 Hz repetition rate) was split in a 1/9 ratio to generate a white light continuum probe pulse and a pump pulse, respectively. The pump pulse was subsequently routed through an optical parametric amplifier to generate the desired 350 nm pump beam with a pulse duration of ~ 180 fs. Pump power was modulated by the use of absorptive neutral density filters before illuminating the sample. The pump and probe beams were overlapped spatially and temporally at the sample and the spectra were recorded after excitation with the pump and interrogation with the probe over a delay interval of 0-1000 ps between the pump and probe pulses. Variation in time delay was achieved by a motor-controlled translation stage with 1 μm resolution (6 fs time resolution). The difference absorption of each sample was measured over the aforementioned interval two times and the data averaged to achieve lower overall noise.

2.4.1.5 Estimation of QD concentration, size and shell thickness calculation

The size of PbS QDs and the PbS cores in core/shell QDs was calculated based on bandgap energy estimated from the first exciton absorption peak [40, 80, 90]:

$$E = 0.41 + 1/(0.0252 d^2 + 0.283d) \quad (2.4)$$

The band gap energy was calculated from the absorption peak following the equation:

$$E = hc/\lambda \quad (2.5)$$

where E represents band gap energy, d represents the diameter of a PbS QDs or a PbS core in PbS/CdS

core/shell QDs, h is Planck constant and λ represents the first excitation absorption peak position.

The only exception was 2.7 nm PbS/CdS core/shell QDs, for which the relationship between photoluminescence (PL) peak energy and bandgap energy was used to estimate the bandgap energy, and thereby the average size of PbS cores, due to the lack of a clear exciton absorption peak [91]. Since the overall size of PbS/CdS core/shell QDs remained the same as that of initial PbS QDs, the CdS shell thickness was estimated by subtracting the radius of PbS cores in PbS/CdS core/shell QDs from the radius of initial PbS QDs [92].

The size of PbS/CdS/ZnS core/shell/shell water dispersible QDs was measured by TEM with good precision. More than 150 QDs were analyzed for each sample; the size distribution was analyzed with a Gaussian distribution.

The concentration of purified PbS QDs in toluene was determined using the Beer-Lambert's law [40]:

$$A = \varepsilon CL \quad (2.6)$$

where A is the absorbance at the peak position of the first exciton absorption peak for a given sample, C is the molar concentration of QDs, ε is the extinction coefficient per mole of QDs and L is the light path length. ε was determined using:

$$\varepsilon = 19600 d^{2.32} \quad (2.7)$$

where d is the radius of QDs.

2.4.2 Theoretical calculation of wave functions

To calculate the electron and hole wave functions, we solved the stationary Schrödinger equation in spherical geometry, in which we used the bulk values for the effective masses of electrons (m_e^*) and holes (m_h^*), namely $m_e^* = 0.085 m_e$ and $m_h^* = 0.085 m_e$ for PbS, and $m_e^* = 0.2 m_e$ and $m_h^* = 0.7 m_e$ for CdS, where m_e is the electron mass at rest in vacuum [93]. The potentials for electrons and holes as a function of position were approximated as the lowest unoccupied molecular orbital and highest occupied molecular orbital levels, respectively, for the bulk materials [94]. For PbS, these levels are -4.5 and -4.91 eV, respectively, while for CdS they are -3.3 and -5.8 eV, respectively [93]. Outside the QD,

the potentials were set as 0 and -9.8 eV for electrons and holes, respectively. The interaction between electrons and holes was neglected in the calculations.

2.4.3 Cytotoxicity study of PbS/CdS/ZnS QDs

In order to use the water dispersible PbS/CdS/ZnS core/shell/shell QDs for bio-application, the cytotoxicity effects of these QDs were first tested. HeLa cells were plated at 5×10^5 cells/well into a 96-well plate and incubated for 24 h in DMEM (100 μ L) containing 10% fetal bovine serum (FBS). Then, DMEM was removed and at this point, live cells were attached onto the bottom of the wells. QDs dispersions in PBS were diluted with DMEM to make a series of concentrations (1 nM, 3 nM, 5 nM and 50 nM). These dispersions of QDs in DMEM (100 μ L) were dispensed to 96 wells. Blank controls without any QDs, only with pure DMEM ran simultaneously. Cell viability was measured using CellTiter 96 Non-Radioactive Cell Proliferation Assay Kit (MTT, Promega) according to manufacturer's instruction. Briefly, MTT solution (15 μ L) was added into each well. After 24 h incubation, the medium containing unreacted MTT was carefully removed. DMSO (100 μ L) was added into each well in order to dissolve the formed formazan blue crystals, and then the absorbance at $\lambda = 570$ nm was recorded using Powerwave HT Microplate Reader (Bio-Tek). Each concentration was 12-replicated. Cell viability was calculated as the percentage ratio.

2.4.4 In vivo fluorescence imaging on mice

For the animal experiments, we used six female athymic nude mice (Harlan, Holand) aged 7 weeks. The animals were subcutaneously inoculated in both flanks with 10×10^6 MDA-MB-231 cells per flank in a volume of 200 μ L of PBS to generate the human tumor xenografts. When the estimated tumor volume reached 90 mm³, we proceeded to carry out imaging experiment. For the imaging, the mice were anesthetized with 2% isoflurane and 50 μ L PBS solution containing PbS/CdS/ZnS QDs (0.2 mg/mL) was injected into each tumor. The tumors were then irradiated with an 808 nm laser diode (LIMO) at a power density of 0.04 W/cm² and NIR fluorescence images were acquired by using an InGaAs camera (XEva1.7-320) with enhanced sensitivity in the 1000-1700 nm spectral range. A long pass filter with

cut-off wavelength at 850 nm was used to remove the 808 nm pump background. The exposure time for all the images shown in the paper was shorter than 1 ms. All the experimental procedures with animals were carried out in compliance with the 2010/63/UE European guideline and were approved by the Ethics Committee from Universidad Autónoma de Madrid (CEIT) in the frame of the project FIS-MAT2013-47395-C4-1-R supported by the Spanish Ministerio de Economía y Competitividad.

Fluorescence nanothermometry experiments were carried out by optically pumping a cuvette containing the 1270 nm emitting QDs solution in PBS. The solution temperature was varied by placing the cuvette on a temperature controlled microscope stage (Linkam PE120) operating in the 5-55 °C range with a temperature accuracy of ± 0.5 °C. The thermal contact between the cuvette and the platform was guaranteed using silver filler. Thermal stabilization of the cuvette was ensured by setting heating and cooling ramps as low as 1 °C/min and performing spectral acquisitions after stabilization times close to 10 min thus guaranteeing the reported temperature value had been reached throughout the whole sample.

The optical pumping was provided by a multi-mode fiber coupled laser diode operating at 808 nm (LIMO GmbH). Pump power was kept below 50 mW for all experiments. The 808 nm radiation was focused into the cuvette by using a low numerical aperture microscope objective (10X, 0.2 NA). The NIR luminescence was collected with the same objective and spectrally analyzed by a high-resolution spectrometer (Horiba HIR 320) connected to an AsGaIn detector.

In order to determine whether the PbS/CdS/ZnS can be used for bio-imaging, we investigated the toxicity and cell viability of the HeLa epithelial cancer cells after treatment with the PbS/CdS/ZnS 1270 nm emitting QDs. For this purpose, we used the MTT assay, a method based on the activity of mitochondrial dehydrogenases, which will be functionally affected by QDs *in vitro*. As can be observed, the PbS/CdS/ZnS QDs did not show toxicity in HeLa cells with two concentrations used (1:50 and (b) 1:100 of an aqueous solution of those aforementioned QDs with an original concentration of 5 mg/ml). *In vitro* cell viability/cytotoxicity studies. This study was undertaken using a cervical cancer cell line,

HeLa. Cells were routinely cultivated using Dulbecco modified Eagle medium (DMEM) containing 10% (vol/vol) fetal calf serum (FCS), 50 units/mL penicillin, 50 µg/mL streptomycin. Cell cultures were performed at 37 °C in a humidified atmosphere containing 5% CO₂.

The MTT (3-(4,5-dimethylthiazol-2-yl)-2,5-diphenyltetrazolium bromide) assay is a simple non-radioactive colorimetric assay to measure cell cytotoxicity, proliferation or viability. MTT is yellow, water dispersible, tetrazolium salt. Metabolically active cells are able to convert this dye into a water-indispersible dark blue formazan by reductive cleavage of the tetrazolium ring⁴. Formazan crystals, then, can be dissolved in an organic solvent such as dimethylsulphoxide (DMSO) and quantified by measuring the absorbance of the solution at 540 nm, and the resultant value is related to the number of living cells. To determine cell cytotoxicity/viability, the cells were plated in a 24 well plate at 37 °C in 5% CO₂ atmosphere. After 48 h of culture, the medium in the well was replaced with the fresh medium containing QDs of varying concentrations (see Figure S2 caption) and cells were incubated for different periods of time. After incubation, the medium was removed and added completed medium without QDs. After 24 h, 0.5 ml of MTT dye solution (0.05 mg/ml of MTT, Sigma) was added to each well. After 2-3 h of incubation at 37 °C and 5% CO₂, the medium was removed and formazan crystals were solubilized with 0.5 ml of DMSO and the solution was vigorously mixed to dissolve the reacted dye. The absorbance of each well was read on a microplate reader at 540 nm. The spectrophotometer was calibrated to zero absorbance-using culture medium without cells.

The optical pumping was provided by a multi-mode fiber coupled laser diode operating at 808 nm (LIMO GmbH) with a maximum excitation power < 3 W. The laser beam was uncollimated, allowing us to take advantage of the divergence of the laser light exiting the fiber to excite the entire body of the mouse under study. That resulted in a laser-excited area of ~80 cm. The fluorescence signal from the mouse body was recorded by a Xeva-1.7 infrared camera (Xenics Inc.) capable of detecting fluorescence emission in the 900-1700 nm spectral range. The detector was fixed on a scaffold superstructure just orthogonally above the specimen where the entire body of the mouse was within its

optical field (see Figure 2.4) [95]. Residual 808 nm radiation and any residual autofluorescence from mouse's body were blocked by using a set of longpass fluorescence filters with cut-off wavelength of 1000 nm.

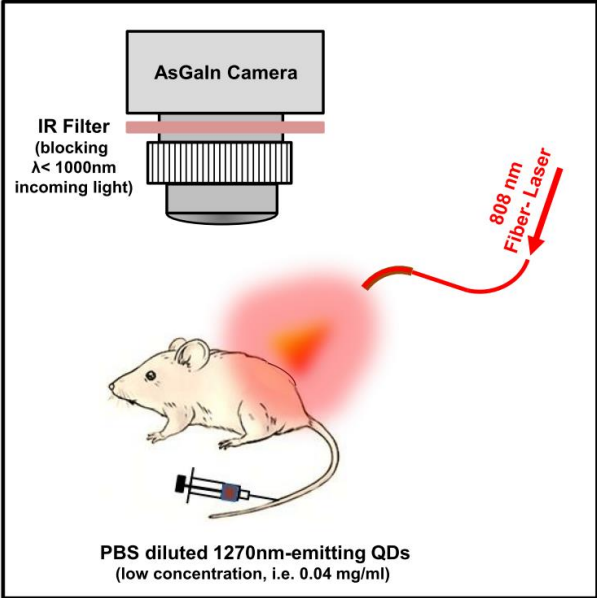


Figure 2.4 Scheme of the in vivo fluorescence imaging experiments.

CHAPTER 3 RESULTS

The results chapter is presented in two different parts. The first part is focused on the investigation of synthesis and optical properties of PbS/CdS core/shell QDs. It is divided into two sections according to different research objects (Section I and Section II). In Section I, a reproducible and controllable microwave-assisted cation exchange approach was developed to quickly synthesize high-quality NIR emitting PbS/CdS core/shell QDs. In Section II, anomalous size-dependent PL intensity variation of PbS QDs with the formation of a thin CdS shell was studied. Part II is focused on the synthesis, photo and colloidal stability of water dispersible PbS/CdS/ZnS core/shell/shell QDs (Section III) and their bio-applications (Section IV).

3.1 Part I: Quantum dots in organic phase

As introduced in Chapter 1, NIR QDs have attracted worldwide attention in recent years owing to their unique features, such as size-tunable optical and electronic properties, as well as their potential applications in NIR photodetectors, light-emitting diodes, solar cells and biological sensors. Due to their tremendous surface-to-volume ratio, their optical properties are extremely sensitive to surface states. Poor surface passivation and related surface defects will lead to either trap-state emission or non-radiative recombination, resulting in low PL QY. To achieve better optical properties and fully meet the requirements of practical applications, appropriate manipulation and modification of the QD surface is needed. In this part, we firstly synthesized a series of differently sized PbS QDs by using traditional hot inject method, then these PbS QDs were coated with a thin CdS shell to form PbS/CdS core/shell structure by our new microwave-assisted cation exchange approach, finally the optical properties of these core/shell QDs were studied.

To be more specific, part I is divided into two sections, each corresponding to an article. In Section I, we develop a reproducible and controllable microwave-assisted cation exchange approach, for the first time, to quickly synthesize high-quality, NIR emitting PbS/CdS core/shell QDs [82]. In Section II, we report anomalous size-dependent PL intensity variation of PbS QDs with the formation of a thin CdS shell via

the same microwave-assisted cation exchange approach.

Section I Microwave-assisted cation exchange toward synthesis of near-infrared emitting PbS/CdS core/shell quantum dots with significantly improved quantum yields through a uniform growth path

The synthesis of PbS QDs was developed over the last decade, the very uniform and narrow size distribution of QDs can be achieved, however, the QY of the larger-sized QDs emitting in the range of 1300-1600 nm is still relatively lower, compared with the smaller-sized QDs emitting in the range of 1100-1300 nm. Therefore, it is highly desirable but also challenging to develop a feasible approach for synthesizing high-quality PbS-based QDs with high QY in the longer wavelength range. Recent studies have revealed that the core/shell approach is one of the most efficient ways to produce high QY ultraviolet (UV)-visible or NIR emitting QDs due to the improved surface passivation of the core semiconductors.

In this section, we develop, for the first time, a reproducible and controllable microwave-assisted cation exchange approach to synthesize NIR-emitting PbS/CdS core/shell QDs, which show a QY as high as 57% in the emission range of 1300-1600 nm. Owing to their uniform shape and size, the as-synthesized PbS/CdS QDs can self-assemble nearly perfectly and easily on a large area at the micrometer scale. These high quality QDs may serve as promising materials for telecommunication devices or LED

Nanoscale **5** (2013) 7800–7804.

Cet article a dû être retiré de la version électronique en raison de restrictions liées au droit d'auteur.
Vous pouvez le consulter à l'adresse suivante :
DOI : 10.1039/C3NR02181E

Section II Towards Understanding Unusual Photoluminescence Intensity Variation of Ultrasmall Colloidal PbS Quantum Dots with the Formation of Thin CdS Shell

The core/shell strategy has been widely employed as a useful means to enhance the photophysical properties of QDs. Normally, the core/shell structure can improve the QY and stability with respect to the initial, “shell-free” QDs. However, an optimal shell thickness exists in the core/shell system, beyond certain shell thicknesses, PL intensity decreases as compared to that of the initial QDs due to the introduction of new defects. This was proved by our previous published work [92, 96]. In the last Section, we found that the QY of PbS QDs with PL peak from 1340 nm to 1560 nm (diameter from 4.5 to 5.9 nm) was largely enhanced after coating with a CdS shell of optimal thickness, mainly due to the improved surface passivation of the PbS core.

In this section, we report anomalous size-dependent photoluminescence (PL) intensity variation of PbS QDs with the formation of a thin CdS shell via a microwave-assisted cation exchange approach. We observed an unusual PL decrease in ultrasmall QDs upon shell formation. We attempted to understand this abnormal phenomenon from the perspective of trap density variation and the probability of electrons and holes reaching surface defects.

Submitted to Physical Chemistry Chemical Physics, under review.

Cet article a dû être retiré de la version électronique en raison de restrictions liées au droit d’auteur.
Vous pouvez le consulter à l'adresse suivante :
DOI : 10.1039/C6CP05786A

Supporting information for

Towards Understanding Unusual Photoluminescence Intensity Variation of Ultrasmall Colloidal PbS Quantum Dots with the Formation of Thin CdS Shell

Fuqiang Ren,^{†,‡} Sarah A. Lindley,^{‡,‡} Haiguang Zhao,[†] Long Tan,[†] Belete Atomsa Gonfa,[†] Ying-Chih Pu,[‡] Fan Yang,[†] Xinyu Liu,[§] François Vidal,[†] Jin Z. Zhang,^{*,‡} Fiorenzo Vetrone,^{†, ∇} Dongling Ma^{*,†}

[†] Institut National de la Recherche Scientifique - Énergie, Matériaux et Télécommunications, 1650
Boul. Lionel-Boulet, Varennes, Québec J3X 1S2, Canada

[‡] Department of Chemistry and Biochemistry, University of California, Santa Cruz, CA 95064, USA

[§] Department of Mechanical Engineering, McGill University, 817 Sherbrooke Street West, Montreal,
Quebec H3A 0C3, Canada

[∇] Centre for Self-Assembled Chemical Structures, McGill University, Montreal, Quebec H3A 2K6,
Canada

Contents

- 1. Materials**
- 2. Synthesis of smaller PbS quantum dots (QDs; 2.7 and 2.9 nm in diameter)**
- 3. Synthesis of larger PbS QDs (3.4 to 6 nm in diameter)**
- 4. Synthesis of colloidal PbS/CdS QDs.**
- 5. Structural and optical characterization of QDs**
- 6. Theoretical calculation of wave functions**

Figures S1-6 with captions

References

Materials and Methods

I. Materials

Lead chloride (98%), Nitric acid (70%), lead acetate trihydrate ($\text{Pb}(\text{OAc})_2 \cdot 3\text{H}_2\text{O}$; $\geq 99.9\%$), bis(trimethylsilyl) sulfide ($(\text{TMS})_2\text{S}$; synthesis grade), Trioctylphosphine (TOP; technical grade, 90%), sulfur (100%), oleylamine (OLA; technical grade, 70%), cadmium oxide (99%), cardiogreen (IR-125), 1-Benzothiopyrylium (IR-26), methanol (anhydrous, 99.8%) and octadecene (ODE) were obtained from Sigma-Aldrich Inc. Hexane, oleic acid (OA), toluene and ethanol were purchased from Fisher Scientific Company. All chemicals were used as purchased.

II. Synthesis of smaller PbS quantum dots (QDs; 2.7 and 2.9 nm in diameter)

PbS QDs were synthesized following a previously reported method.^{1, 2} In a typical procedure, a mixture of $\text{Pb}(\text{OAc})_2 \cdot 3\text{H}_2\text{O}$ (760 mg), OA (2.4 ml) and ODE (15 ml) was stirred and heated to 150 °C for 1 h under N_2 flow. It was then cooled to 130 °C under vacuum and the N_2 flow was recovered. After that, a mixture (2 ml) of $(\text{TMS})_2\text{S}$ and TOP (1:10 ratio by volume) was quickly injected into the flask, resulting in a quick drop in temperature. The reaction was then quenched with cold water after about 5 minutes. The QDs were precipitated by centrifugation and then re-dispersed in cold hexane. After keeping the QD dispersion at 4 °C for two days, the QD dispersion was centrifuged at 8000 rpm for 30 minutes and the sediment was discarded. Following methanol addition, the QD dispersion was centrifuged at 3000 rpm for 5 minutes. After removing the supernatant, the QDs were dispersed in toluene. This purification step was repeated one more time.

III. Synthesis of larger PbS QDs (3.4 to 6 nm in diameter)

Larger PbS QDs were synthesized by using OLA as capping ligands.³ In a typical reaction, PbCl_2 (10 g) and OLA (24 mL) were heated by oil bath to 160 °C and kept at this temperature for 1 h under the protection of N_2 . The solution was then cooled to 120 °C and pumped for 30 min. The flask was then reopened and the N_2 flux was restored. Sulfur (115 mg) in OLA (4 mL) at room temperature was quickly injected into the PbCl_2 -OLA suspension under vigorous stirring. The reaction cell was quenched with cold water after the reaction was conducted at 100 °C for 1-30 min to obtain PbS QDs of different sizes. The purification procedure was carried out in air using anhydrous solvents. Hexane and ethanol were added to the reaction solution followed by centrifugation to separate QDs. Obtained PbS QDs were purified one more time by redispersion and centrifugation processes. Ligand exchange with oleic acid was then performed following routine procedure.⁴ Finally, the QDs were dispersed in toluene for characterizations or for the synthesis of PbS/CdS QDs.

IV. Synthesis of colloidal PbS/CdS QDs.

Core/shell QDs were synthesized following our previously reported microwave-assisted cation exchange approach.⁵ CdO (3 g), OA (15 mL) and ODE (20 mL) were mixed and heated to 200-250 °C by oil bath until the solution turned colorless. The mixture was cooled to 100 °C and degassed under vacuum for 30 min. The temperature was further decreased to 20 °C and 12 mL of PbS QD dispersion was added *via* syringe. Then, 20 mL of this mixture was introduced into a 35 mL microwave reaction tube and heated *via* microwave (Discover; CEM Corporation). The reaction was conducted at 100 °C for different time. To purify the PbS/CdS QDs, ethanol was added to precipitate the QDs. The precipitate was subsequently redispersed in toluene and again precipitated with ethanol. The redispersion/precipitation procedure was repeated additionally once or twice.

Structural and optical characterization of QDs

The morphology of PbS and PbS/CdS QDs was characterized by a transmission electron microscope (TEM; JEOL 2100F). Absorption spectra were acquired with a Cary 5000 UV-Vis-NIR spectrophotometer (Varian) with a scan speed of 600 nm/min. Fluorescence spectra were taken with a Fluorolog®-3 system (Horiba Jobin Yvon) using charge coupled device or photomultiplier tube detectors, depending on emission wavelengths. The quantum yield (QY) of smaller sized QDs (≤ 2.9 nm) was measured by using dye IR-125 as a reference and the QY of larger sized QDs (≥ 3.4 nm) was measured by using dye IR-26 as a reference. The size of PbS QDs and the PbS cores in core/shell QDs was calculated based on bandgap energy estimated from the first exciton absorption peak.⁶⁻⁸ The only exception was 2.7 nm PbS/CdS core/shell QDs, for which the relationship between photoluminescence (PL) peak energy and bandgap energy was used to estimate the bandgap energy, and thereby the average size of PbS cores, due to the lack of a clear exciton absorption peak.⁹ Since the overall size of PbS/CdS core/shell QDs remained the same as that of initial PbS QDs, the CdS shell thickness was estimated by subtracting the radius of PbS cores in PbS/CdS core/shell QDs from the radius of initial PbS QDs.¹⁰

The PL lifetimes of PbS and PbS/CdS nanocrystals in toluene were measured using a pulsed laser diode of 2.79 eV, photomultiplier tube detectors, and a fast multichannel scaler mode. PL decay curves were fit with a typical biexponential function.¹¹ Average lifetime (τ) was calculated from two lifetime components, τ_1 and τ_2 , by using the following equation:

$$\tau = (B_1\tau_1^2 + B_2\tau_2^2) / (B_1\tau_1 + B_2\tau_2),$$

where B_1 and B_2 represent the relative amplitude of τ_1 and τ_2 , respectively, and were also obtained from the fitting of the biexponential function. The error on τ was obtained through differentiation of the above definition and expressed as a function of

the uncertainty on the fitting parameters B_1 , B_2 , τ_1 , and τ_2 . These uncertainties were calculated automatically from the software (DAS6 Fluorescence Decay Analysis).

The contents of Pb and S elements were characterized by an Inductively Coupled Plasma-Optical Emission Spectrometer (ICP-OES; Agilent Technologie, 5100). Basically, PbS QDs were precipitated with ethanol, centrifuged, and then dried in vacuum. Then, the PbS QD powder was completely dissolved by nitric acid to make aqueous solution for measuring ICP-OES.

Transient absorption (TA) spectroscopy was performed with a Quantronix-designed femtosecond transient absorption laser system comprising an Er-doped fiber oscillator, regenerative amplifier, and a diode-pumped, Q-switched, second-harmonic Nd:YLF pump laser (527 nm, 10 W capacity). After amplification, the as-generated fundamental beam (~ 800 nm, 760 Hz repetition rate) was split in a 1/9 ratio to generate a white light continuum probe pulse and a pump pulse, respectively. The pump pulse was subsequently routed through an optical parametric amplifier to generate the desired 350 nm pump beam with a pulse duration of ~ 180 fs. Pump power was modulated by the use of absorptive neutral density filters before illuminating the sample. The pump and probe beams were overlapped spatially and temporally at the sample and the spectra were recorded after excitation with the pump and interrogation with the probe over a delay interval of 0–1000 ps between the pump and probe pulses. Variation in time delay was achieved by a motor-controlled translation stage with 1 μm resolution (6 fs time resolution). The difference absorption of each sample was measured over the aforementioned interval two times and the data averaged to achieve lower overall noise.

Theoretical calculation of wave functions

To calculate the electron and hole wave functions, we solved the stationary Schrödinger equation in spherical geometry, in which we used the bulk values for the effective masses of electrons (m_e^*) and holes (m_h^*), namely $m_e^* = 0.085 m_e$ and $m_h^* = 0.085 m_e$ for Pbs, and $m_e^* = 0.2 m_e$ and $m_h^* = 0.7 m_e$ for CdS, where m_e is the electron mass at rest in vacuum.¹² The potentials for electrons and holes as a function of position were approximated as the lowest unoccupied molecular orbital and highest occupied molecular orbital levels, respectively, for the bulk materials.¹³ For PbS, these levels are -4.5 and -4.91 eV, respectively, while for CdS they are -3.3 and -5.8 eV, respectively.¹² Outside the QD, the potentials were set as 0 and -9.8 eV for electrons and holes, respectively. The interaction between electrons and holes was neglected in the calculations.

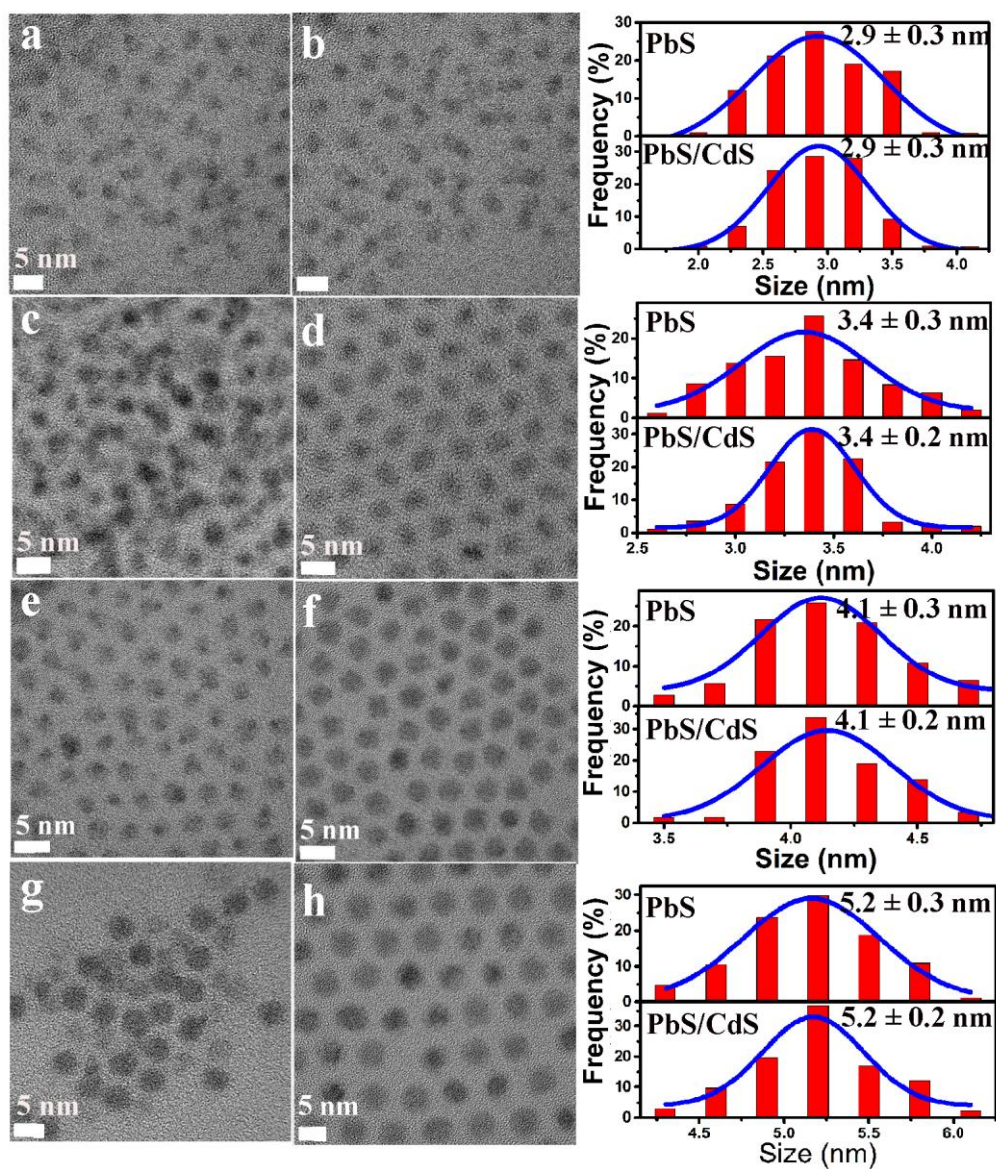


Figure S1. TEM images of differently sized PbS (a: 2.9 ± 0.3 nm, c: 3.4 ± 0.3 nm, e: 4.1 ± 0.3 nm, g: 5.2 ± 0.3 nm) and PbS/CdS (b: 2.9 ± 0.3 , d: 3.4 ± 0.2 nm, f: 4.1 ± 0.2 nm, h: 5.2 ± 0.2 nm) QDs and their corresponding histograms (right).

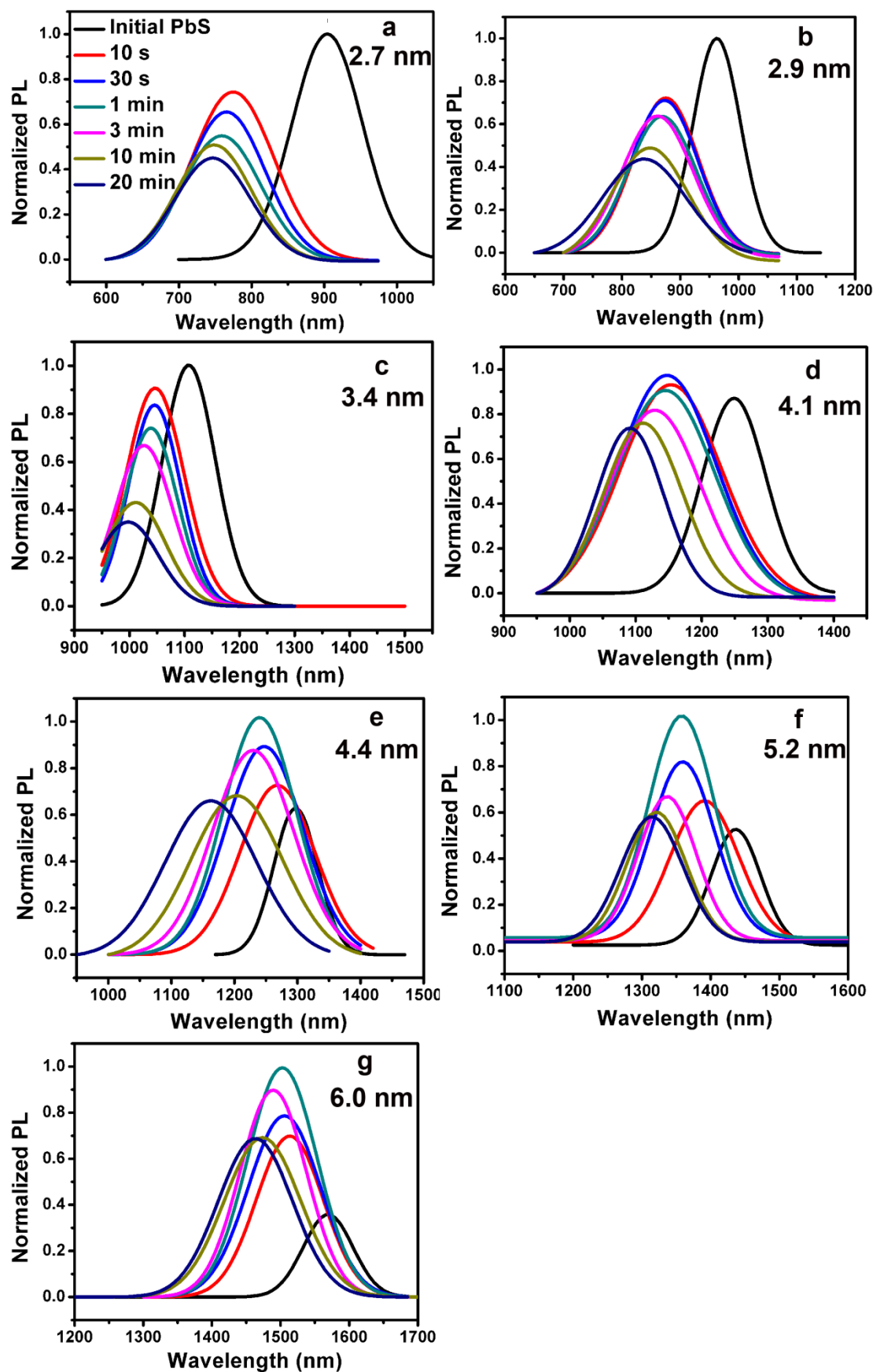


Figure S2. PL spectra of differently sized PbS QDs and PbS/CdS core/shell QDs synthesized by microwave-assisted cation exchange at different reaction time.

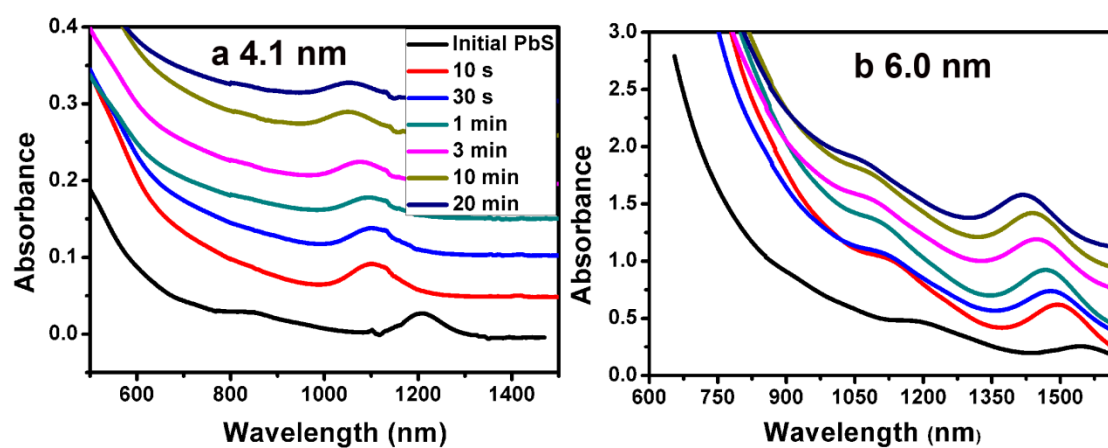


Figure S3. Typical absorption spectra evolution of QDs during microwave-assisted cation exchange (a: 4.1 nm, b: 6 nm).

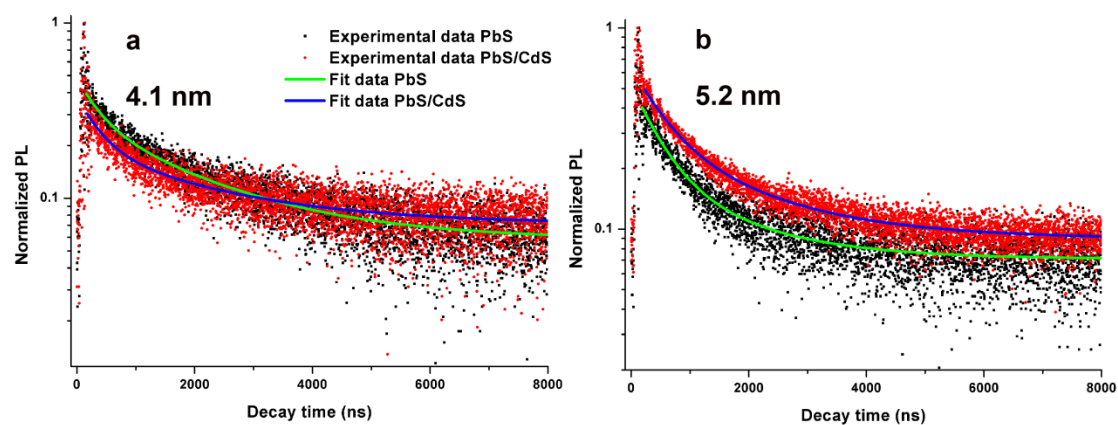


Figure S4. Typical PL decay curves of PbS and PbS/CdS QDs of different size (a: 4.1 nm, b: 5.2 nm).

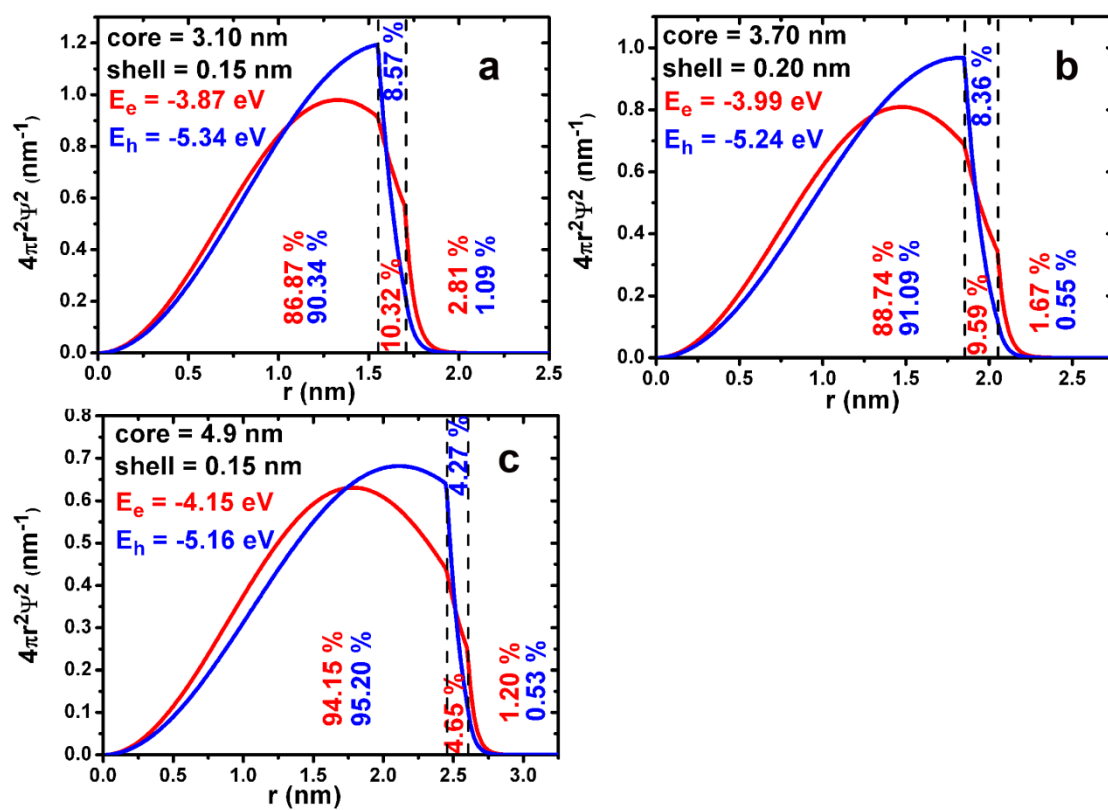


Figure S5. The energies for electrons and holes of differently sized PbS/CdS QDs (a: 3.4 nm, b: 4.1 nm, c: 5.2 nm) and the probability of finding them in each of the 3 regions (core, shell, outside).

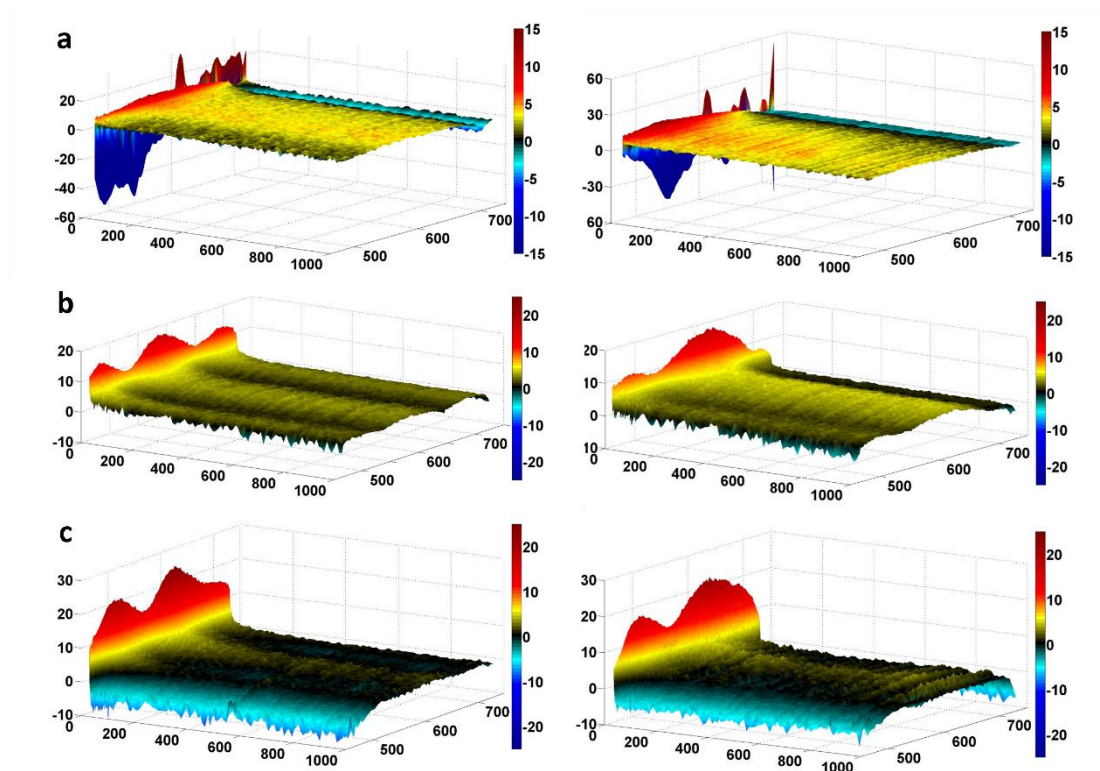


Figure S6. 3D transient absorption difference absorption spectra of PbS (left) and PbS/CdS (right) of different particle size a: 2.9 nm, b: 4.4 nm, c: 6 nm at probe wavelengths spanning 480 – 720 nm after 750 nm, 2.5 μJ /pulse excitation.

References

- (1) Hines, M. A.; Scholes, G. D., Colloidal PbS nanocrystals with size - tunable near - infrared emission: observation of post - synthesis self - narrowing of the particle size distribution. *Advanced Materials* **2003**, 15, (21), 1844-1849.
- (2) Zhang, T.; Zhao, H.; Riabinina, D.; Chaker, M.; Ma, D., Concentration-dependent photoinduced photoluminescence enhancement in colloidal PbS quantum dot solution. *The Journal of Physical Chemistry C* **2010**, 114, (22), 10153-10159.
- (3) Cademartiri L.; Montanari E.; Calestan G.; Migliori A.; Guagliardi A.; Ozin G. A.; Size-dependent extinction coefficients of PbS quantum dots. *Journal of the American Chemical Society* **2006**, 128, (31), 10337-10346.

- (4) Yuan, M.; Kemp, K. W.; Thon, S. M.; Kim, J. Y.; Chou, K. W.; Amassian, A.; Sargent, E. H., High - Performance Quantum - Dot Solids via Elemental Sulfur Synthesis. *Advanced Materials* **2014**, 26, (21), 3513-3519.
- (5) Ren, F.; Zhao, H.; Vetrone, F.; Ma, D., Microwave-assisted cation exchange toward synthesis of near-infrared emitting PbS/CdS core/shell quantum dots with significantly improved quantum yields through a uniform growth path. *Nanoscale* **2013**, 5, (17), 7800-7804.
- (6) Moreels, I.; Lambert, K.; Smeets, D.; De Muynck, D.; Nollet, T.; Martins, J. C.; Vanhaecke, F.; Vantomme, A.; Delerue, C.; Allan, G., Size-dependent optical properties of colloidal PbS quantum dots. *ACS nano* **2009**, 3, (10), 3023-3030.
- (7) Moreels, I.; Justo, Y.; De Geyter, B.; Haustraete, K.; Martins, J. C.; Hens, Z., Size-tunable, bright, and stable PbS quantum dots: a surface chemistry study. *Acs Nano* **2011**, 5, (3), 2004-2012.
- (8) Cademartiri, L.; Montanari, E.; Calestani, G.; Migliori, A.; Guagliardi, A.; Ozin, G. A., Size-dependent extinction coefficients of PbS quantum dots. *Journal of the American Chemical Society* **2006**, 128, (31), 10337-10346.
- (9) Ushakova, E. V.; Litvin, A. P.; Parfenov, P. S.; Fedorov, A. V.; Artemyev, M.; Prudnikau, A. V.; Rukhlenko, I. D.; Baranov, A. V., Anomalous size-dependent decay of low-energy luminescence from PbS quantum dots in colloidal solution. *ACS nano* **2012**, 6, (10), 8913-8921.
- (10) Zhao, H.; Chaker, M.; Ma, D., Effect of CdS shell thickness on the optical properties of water-soluble, amphiphilic polymer-encapsulated PbS/CdS core/shell quantum dots. *Journal of Materials Chemistry* **2011**, 21, (43), 17483-17491.
- (11) Lakowicz, J., Springer; New York: 2006. *Principles of Fluorescence Spectroscopy*.

- (12) Gopidas, K.; Bohorquez, M.; Kamat, P. V., Photophysical and photochemical aspects of coupled semiconductors: charge-transfer processes in colloidal cadmium sulfide-titania and cadmium sulfide-silver (I) iodide systems. *Journal of Physical Chemistry* **1990**, 94, (16), 6435-6440.
- (13) De Geyter, B.; Justo, Y.; Moreels, I.; Lambert, K.; Smet, P. F.; Van Thourhout, D.; Houtepen, A. J.; Grodzinska, D.; de Mello Donega, C.; Meijerink, A., The different nature of band edge absorption and emission in colloidal PbSe/CdSe core/shell quantum dots. *ACS nano* **2010**, 5, (1), 58-66.

3.2 Part II: Water dispersible quantum dots and their applications

It was introduced in Chapter 1 that NIR emitting QDs show potential biological application in the NIR spectral windows by improving the sensitivity and increasing the penetration depth of in vivo imaging. This part is focused on the development of water dispersible PbS/CdS/ZnS core/shell/shell QDs and their potential bio-applications. It is divided into two sections, corresponding to synthesis and their stability (Section III) and potential bio-applications (Section IV), respectively. In section III, NIR water dispersible PbS/CdS/ZnS core/shell/shell QDs were first synthesized by growing a biocompatible ZnS shell on the PbS/CdS core/shell QDs surface and simultaneously functionalizing the surface with mercaptopropionic acid ligands. Their colloidal and photo stability as well as their cytotoxicity effects were investigated. At the end, the ultrastable and biocompatible QDs were used for tumour imaging tests in mouse. In Section IV, we developed a QD-based imaging system based on NIR-emitting PbS/CdS/ZnS QDs to obtain fluorescence imaging nanoprobe with optimal penetration depths in biological tissue. The system is also capable of acting as a biological nanothermometer, based on the reliable thermal-dependent behavior of the fluorescence signal.

Section III Development and Investigation of Ultrastable PbS/CdS/ZnS Core /shell/shell Quantum Dots in the First and Second Biological Windows and their Application in Tumor Imaging

For biomedical applications, QDs are required to not only be dispersible in water, but also show high QY and good PL stability in buffer. In this section, high quality PbS/CdS/ZnS core/shell/shell QDs emitting at 930 nm in the first biological window and at 1220 nm in the second biological window were synthesized, for the first time, by growing a biocompatible thin ZnS shell on the surface of PbS/CdS core/shell QDs and simultaneously replacing initial oleic acid with MPA ligands, which endowed QDs aqueous dispersibility and stability. These synthesized core/shell/shell QDs are very stable in three commonly used biological buffers and show long time stability up to at least 14 months in PBS buffer. The QDs cytotoxicity studies show that these core/shell/shell QDs show negligible toxicity on cultured cells even at a very high QDs concentration (50 nM). The ultrastable and biocompatible QDs were further used for tumour imaging tests in mouse.

Submitted to particle and particle systems characterization, under review.

Development and Investigation of Ultrastable PbS/CdS/ZnS Quantum Dots for Near-Infrared Tumor Imaging

Fuqiang Ren,[†] Blanca del Rosal,[‡] So Young An,[§] Fan Yang,[†] Elisa Carrasco,[‡] Antonio Benayas,[†] Jung Kwon Oh,[§] Daniel Jaque,^{*,‡} Ángeles Juarranz de la Fuente,[‡] Fiorenzo Vetrone,^{*,†,∇} Dongling Ma^{*,†}

[†] Institut National de la Recherche Scientifique - Énergie, Matériaux et Télécommunications, Université du Québec, 1650 Boul. Lionel-Boulet, Varennes, Québec J3X 1S2, Canada

[‡] Fluorescence Imaging Group, Departamento de Física de Materiales, Facultad de Ciencias, Universidad Autónoma de Madrid, Madrid 28049, Spain.

[§] Department of Chemistry and Biochemistry, Concordia University, Montreal, Quebec H4B 1R6, Canada

[∇] Centre for Self-Assembled Chemical Structures, McGill University, Montreal, Quebec H3A 2K6, Canada

[‡] Grupo de Dermatología Experimental, Instituto Ramón y Cajal de Investigación Sanitaria, IRYCIS, Madrid 28034, Spain

KEYWORDS. Quantum dots, near-infrared, tumor imaging, photoluminescence

***Address correspondence to:**

daniel.jaque@uam.es;

fiorenzo.vetrone@emt.inrs.ca;

ma@emt.inrs.ca

ABSTRACT Achieving bright, reliable, robust and stable probes for in vivo imaging is becoming extremely urgent for the cancer imaging research community. Despite this fact, to date very few works have reported on elucidating, for a given imaging probe, the strict requirements that need to be fulfilled for it to safely and harmlessly act in the varied and chemically complex biological milieu. We report for the first time detailed investigations of the synthesis of near-infrared, water dispersive, strongly luminescent and highly stable PbS/CdS/ZnS core/shell/shell quantum dots (QDs), their properties in different buffers, their cytotoxicity and further their applications in tumor imaging. In particular, we focus on the QDs emitting at 930 nm and 1220 nm, within the first and second biological windows, respectively. These QDs were synthesized via our recently developed microwave-assisted approach to grow a ZnS shell and to simultaneous exchange initial ligand with mercaptopropyl acid on the PbS/CdS core/shell QDs dispersed in an organic phase. These QDs were extremely stable in commonly used biological buffers and remarkably, they could keep their initial morphology, dispersion status and photoluminescence (PL) in phosphate buffered saline buffer (PBS) for as long as 14 months, which was the longest time we investigated with both transmission electron microscopy and PL spectroscopy herein. PL image taken on the 930 nm emitting PbS/CdS/ZnS core/shell/shell QDs revealed that they could still emit strongly after 30-month storage in PBS. Such long term stability of water dispersible QDs is rarely reported in the literature. Their colloidal stability was further investigated by keeping them in high ionic concentration conditions. Their PL intensity did not show a noticeable

change for at least 3 weeks at high NaCl concentration up to 400 mM. The QDs also showed excellent photostability and could keep approximately 80% of their initial PL intensity after 1 hour continuous, strong UV illumination. More interestingly, they showed negligible toxicity to cultured cells even at high QDs concentration (50 nM). Given these outstanding properties, the ultrastable and biocompatible QDs were explored for the first time for in vivo, tumor imaging in mice. With one order of magnitude lower QD concentration (0.04 mg/mL), significantly weaker laser intensity (0.04 W/cm^2 vs $\sim 1 \text{ W/cm}^2$) and considerably shorter signal integration time ($\leq 1 \text{ ms}$ vs several hundreds of ms) as compared to the best reported rare earth doped nanoparticles, the QDs showed high emission intensity even at injection depth of ~ 2.5 mm, hard to achieve with visible QDs and other NIR PL probes.

INTRODUCTION

Every year there are millions of newly diagnosed cases of cancer, which puts a strain on our health care system.^{1,2} It is more challenging to detect cancer at an early stage rather than at an advanced stage, by then, however, the primary tumor usually has metastasized and invaded other organs, and is then often beyond surgical intervention. From a therapeutic viewpoint, current chemo- and radiation therapies have relatively poor specificity toward malignant tissues, resulting in damage to healthy cells or tissues along with the diseased ones. Therefore, the development of new probes for diagnosis at an earlier stage and advanced therapies with high selectivity is of paramount importance in cancer treatment. Fluorescence-based optical imaging benefiting from fast feedback as well as relatively good spatial resolution has been

shown to be useful for both *in vitro* and *in vivo* imaging.³ But since it is mostly based on the visible wavelength regime (400-700 nm), it has been greatly limited by tissue penetration to approximately 1 mm.⁴ For deep tissue imaging, NIR fluorescence probes, which allow much lower tissue absorption and scattering, lower undesirable NIR autofluorescence and deeper penetration depth are more desirable.^{5,6} In particular, two optimal wavelength ranges between 650-950 nm and 1000-1350 nm, now known as the first and second biological windows (I-BW and II-BW), respectively, have been identified.⁷ However, there are only limited choices of NIR-emitting fluorophores, such as single-walled carbon nanotubes (SWCNTs),^{8,9} Nd³⁺ and Er³⁺ doped nanoparticles,¹⁰⁻¹³ certain types of QDs,¹⁴⁻¹⁶ and a few organic dyes^{17,18}. The relatively low fluorescence quantum yields (QYs) and absorption coefficients, and/or poor biocompatibility of SWCNTs, dyes and rare-earth doped nanoparticles have limited their widespread use for *in vivo* imaging.^{19,20} It has also been reported that carbon nanotubes can impale pulmonary cells like needles.^{21,22} NIR QDs owing to their remarkable photostability, brightness and unique size-tunable PL have recently been explored as highly promising, new biomedical imaging probes.²³ There are several types of QDs including InAs and InP (III-V),^{24,25} PbSe and PbS (IV-VI),^{26,27} Ag₂S and Ag₂Se (I-VI),^{14,28} which can be tuned to emit in the NIR range. Among them, Ag₂S QDs with relatively high fluorescence in the second biological window have been used for NIR *in vivo* imaging.^{29,30} Imaging with these Ag₂S QDs afforded deep inner organ registration, dynamic tumor contrast, and fast tumor detection. However, their low photostability can be a major issue for some applications. It has

been reported that their PL intensity decreased by half in the first 200 s under continuous illumination with a 808 nm laser diode.²⁹

Lead-based QDs (PbSe and PbS) have gained considerable attention in the last decade due to their potential applications in, for instance, solar cells, bioimaging, telecommunications and light emitting diodes.³¹⁻³³ They are usually synthesized in an organic phase. For biomedical applications, QDs are required to not only be dispersible in water, but also show high QY and good PL stability in biological media. In this case, surface modification of QDs is indispensable, which is usually achieved through ligand exchange, silica coating or intercalation process³⁴⁻³⁶. One of the earliest reports on surface modification of Pb-based QDs was published by Colvin's group, where 11-mercaptoundecanoic acid was used to replace the oleate ligand on the surface of PbSe QDs.³⁷ Such prepared water dispersible QDs were found to be stable in water, but not in physiological buffers. Subsequently, Hinds *et al.* transferred PbS QDs from organic solvent to aqueous solution by replacing the oleate ligand with (1-mercaptoundec-11-yl) tetra (ethylene glycol).³⁸ These PbS QDs exhibited improved colloidal stability in buffer for about 5 days. Recently, van Veggel's group used a modified polymer approach to functionalize PbS/CdS core/shell QDs and transfer them into water.³⁵ These QDs showed significantly enhanced long term colloidal stability in buffers, however, no information was provided on the photostability of these QDs under continuous illumination in buffers, which is an important requirement for biomedical applications when long term tracking of biological processes is needed.³⁹

When QDs containing heavy metals of Pb or Cd are used for biological applications, toxicity remains a strong concern. To the best of our knowledge, so far there are no in-depth studies on the toxic effects of Pb-based QDs. However, several reports have demonstrated the toxicity of Cd-based QDs in both cell culture and small animal studies. Derfus *et al.* reported that CdSe QDs dispersed in aqueous solution could release Cd²⁺ ions and the concentration of the Cd²⁺ ions was directly correlated with the level of cytotoxicity.⁴⁰ Their research also demonstrated that Cd²⁺ ion release was enhanced by oxidation, either through exposure to air or UV irradiation, but was suppressed by encapsulating the QDs with appropriate shells, such as ZnS or an additional organic shell. Kirchner *et al.* investigated the cytotoxicity of CdSe and CdSe/ZnS QDs undergoing different surface modifications, such as coating with mercaptopropionic acid, silica and polymer. They claimed that coating of CdSe QDs with a ZnS shell increased the critical concentration, up to which no toxic effects could be observed, by almost a factor of 10, with respect to the CdSe QDs capped only by mercaptopropionic acid.⁴¹ The reason was that a ligand shell of mercaptopropionic acid around the QDs was not very stable and could not prevent the release of Cd²⁺ ions from the QD surface.⁴¹ Ye *et al.* demonstrated that rhesus macaques injected with phospholipid micelle-encapsulated CdSe/CdS/ZnS QDs did not exhibit any evidence of toxicity.⁴² Blood and biochemical markers remained within normal ranges following the treatment, and histology of major organs showed no abnormalities after 90 days.

We previously reported on the important role of CdS in effectively preventing the

release of heavy metal Pb^{2+} ions, as well as significantly enhancing the PL intensity, colloidal stability and photostability of PbS/CdS core/shell QDs with respect to PbS QDs.⁴³⁻⁴⁵ Subsequently, we further developed water dispersible and biocompatible PbS/CdS/ZnS core/shell/shell QDs by synthesizing a thin ZnS shell around PbS/CdS QDs and simultaneously replacing the hydrophobic oleic acid ligand with the mercaptopropyl acid ligand during a facile microwave-assisted ZnS shell formation process. After carefully tailoring the synthesis parameters to optimize reactions and structures (such as the thickness of the intermediate CdS shell), we achieved high quality, water dispersible PbS/CdS/ZnS core/shell/shell QDs. In PBS buffer, these QDs showed excellent long term colloidal stability and retention of luminescence, while their morphology, PL shape and intensity remained unchanged for at least 14 months (the longest time we investigated with both electron microscopy and PL spectroscopy). Equally important was the observation that their PL kept 80% of its initial intensity after 1 hour of continuous illumination with a 4 W UV lamp. Their excellent colloidal stability and photostability confirm their promising potential for diverse biological applications, as already partially demonstrated in our recent work.⁴⁶ Nonetheless, in that work, neither their cytotoxicity nor their applicability in tumor imaging was explored in depth. Herein, the cytotoxicity of these QDs was assessed against HeLa cancer cells at different QD concentrations and no obvious toxicity was observed even at a high QD concentration. These QDs were then injected into mice for tumor imaging in small animals and showed high brightness even at quite low concentrations, under very reduced NIR laser density excitations, with very short

signal integration time and deep injection. This feature paves the way for the use of low injection doses thus further reducing the risk of adverse health effects caused by the QDs. Together, these results strongly reveal the great potential of PbS/CdS/ZnS QDs in deep tissue imaging, including, but not limited to tumor imaging.

RESULTS AND DISCUSSION

To synthesize PbS/CdS/ZnS core/shell/shell QDs emitting in the first and second biological windows, initial PbS QDs with diameters of 3.5 ± 0.3 nm and 4.6 ± 0.4 nm were synthesized through the hot injection method in an organic medium.^{27, 47, 48} In order to improve their photo- and thermal- stability, a uniform CdS shell (0.2 ~ 0.6 nm) was grown on the PbS surface to form PbS/CdS core/shell QDs by using a microwave-assisted cation exchange method.⁴³ The size of PbS QDs and the PbS cores in core/shell QDs was calculated based on bandgap energy estimated from the first exciton absorption peak.^{27, 49, 50} Since the overall size of PbS/CdS core/shell QDs remained the same as that of initial PbS QDs, the CdS shell thickness was estimated by subtracting the radius of PbS cores in PbS/CdS core/shell QDs from the radius of initial PbS QDs.⁴⁴ The OA capped core/shell PbS/CdS QDs were further modified by the simultaneous growth of a thin ZnS shell and functionalization of the surface with MPA capping ligands. This approach avoided a separate ligand exchange step, which is known to induce surface defects and significantly reduce QY.^{45, 51-53} Figure 1 shows the TEM images of the two differently sized water dispersible PbS/CdS/ZnS QDs emitting in the first and second biological windows, respectively, and it is clear that both QD samples showed a uniform size distribution. Figure 2

presents the PL spectra of the initial PbS QDs and that of the QDs after the first CdS shell and the second ZnS shell formation. The thin CdS shell (tunable from 0.2 to 0.6 nm) was formed by the gradual replacement of Pb^{2+} ions with Cd^{2+} ions through sharing of a face centered cubic sublattice of S anions.⁵⁴ The overall QD size remained almost unchanged during this cation exchange process. However, due to the shrinking of the PbS core size, a blue shift of their PL was observed for both small and larger PbS/CdS QDs. Following the growth of another shell of ZnS, and their subsequent transfer into water, another small blue shift was observed for the larger PbS/CdS/ZnS QDs (in this specific case, CdS thickness: 0.41 nm; ZnS thickness: 0.8 nm), while the PL peak of the smaller QDs (in this specific case, CdS thickness: 0.42 nm; ZnS thickness: 1.1 nm) remained unchanged.

The PL properties and stability of PbS QDs can be profoundly influenced by their surface chemistry and surrounding medium. Coating PbS QDs with a CdS shell can usually improve their PL intensity, thermal- and photo-stability.^{55, 56} The essential reason is that the surface passivation by a larger bandgap, robust inorganic shell can bury the PbS semiconductor in a potential energy well and also diminish the impact from the environment. We already proved that by controlling the thickness of the CdS shell to 0.2-0.3 nm, the QY of core PbS QDs at certain wavelengths can reach the highest value reported to date.⁴³ However, in the process of coating another ZnS shell and transferring them into water, this thickness did not seem to be thick enough to protect the core PbS from the influence of various external factors. Even with a thicker shell of ~0.4 nm, a slight blue shift of the QDs (with the final PL peak at 1220

nm) was observed after the ZnS formation and water transfer process (Figure 2 right). It is possibly due to the slight decrease of the PbS core size, arising from solvent and/or ligand etching during the ZnS shell synthesis process.^{45,57} We investigated the effect of CdS shell and ZnS shell reaction time on the PL property of water dispersible PbS/CdS/ZnS QDs. For the PbS QDs emitting at 1340 nm with reaction time increasing from 1 min to 20 min, the CdS shell thickness was estimated to increase from 0.21 to 0.54 nm during the microwave assisted cation exchange process. As shown in Figure S1, the PL intensity first increased and then decreased with the uniform CdS shell coating. This general trend was already well illustrated and explained in our previous work.⁴³ Briefly, although thin CdS coating can offer better surface passivation to enhance PL; beyond certain thickness, it can introduce new defects. In the current specific case, the maximum PL intensity was achieved at 0.21 nm CdS thickness. However, after growing another ZnS shell and transferring them into water, the PL intensity reached its maximum at a CdS thickness of about 0.41 nm (Figure S2). There is thus a shift in the optimal CdS thickness for PbS/CdS QDs in an organic phase and PbS/CdS/ZnS QDs in PBS. During the ZnS coating and water transfer process, surface defects may be introduced and also in aqueous systems, PL quenching by different species can be involved.^{38, 45} Generally speaking, these negative effects can be minimized by using a thicker CdS shell. But as mentioned above, thicker CdS coating can introduce defects, detrimental to PL, by itself also. Therefore, the different optimal CdS shell thicknesses were the result of interplay of all these factors. It is reasonable that the optimal CdS shell thickness in final QDs was

larger than that in the core/shell QDs dispersed in an organic phase.

For the ultrasmall 1030 nm emitting PbS QDs (3.5 nm), unexpectedly, their PL intensity didn't show any increase with CdS shell formation, while monotonically decreasing (Figure S3). We also repeated this experiment with traditional oil heating and observed the same trend. Although the exact reason is currently under investigation, the trend was quite reproducible. After growing another ZnS shell and transferring them into water, the PL intensity showed its maximum at a CdS thickness of about 0.42 nm (Figure S4), which perhaps represented the best value to minimize environmental effects.

We further studied the effect of the ZnS shell reaction time on the PL intensity. As show in Figures S5 and S6, the PL intensity of both small and larger QDs did not change in a significant way with reaction time. The ICP-OES results indicate that the ZnS shell thickness did not change when increasing reaction time from as short as 1 minute up to 1 hour (Figure S7 and S8). Quite likely, the ZnS formation was very fast under our reaction conditions and most precursors were used for ZnS formation in a short time. Nonetheless, we noticed that the stability of the core/shell/shell QDs was different in the aqueous system with ZnS reaction time. Since ligand exchange took place during the same process, we believe it was because that optimal ligand arrangement on the ZnS surface required a certain time that was longer than 1 minute. Further considering manipulation reproducibility and easiness, we choose 10 minute as the optimal reaction time for the ZnS shell formation in all the samples discussed below.

The optimized PbS/CdS/ZnS QDs (CdS: ~ 0.42 nm; ZnS: 1.1 nm) emitting at 930 nm showed a QY as high as 30%, in PBS. The atomic ratio of the Pb, Cd and Zn was found to be $\sim 1:7:70$ as measured by ICP-OES (Figure S7). Their PL decay time was 1449 ± 78 ns, much shorter than that (1881 ± 90 ns) of parent 1030 nm emitting PbS QDs (Figure S9). The optimized PbS/CdS/ZnS QDs emitting at 1220 nm showed a QY as high as 20%, when the CdS shell thickness was adjusted to be around 0.41 nm and ZnS shell thickness around 0.8 nm. The atom ratio of the Pb, Cd and Zn in these QDs was $\sim 1:2:18$ based on ICP-OES data (Figure S10). Similar to 930 nm emitting PbS/CdS/ZnS QDs, the PL decay time decreased from 1175 ± 25 ns for parent 1340 nm emitting PbS QDs to 724 ± 40 ns for PbS/CdS/ZnS QDs (Figure S10). The decrease of the decay time was probably due to the complicated interactions among water molecules, QD surfaces and different types of capping ligands.⁵³ The QY of both the smaller and larger sized QDs, became lower after being transferred from an organic phase into water, in line with the shortening of the lifetime. However, these values (20%-30%) are comparable to the best values reported for water dispersible NIR QDs.⁵⁸ The decrease of the lifetime and QY is also consistent with what reported for UV-visible QDs following the water transfer process.^{59, 60}

For comparison and highlighting the significance of the CdS shell, we also tried to directly coat the PbS QDs with a ZnS shell, without the first deposition of the intermediate CdS shell. Once PbS QDs were mixed with phosphorous pentasulfide solution, aggregation and precipitate were immediately observed. The reason is that the lattice mismatch (8.8%) between PbS (rock salt, $a = 5.93$ Å) and ZnS (zinc blende,

$a = 5.41 \text{ \AA}$) is much larger than that (1.9%) between CdS (zinc blende, $a = 5.82 \text{ \AA}$) and PbS.^{44, 54, 61} The CdS shell with a lattice constant in between those of PbS and ZnS was introduced as a buffer layer to reduce the strain.⁶² With increasing CdS thickness, PL intensity increased and reached its maximum at a CdS thickness of about 0.4 ~ 0.5 nm, after which it decreased. This behavior clearly indicated that the CdS shell played a critical role in the process of transferring PbS QDs into water and in determining the final QY of water dispersible QDs.

Colloidal Stability

Most biomedical applications involving nanoparticles, such as *in vivo* imaging and targeted labeling, require the use of colloidal nanocrystals.⁶³ The complicated nature of biological environments makes it preferable to use nanocrystals showing superior stability in diverse biological media with different conditions (salt concentrations, pH values, etc.), which has been a significant challenge.^{51, 64, 65}

Herein the new method we developed allows PbS/CdS core/shell QDs to be surface passivated by the robust, inorganic ZnS shell and functionalized with water dispersible MPA simultaneously in a single step. Aiming for biomedical applications, the colloidal stability of water dispersible PbS/CdS/ZnS QDs emitting in the first and second biological windows (*i.e.*, 930 nm and 1220 nm QDs) were evaluated by dispersing them in three commonly used biological buffers: PBS, Tris, and borate. Impressively, the core/shell/shell QDs of both sizes showed remarkable long-term stability in PBS buffer; as shown in Figures 3a and c, their PL peaks showed no noticeable changes throughout the 14 months that they were kept in PBS buffer,

which was the longest time point that we investigated by using both TEM and PL spectroscopy for both sizes of QDs herein. Figure 3b (left) shows the optical image of an aqueous dispersion of 930 nm emitting PbS/CdS/ZnS core/shell/shell QDs after 30 month storage in PBS and their NIR luminescence image (Figure 3b, right). High optical transparency, lack of any precipitates and strong NIR emission strongly support once again the superior quality, excellent stability and a very long shelf life of these QDs in the buffer. Their excellent stability was further confirmed by TEM observations straightforwardly and as shown in Figures 3d and e, both 930 nm and 1220 nm QDs were still homogenous, non-agglomerated and exhibited the same uniform size distributions as freshly prepared QDs. The main reason for such long-term stability is that the MPA ligand endowed the QDs excellent dispersion stability, while the CdS and ZnS double shells prohibited the attack of water molecules, salts or other ions to the PbS core, which dominated the overall optical characteristics of the QDs.

We further studied the stability of our QDs in two other buffers, Tris and borate. As shown in Figure 4, no significant PL peak position and peak width changes could be observed after three weeks compared to freshly prepared QDs initially dispersed in these buffers, which once again indicates the average QD size remained unchanged in these buffers. Moreover, the PL intensity also remained relatively unchanged in borate or tris buffers for the 930 nm QDs, while showing a slight decrease of 8% in the borate buffer and 25% in the Tris buffer for the 1220 nm QDs. The possible reason is that smaller QDs having a higher Pb:S ratio are more stable than larger QDs.⁶⁶ Even

with certain decrease, we would like to emphasize that these QDs showed, to the best of our knowledge, the highest long term stability in buffers reported in the literature.

In addition to the colloidal stability in common buffers at typical salt concentrations, the stability of both 930 and 1220 nm PbS/CdS/ZnS core/shell/shell QDs in PBS buffer solution were further investigated at various NaCl concentrations from 0 to 400 mM with a buffer pH value fixed at 7.4. Moreover, at the highest salt concentration of 400 mM, the PL properties were further monitored for three weeks. As shown in Figure 5, in the tested concentration range (0-400 mM) and period (up to three weeks), little or no change in both PL intensity and peak shape was observed for the two differently sized QDs. These results further highlight the stability of PbS/CdS/ZnS core/shell/shell QDs under high ionic concentration conditions.

Photostability

When QDs are used as fluorescence tracers, either *in vitro* or *in vivo*, they are required to be photostable.⁶³ Although QDs are usually more stable than organic fluorescence dyes, they still suffer from photobleaching and photooxidation under certain circumstances, especially those capped only by hydrophilic molecules. For example, Chen's group studied the photochemical instability of thiol-capped CdTe QDs.⁶⁷ They found that thiol detachment and QDs aggregation occurred after laser irradiation. Later, the same group claimed that the photostability of bovine serum albumin coated CdSe/CdS/ZnS QDs was largely improved, up to 4-5 times higher than plain CdTe QDs capped only by thiols.³⁹ Wang's group found that the CdTe/CdS/ZnS core/shell/shell QDs not only exhibited excellent photostability, which

was 17-fold more stable than bare CdTe QDs, but also showed favorable biocompatibility and non-cytotoxicity to K562 cells.⁶⁸

We tested the photostability of PbS/CdS/ZnS core/shell/shell QDs dispersed in PBS buffer by placing them under continuous illumination of a 4 W UV lamp. As shown in Figure 6, the only change observed for the 930 nm QDs during 2 hours irradiation was a drop in PL intensity; no PL peak broadening and shift were observed. The 1220 nm QDs revealed the same trend in PL intensity with irradiation time as the 930 nm QDs. However, a small blue shift of 6 nm was observed for the 1220 nm QDs, which was possibly due to their surface oxidation or photo-accelerated ligand etching.^{44, 69} Small PbS QDs were reported to be more stable than larger ones, due to the higher Pb to S ratio on their surface as well as their more compact ligand structure.^{66, 70} For bulk PbS, it was found that the kinetics of oxidation depends on its stoichiometry: sulfur rich samples oxidize much faster than sulfur deficient samples.⁷¹ Here, although PbS core dots were capped by CdS and ZnS shells, oxidation may not be completely prevented. Importantly, for both sized QDs, the PL intensity could still keep about 80% of its initial value after 1 hour continuous, strong UV illumination. This represents significant improvements as compared with some commonly used, traditional fluorophores, such as fluorescein isothiocyanate (FITC) that totally lose their fluorescence in as short as 3 minutes.⁶⁸ The excellent photostability of these QDs suggest their high potential for biomedical applications, including highly challenging, long term tracking of biological events.

Cytotoxicity

The cytotoxicity of the PbS/CdS/ZnS core/shell/shell QDs developed here as effective QDs probes for cancer cell imaging was evaluated on HeLa cancer cells using a MTT colorimetric assay. HeLa cells were incubated with various concentrations of QDs for 24 h and the viability was determined by the ratio of absorbance at $\lambda = 570$ nm (using the MTT assay) in the presence to absence of QDs. As shown in Figure 7, the viability of HeLa cells was as high as 95% in the presence of both 930 and 1220 nm QDs up to 50 nM, suggesting that these QDs exhibit negligible toxicity to cultured cells in the investigated concentration range and even at quite high QDs concentration (50 nM).⁷²

⁷³ Such non-toxicity is mainly attributed to the presence of the ZnS protective shell, which could isolate the heavy metals of Pb and Cd from exposing to the biological milieu as well as preventing their leakage with time. Another reason could consist in the surface potential of the QDs. Fisher *et al* found that cationic nanoparticles could cause high cytotoxic effects, due to their electrostatic interactions with negatively charged glycocalyx on cell membranes.⁷⁴ As reported in our previous work,⁷⁵ MPA capped QDs possess a negatively charged surface in most biological environments with a zeta-potential value of -24.2 mV at pH = 7. The negatively charged QDs could show less cytotoxic effects.⁷⁴ They may also be helpful from the bio-distribution point of view. According to Tang, Y. *et al.*, negatively charged particles preferentially render abundant accumulation in the liver other than in the lung where the cationic particles would deposit.⁷⁶ Because of this, the negatively charged QDs can be easily eliminated from the body and reduce overall toxicity, if there is any.

Tumor imaging

Motivated by their excellent colloidal stability, photo-stability and non-cytotoxicity, we further used these QDs for *in vivo* tumor imaging. Figure 8 (up) shows the scheme of the experimental procedure. Briefly, an 808 nm diode laser (0.04 W/cm² intensity) was used to excite the QDs directly injected into tumors with the estimated injection depth of around 2.5 mm and imaged with a Peltier-cooled InGaAs camera. The use of the 808 nm excitation radiation not only provides large penetration depths but also minimizes the risk of QDs photo-dissociation.^{77,78} In order to get high brightness, most of the published work used high concentration imaging agents, high laser intensity and/or long integration time. For example, in imaging with Ag₂S QDs emitting at a similar wavelength of 1200 nm, a QD concentration of 1.34 mg/ml, the laser intensity of 0.14 W/cm² and an integration time of 100 ms were used.²⁹ This high laser intensity and/or long exposure time were also used for other promising imaging agents, such as SWCNTs (0.14 W/cm², 50 ms),⁷⁹ NaGdF₄:Yb³⁺, Er³⁺@NaGdF₄:Nd³⁺,Yb³⁺ (0.2 W/cm², 100 ms) and NaYF₄:Yb³⁺, Er³⁺ (0.14 W/cm², 50 ms).⁸⁰ In the current case, the outstanding fluorescence brightness of our QDs allowed us to use almost one order of magnitude lower QD concentration (0.04 mg/ml), a significantly weaker laser excitation density (0.04 W/cm² vs ~1 W/cm²) and considerably shorter exposure time (\leq 1 ms vs several hundreds of ms) compared with rare earth doped nanoparticles. As shown in Figure 8, after injecting these two differently sized QDs into tumors, the emission signal from both 930 nm and 1220 nm QDs can be distinctly identified and moreover the injection depth (2.5 mm) is much deeper than that for visible imaging agents (1 mm).⁴ It is known that excitation and

emission both in the NIR range can largely reduce the chance of auto-fluorescence and increase signal-to-noise ratios, which represent one of major advantages of our NIR QDs.¹⁰

To spectrally differentiate the relative amount of signal emitted, we have placed different filters through the collection optical path going from the specimen to the NIR camera. When using a 1000 nm long pass filter, we could clearly see the emission from both QDs. Further increasing the wavelength of long pass filters from 1100 nm to 1200 nm, the collected intensity signal from 930 nm QDs became much weaker and then completely disappeared in the camera. In contrast, with a 1200 nm long pass filter, the emission from the 1220 nm QDs could still be clearly resolved, although it got weaker than that with the 1000 nm long pass filter. All these observations were in very good agreement with their PL spectrum features. These results demonstrate the feasibility of the PbS/CdS/ZnS core/shell/shell QDs as tumor imaging agents, yielding high signal-to-noise ratios for cancer detection. With the subsequent development of these NIR imaging probes, it is straightforward to envision further application of these QDs as deep tumor imaging probes, once functionalized with appropriate targeting moieties. The work on this aspect is on-going.

CONCLUSIONS

High quality PbS/CdS/ZnS core/shell/shell QDs emitting at 930 nm in the first biological window and at 1220 nm in the second biological window were synthesized by growing a biocompatible thin ZnS shell on the surface of PbS/CdS core/shell QDs

and simultaneously replacing initial oleic acid with MPA ligands, which endowed the QDs aqueous dispersibility and stability. By systematically studying the effect of the reaction time of the first CdS shell and the second ZnS shell (thereby shell thickness) on the PL properties of the QDs, the optimal QDs were obtained, which led to high QYs of 30% and 20% for 930 nm and 1220 nm QDs, respectively. The synthesized core/shell/shell QDs were highly stable in commonly used biological buffers: PBS, Tris, and borate. In particular, in our long term studies up to 14 months on the QDs dispersed in PBS buffer, it was found that the QDs exhibited remarkable stability, without any detectable morphology and optical property changes for at least 14 months. Our investigations on their stability at various NaCl concentrations further revealed that they were also extremely stable under high ionic concentration conditions. The QDs also demonstrated excellent photostability under continuous, strong UV illumination. These excellent properties of the QDs along with their non-cytotoxicity (at even high concentration of 50 nM) evaluated by using MTT assays motivated us to conduct tumor imaging in mice with both excitation and imaging in the NIR range. At relatively deep position of ~2.5 mm, the tumor could be clearly imaged with high brightness using rather low QD concentration, rather weak excitation and very short signal integration time. All these studies strongly suggest these QDs have high potential to serve as a next generation of deep bioimaging probes with high signal-to-noise ratios and high sensitivity for cancer diagnostics.

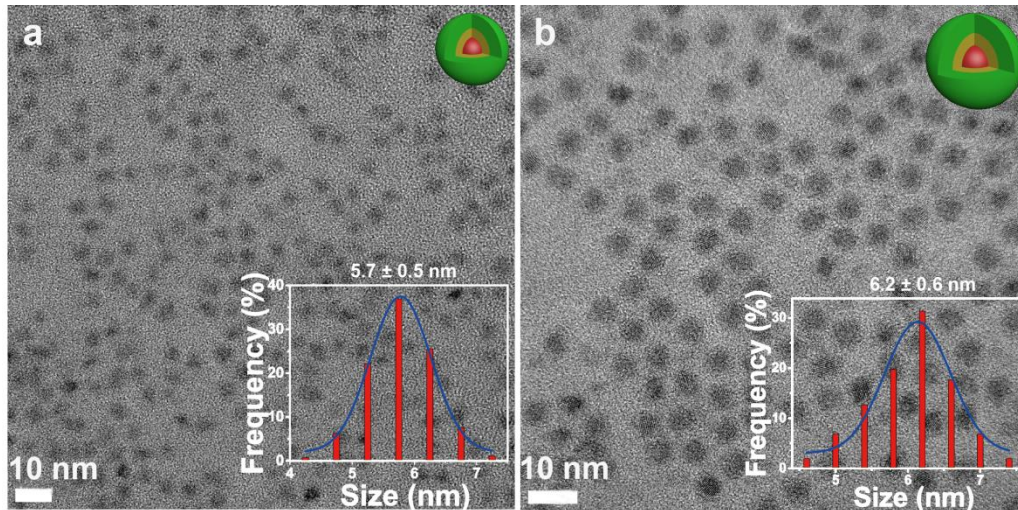


Figure 1. TEM images of PbS/CdS/ZnS QDs emitting at (a) 930 nm and (b) 1220 nm, respectively. Corresponding size distributions are shown as insets.

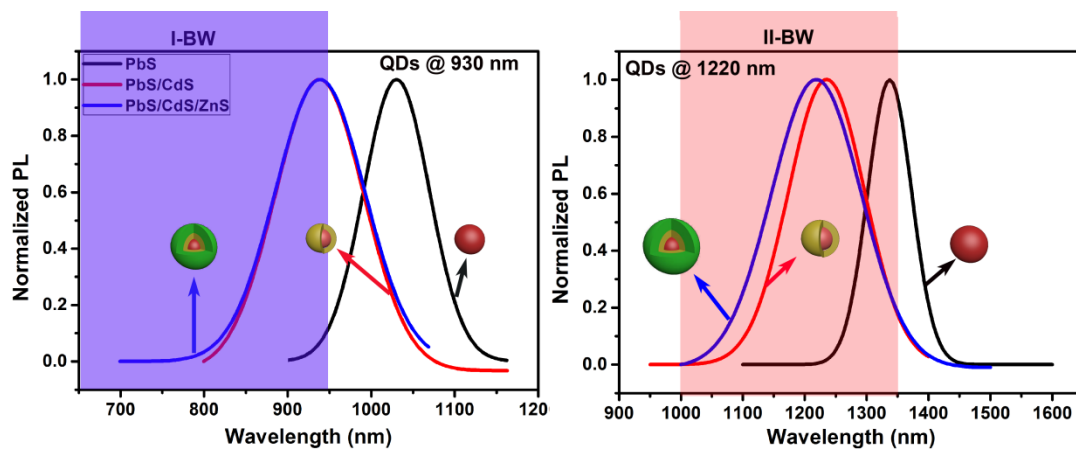


Figure 2. PL spectra of initial PbS QDs (dispersed in toluene), PbS/CdS QDs (dispersed in toluene), and final PbS/CdS/ZnS QDs (dispersed in PBS buffer) emitting at 930 nm (left) and 1220 nm (right).

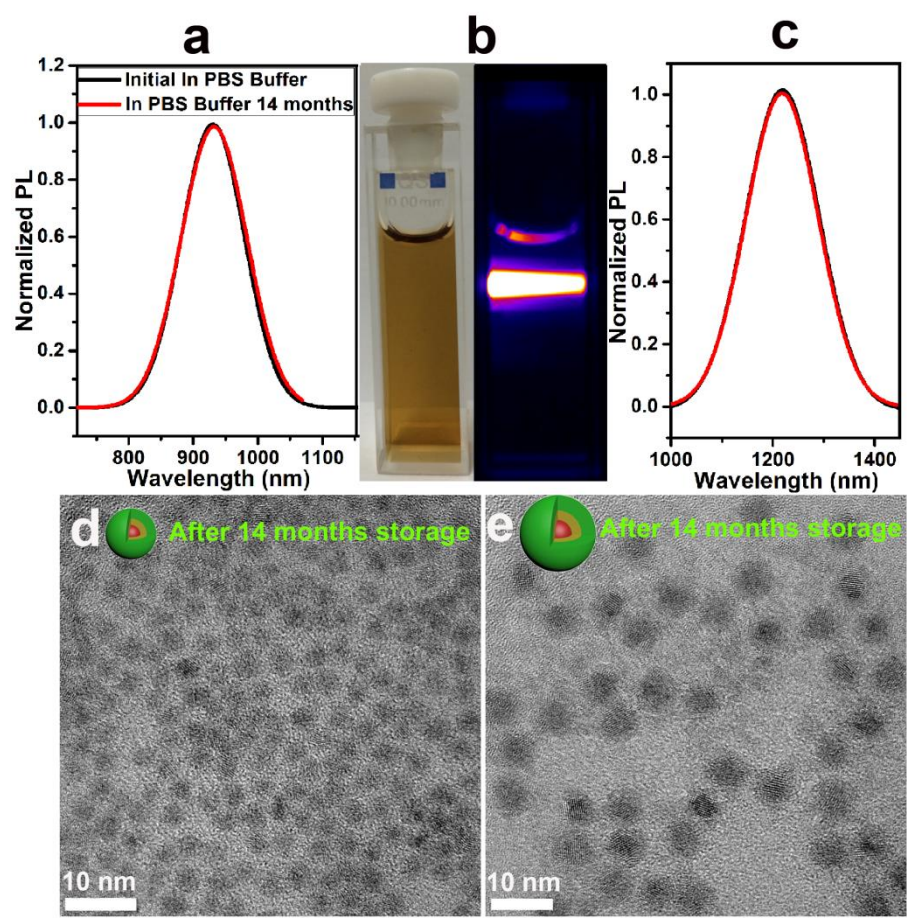


Figure 3. PL spectra of (a) 930 nm and (c) 1220 nm emitting PbS/CdS/ZnS core/shell/shell QDs freshly prepared and dispersed in PBS buffer as well as after 14 month storage in the PBS buffer. Optical (left) and luminescence (right) images of (b) 930 nm emitting PbS/CdS/ZnS core/shell/shell QDs stored in PBS buffer for 30 months. TEM images of (d) 930 nm and (e) 1220 nm PbS/CdS/ZnS core/shell/shell QDs stored in PBS buffer for 14 months.

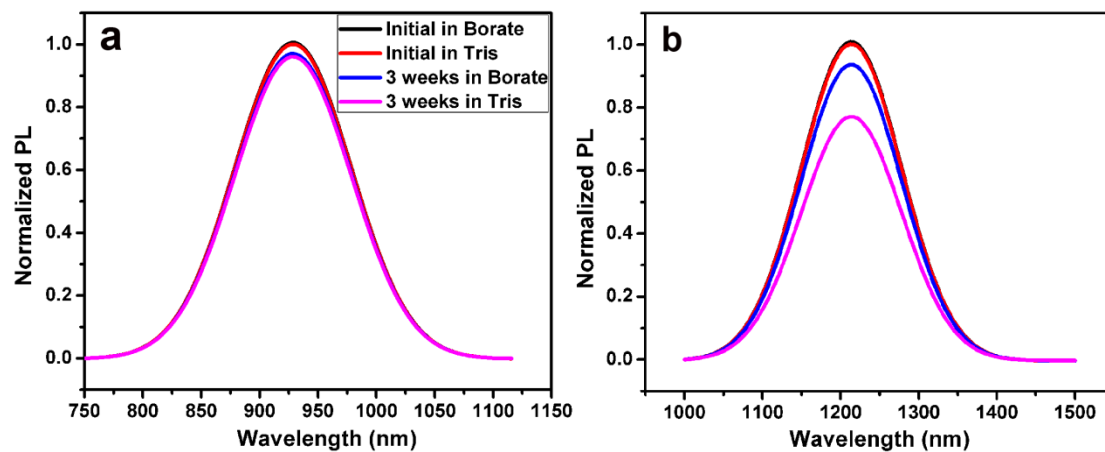


Figure 4. PL spectra of (a) 930 nm and (b) 1220 nm emitting PbS/CdS/ZnS core/shell/shell QDs freshly prepared and dispersed in two different buffers as well as after the storage for 3 weeks.

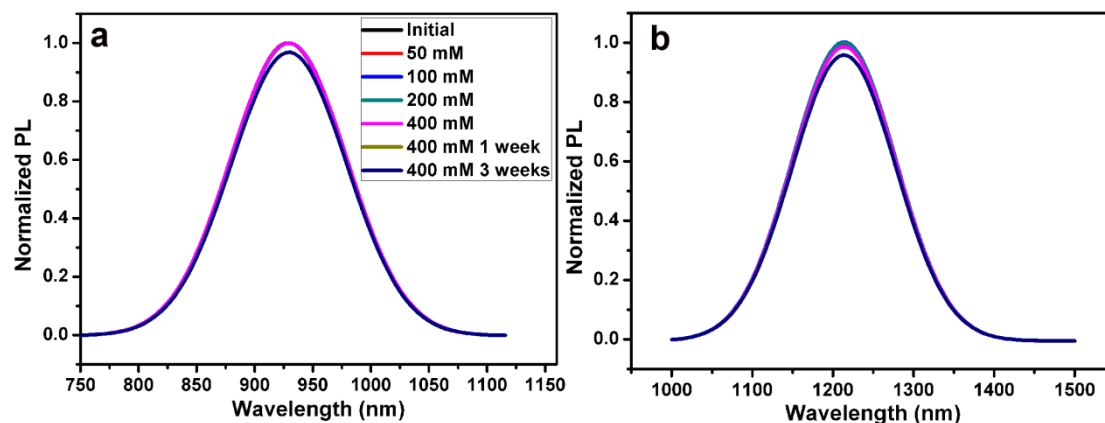


Figure 5. PL spectra of (a) 930 nm and (b) 1220 nm emitting PbS/CdS/ZnS core/shell/shell QDs in PBS buffer containing NaCl at different concentrations.

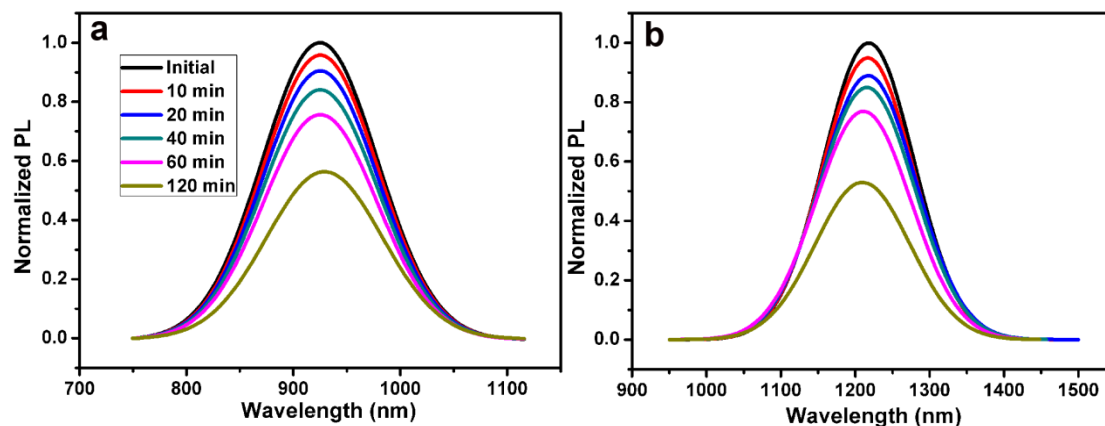


Figure 6. PL spectra of (a) 930 nm and (b) 1220 nm PbS/CdS/ZnS core/shell/shell

QDs in PBS buffer under continuous UV illumination for different time.

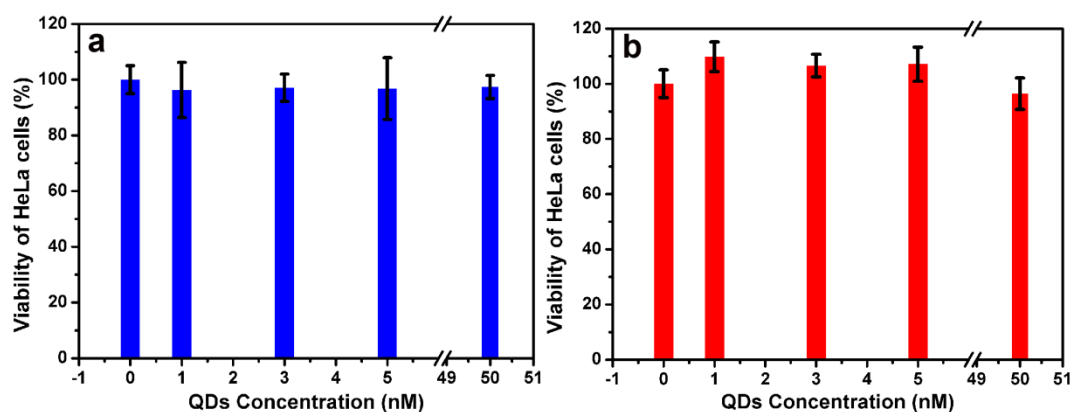


Figure 7. Cell viability in the presence of (a) 930 nm and (b) 1220 nm QDs at their different concentrations up to 50 nM.

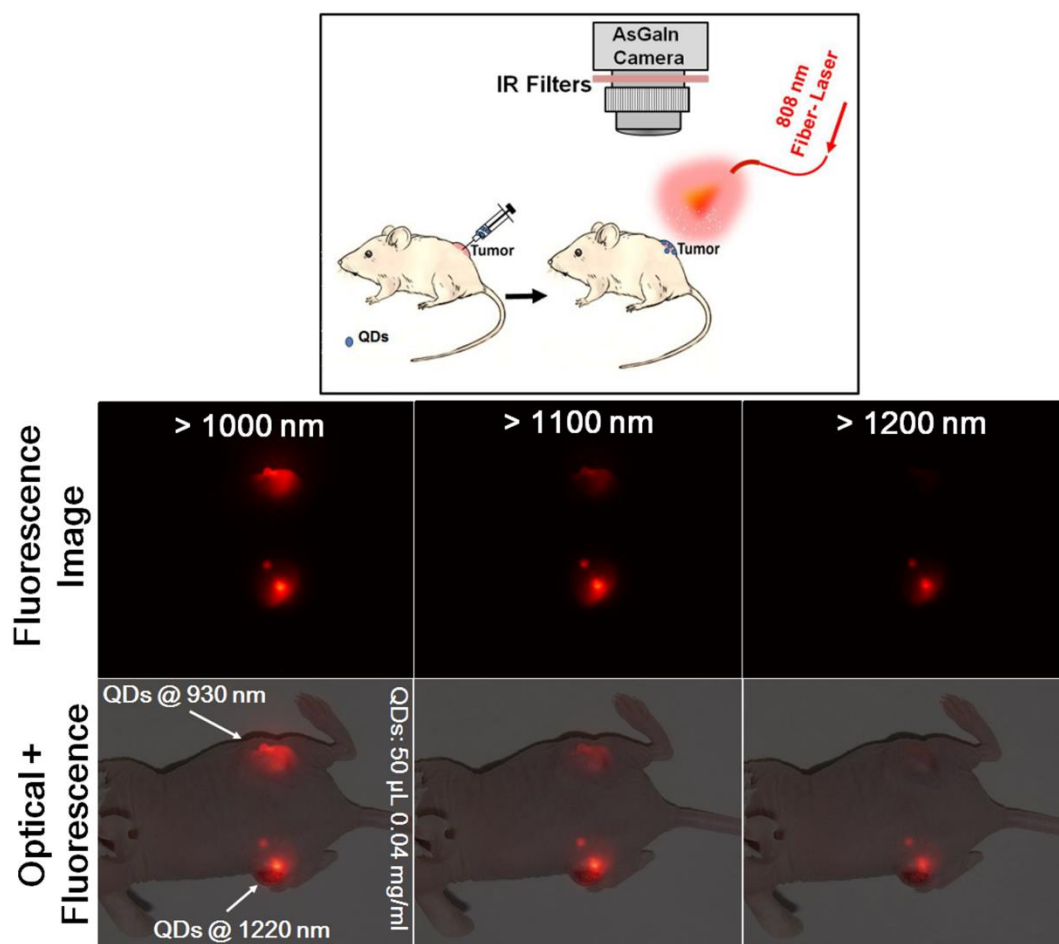


Figure 8. Up: Scheme of the experimental procedure for tumor imaging. 50 μL PBS buffer solutions containing QDs were directly injected into tumors and the estimated depth of the injection was around 2.5 mm. An 808 nm diode laser (0.04 W/cm²

intensity) was used to excite the QDs. NIR luminescence generated by the QDs was recorded with a Peltier-cooled InGaAs camera, capable of real-time image processing in the 900–1700 nm spectral range. *In vivo* experiments: fluorescence (middle) and optical + fluorescence images (bottom) of the mouse after injection with the two differently sized QDs solutions emitting in the first and second biological windows, respectively.

MATERIALS AND METHODS

Materials

Lead chloride (98%), lead acetate trihydrate ($\geq 99.99\%$), bis(trimethylsilyl) sulfide ((TMS)₂S; synthesis grade), trioctylphosphine (TOP) (technical grade, 90%), sulfur (100%), oleylamine (OLA) (technical grade, 70%), cadmium oxide (99%), cardiogreen (IR 125), methanol (anhydrous, 99.8%), octadecene (ODE), mercaptopropyl acid (MPA; $\geq 99.0\%$), 1-methyl-2-pyrrolidinone (NMP; $\geq 99\%$), butylamine (99.5%), Dulbecco's modified Eagle's medium (DMEM), dimethyl sulfoxide (DMSO), 3-(4,5-dimethylthiazol-2-yl)-2,5-diphenyltetrazolium bromide (MTT), phosphorous pentasulfide (99%) and zinc chloride (99.999%) were obtained from Sigma-Aldrich Inc. Hexane, borate buffered saline solution (pH 9.2) traceable to National Institute of Standards and Technology, 10X Tris-EDTA solution (pH 7.6), phosphate buffered saline (PBS; pH 7.4), oleic acid (OA), toluene, and ethanol were purchased from Fisher Scientific Company. All chemicals were used as purchased.

Synthesis of smaller PbS QDs (used for preparing core/shell/shell QDs for the first biological window imaging)

PbS QDs were synthesized following a previously reported method.^{47, 48} In a typical procedure 760 mg of lead acetate trihydrate, 2.4 mL of OA and 15 mL of ODE were added to a three neck round bottom flask. The mixture was heated to 150 °C for 1 h while stirring and purging with a N₂ flow. It was then cooled under vacuum to 130 °C and the N₂ flow was restarted. The mixture of (TMS)₂S and TOP (1:10 ratio by volume; 2 mL in total) was rapidly injected into the flask, quickly cooled to 100 °C and kept at this temperature for approximately 5 min, then quenched with cold water. The PbS QDs were purified by repeated precipitation via centrifugation and redispersion.

Synthesis of larger PbS QDs (used for preparing core/shell/shell QDs for the second biological window imaging)

Larger PbS QDs were synthesized by using OLA as capping ligands.²⁷ In a typical reaction, 10 g of lead chloride and 24 mL of OLA were mixed and heated by oil bath to 160 °C and kept at this temperature for 1 h under the protection of N₂. The solution was then cooled to 120 °C and pumped for 30 min. The flask was then reopened and the N₂ flux was restored. The solution of 115 mg sulfur in 4 mL of OLA at room temperature was quickly injected into the PbCl₂-OLA suspension under vigorous stirring. The reaction cell was quenched with cold water after the reaction was conducted at 100 °C for 4.5 min to obtain PbS QDs with an average diameter 4.6 nm. The QDs were purified by repeated precipitation (by centrifugation) and redispersion. They were finally dispersed in toluene. The concentration of purified PbS QDs in toluene was determined by using the Beer-Lambert's law as we previously reported.⁴³

Synthesis of colloidal PbS/CdS QDs

PbS/CdS core/shell QDs were synthesized following our previously reported method.⁴³ 12 mL of the QD solution with known concentration was mixed with Cd-solution for the growth of the CdS shell. To prepare the Cd precursor solution, 3 g of cadmium oxide, 15 mL of OA and 20 mL of ODE were heated in a separate flask to 200-250 °C using an oil bath until the solution turned colorless. The solution was cooled to 100 °C and degassed under vacuum for 30 min. The temperature was further decreased to 20 °C and 12 mL of PbS QD dispersion was added via syringe. Then, 20 mL of this mixture solution was introduced into a 35 mL reaction tube, and then reacted in a microwave reactor (Discover; CEM Corporation) at 100 °C for different amounts of time to obtain CdS shells of different thicknesses. The PbS/CdS QDs were purified by repeated precipitation (by centrifugation) and redispersion.

Synthesis of water dispersible PbS/CdS/ZnS QDs

PbS/CdS/ZnS core/shell/shell QDs with MPA as the capping ligand were prepared following our very recently developed procedure.⁴⁶ Coating the PbS/CdS QDs with a ZnS shell and replacing OA by MPA was achieved simultaneously. In a typical reaction, 0.045 mmol phosphorous pentasulfide, 0.4 mL MPA and 0.3 mL butylamine were heated at 110 °C for 20 minutes in 10 mL NMP in a sealed vial to dissolve the sulfide. In a separate vial, 0.51 mmol zinc chloride, 0.4 mL MPA and 0.3 mL butylamine were mixed in 10 mL NMP and heated to dissolve zinc chloride in the same way. After cooling down to room temperature, 0.007 g of OLA-capped PbS/CdS QDs were dispersed in the phosphorous pentasulfide solution, and then mixed with

the zinc chloride solution. The mixture was heated at 70 °C for different amounts of time in the microwave reactor, yielding the MPA-capped PbS/CdS/ZnS core/shell/shell QDs. The PbS/CdS/ZnS core/shell/shell QDs were then purified by solvent extraction and ultrafiltration and eventually dispersed in PBS solution with a pH value of 7.5.

Structural and Optical Characterizations

Transmission electron microscopy (TEM) images were obtained using a JEOL 2100F microscope. Absorption spectra were acquired with a Cary 5000 ultraviolet-visible-NIR spectrophotometer (Varian) with a scan speed of 600 nm/min. Fluorescence spectra were taken with a Fluorolog®-3 system (Horiba Jobin Yvon) using a photomultiplier tube detector or a charge coupled device detector. The QY of 930 nm emitting PbS/CdS/ZnS QDs was measured by using dye IR-125 as a reference and the QY of 1220 nm emitting PbS/CdS/ZnS QDs was measured by using dye IR-26 as a reference. The photostability of PbS/CdS/ZnS QDs dispersed in PBS buffer was tested by placing them under continuous illumination with a 4 W UV lamp (115 V, 60 Hz, Model 22-UV, Optical Engineering, UV light Inc.). The NIR luminescence image of 930 nm emitting PbS/CdS/ZnS QDs was obtained under 635 nm excitation with a silicon chip camera (Point Grey) equipped with a 785 long pass filter (Chroma).

The contents of Pb, Cd and Zn elements in the core/shell/shell QDs were characterized by an Inductively Coupled Plasma-Optical Emission Spectrometer (ICP-OES; Agilent Technologie, 5100). Basically, PbS/CdS/ZnS core/shell/shell QDs were first dried in vacuum and then completely dissolved by nitric acid to make

aqueous solution for ICP-OES measurements. Each sample was measured five times. The PL lifetimes of PbS in toluene and PbS/CdS/ZnS QDs in water were measured using a pulsed laser diode of 440 nm, a photomultiplier tube detector, and a fast multichannel scaler mode in the Fluorolog-3 system. PL decay curves were fit with a typical biexponential function. Average lifetime (τ) was calculated from two lifetime components, τ_1 and τ_2 , by using the following equation:

$$\tau = (B_1\tau_1^2 + B_2\tau_2^2) / (B_1\tau_1 + B_2\tau_2),$$

where B_1 and B_2 represent the relative amplitude of τ_1 and τ_2 , respectively, and were also obtained from the fitting of the biexponential function. The error on τ was obtained through differentiation of the above definition and expressed as a function of the uncertainty on the fitting parameters B_1 , B_2 , τ_1 , and τ_2 . These uncertainties were calculated automatically from the software (DAS6 Fluorescence Decay Analysis).

Cell culture and viability assays

HeLa cells were plated at 5×10^5 cells/well into a 96-well plate and incubated for 24 h in DMEM (100 μ L) containing 10% fetal bovine serum (FBS). They were mixed with aliquots of QD dispersions in PBS to adjust the concentration of QDs in DMEM media at (1, 3, 5, and 50 nM). Blank controls without QDs, only with cells themselves, ran simultaneously. Cell viability was measured using the CellTiter 96 Non-Radioactive Cell Proliferation Assay Kit (MTT, Promega), according to the manufacturer's instruction. Briefly, MTT solution (15 μ L) was added into each well. After 24 h incubation, the medium containing unreacted MTT was carefully removed. DMSO (100 μ L) was added into each well in order to dissolve the formed formazan

blue crystals, and then the absorbance at $\lambda = 570$ nm was recorded using a Powerwave HT Microplate Reader (Bio-Tek). Each concentration was 12-replicated. Cell viability was calculated as the percentage ratio.

In vivo tumor fluorescence imaging

For the animal experiments, we used six female athymic nude mice (Harlan, Holand) aged 7 weeks. The animals were subcutaneously inoculated in both flanks with 10×10^6 MDA-MB-231 cells per flank in a volume of 200 μ l of PBS to generate the human tumor xenografts. When the estimated tumor volume reached 90 mm³, we proceeded to carry out imaging experiment. For the imaging, the mice were anesthetized with 2% isoflurane and 50 μ L PBS solution containing PbS/CdS/ZnS QDs (0.2 mg/mL) was injected into each tumor. The tumors were then irradiated with an 808 nm laser diode (LIMO) at a power density of 0.04 W/cm² and NIR fluorescence images were acquired by using an InGaAs camera (XEva1.7-320) with enhanced sensitivity in the 1000-1700 nm spectral range. A long pass filter with cut-off wavelength at 850 nm was used to remove the 808 nm pump background. The exposure time for all the images shown in the paper was shorter than 1 ms. All the experimental procedures with animals were carried out in compliance with the 2010/63/UE European guideline and were approved by the Ethics Committee from Universidad Autónoma de Madrid (CEIT) in the frame of the project FIS-MAT2013-47395-C4-1-R supported by the Spanish Ministerio de Economía y Competitividad.

ASSOCIATED CONTENT

Supporting Information. Optical characterization, decay time and ICP-OES results.

AUTHOR INFORMATION

Corresponding Author

* Fiorenzo Vetrone, E-mail: fiorenzo.vetrone@emt.inrs.ca;
Tel: (514) 228-6847; Fax: (450) 929-8102

* Daniel Jaque, E-mail: daniel.jaque@uam.es

* Dongling Ma, E-mail: ma@emt.inrs.ca;
Tel: (514) 228-6920; Fax: (450) 929-8102

Acknowledgement

This work was supported by the funds from the Natural Sciences and Engineering Research Council of Canada, Fonds de la recherche sur la nature et les technologies and strategic networks “Le Centre québécois sur les matériaux fonctionnels” and “Plasma-Québec”. F.R. greatly appreciates the financial support from the Merit Scholarship Program for Foreign Students from the Ministère de l'Éducation, du Loisir et du Sport du Québec. B.R. acknowledges support from Universidad Autónoma de Madrid through an FPI grant. A.B. thanks the Canadian Institutes of Health Research and the Breast Cancer Society of Canada (CIHR-BCSC), for postdoctoral funding granted to him through an Eileen Iwanicki Fellowship in Breast Cancer Imaging.

References

1. Siegel, R. L.; Miller, K. D.; Jemal, A. Cancer statistics, 2015. *CA: a cancer journal for clinicians* **2015**, 65, 5-29.
2. Ferlay, J.; Soerjomataram, I.; Dikshit, R.; Eser, S.; Mathers, C.; Rebelo, M.; Parkin, D. M.; Forman, D.; Bray, F. Cancer incidence and mortality worldwide: sources, methods and major patterns in GLOBOCAN 2012. *International Journal of Cancer* **2015**, 136, E359-E386.
3. Wang, L. V.; Wu, H.-i. *Biomedical optics: principles and imaging*. John Wiley & Sons: 2012.
4. Wang, L. V.; Hu, S. Photoacoustic tomography: in vivo imaging from organelles to organs. *Science* **2012**, 335, 1458-1462.

5. Hong, G.; Tabakman, S. M.; Welsher, K.; Chen, Z.; Robinson, J. T.; Wang, H.; Zhang, B.; Dai, H. Near-Infrared-Fluorescence-Enhanced Molecular Imaging of Live Cells on Gold Substrates. *Angewandte Chemie International Edition* **2011**, 50, 4644-4648.
6. Del Rosal, B.; Villa, I.; Jaque, D.; Sanz - Rodríguez, F. In vivo autofluorescence in the biological windows: the role of pigmentation. *Journal of biophotonics* **2015**, DOI 10.1002/jbio.201500271.
7. Smith, A. M.; Mancini, M. C.; Nie, S. Bioimaging: second window for in vivo imaging. *Nature Nanotechnology* **2009**, 4, 710-711.
8. Welsher, K.; Liu, Z.; Darancioglu, D.; Dai, H. Selective probing and imaging of cells with single walled carbon nanotubes as near-infrared fluorescent molecules. *Nano Letters* **2008**, 8, 586-590.
9. Liu, Z.; Tabakman, S.; Welsher, K.; Dai, H. Carbon nanotubes in biology and medicine: in vitro and in vivo detection, imaging and drug delivery. *Nano Research* **2009**, 2, 85-120.
10. Villa, I.; Vedda, A.; Cantarelli, I. X.; Pedroni, M.; Piccinelli, F.; Bettinelli, M.; Speghini, A.; Quintanilla, M.; Vetrone, F.; Rocha, U. 1.3 μm emitting $\text{SrF}_2: \text{Nd}^{3+}$ nanoparticles for high contrast in vivo imaging in the second biological window. *Nano Research* **2015**, 8, 649-665.
11. Wang, Y.-F.; Liu, G.-Y.; Sun, L.-D.; Xiao, J.-W.; Zhou, J.-C.; Yan, C.-H. Nd^{3+} -sensitized upconversion nanophosphors: Efficient in vivo bioimaging probes with minimized heating effect. *ACS Nano* **2013**, 7, 7200-7206.
12. Zhan, Q.; Qian, J.; Liang, H.; Somesfalean, G.; Wang, D.; He, S.; Zhang, Z.; Andersson-Engels, S. Using 915 nm laser excited $\text{Tm}^{3+}/\text{Er}^{3+}/\text{Ho}^{3+}$ -doped NaYbF_4 upconversion nanoparticles for in vitro and deeper in vivo bioimaging without overheating irradiation. *ACS Nano* **2011**, 5, 3744-3757.
13. Hemmer, E.; Benayas, A.; L'égaré F.; Vetrone, F. Exploiting the biological windows: current perspectives on fluorescent bioprobes emitting above 1000 nm. *Nanoscale Horizons* 2016, 1, 168-184.
14. Du, Y.; Xu, B.; Fu, T.; Cai, M.; Li, F.; Zhang, Y.; Wang, Q. Near-infrared photoluminescent Ag_2S quantum dots from a single source precursor. *Journal of the American Chemical Society* **2010**, 132, 1470-1471.
15. Shen, S.; Zhang, Y.; Peng, L.; Du, Y.; Wang, Q. Matchstick-Shaped Ag_2S - ZnS Heteronanostructures Preserving both UV/Blue and Near - Infrared Photoluminescence. *Angewandte Chemie International Edition* **2011**, 50, 7115-7118.
16. Bakueva, L.; Gorelikov, I.; Musikhin, S.; Zhao, X. S.; Sargent, E. H.; Kumacheva, E. PbS quantum dots with stable efficient luminescence in the near-IR spectral range. *Advanced Materials* **2004**, 16, 926-929.
17. Peng, X.; Chen, H.; Draney, D. R.; Volcheck, W.; Schutz-Geschwender, A.; Olive, D. M. A nonfluorescent, broad-range quencher dye for Förster resonance energy transfer assays. *Analytical Biochemistry* **2009**, 388, 220-228.
18. Licha, K.; Riefke, B.; Ntziachristos, V.; Becker, A.; Chance, B.; Semmler, W. Hydrophilic Cyanine Dyes as Contrast Agents for Near - infrared Tumor Imaging: Synthesis, Photophysical Properties and Spectroscopic In vivo Characterization. *Photochemistry and Photobiology* **2000**, 72, 392-398.
19. Welsher, K.; Liu, Z.; Sherlock, S. P.; Robinson, J. T.; Chen, Z.; Darancioglu, D.; Dai, H. A route to brightly fluorescent carbon nanotubes for near-infrared imaging in mice. *Nature Nanotechnology* **2009**, 4, 773-780.
20. Resch-Genger, U.; Grabolle, M.; Cavaliere-Jaricot, S.; Nitschke, R.; Nann, T. Quantum dots versus organic dyes as fluorescent labels. *Nature Methods* **2008**, 5, 763-775.
21. Warheit, D. B.; Laurence, B. R.; Reed, K. L.; Roach, D. H.; Reynolds, G. A.; Webb, T. R.

Comparative pulmonary toxicity assessment of single-wall carbon nanotubes in rats. *Toxicological Sciences* **2004**, *77*, 117-125.

22. Lam, C.-W.; James, J. T.; McCluskey, R.; Hunter, R. L. Pulmonary toxicity of single-wall carbon nanotubes in mice 7 and 90 days after intratracheal instillation. *Toxicological Sciences* **2004**, *77*, 126-134.

23. Yong, K. T.; Roy, I.; Ding, H.; Bergey, E. J.; Prasad, P. N. Biocompatible Near-Infrared Quantum Dots as Ultrasensitive Probes for Long-Term in vivo Imaging Applications. *Small* **2009**, *5*, 1997-2004.

24. Allen, P. M.; Liu, W.; Chauhan, V. P.; Lee, J.; Ting, A. Y.; Fukumura, D.; Jain, R. K.; Bawendi, M. G. InAs (ZnCdS) quantum dots optimized for biological imaging in the near-infrared. *Journal of the American Chemical Society* **2009**, *132*, 470-471.

25. Bharali, D. J.; Lucey, D. W.; Jayakumar, H.; Pudavar, H. E.; Prasad, P. N. Folate-receptor-mediated delivery of InP quantum dots for bioimaging using confocal and two-photon microscopy. *Journal of the American Chemical Society* **2005**, *127*, 11364-11371.

26. Pietryga, J. M.; Schaller, R. D.; Werder, D.; Stewart, M. H.; Klimov, V. I.; Hollingsworth, J. A. Pushing the band gap envelope: mid-infrared emitting colloidal PbSe quantum dots. *Journal of the American Chemical Society* **2004**, *126*, 11752-11753.

27. Cademartiri, L.; Montanari, E.; Calestani, G.; Migliori, A.; Guagliardi, A.; Ozin, G. A. Size-dependent extinction coefficients of PbS quantum dots. *Journal of the American Chemical Society* **2006**, *128*, 10337-10346.

28. Gu, Y.-P.; Cui, R.; Zhang, Z.-L.; Xie, Z.-X.; Pang, D.-W. Ultrasmall near-infrared Ag₂Se quantum dots with tunable fluorescence for in vivo imaging. *Journal of the American Chemical Society* **2011**, *134*, 79-82.

29. Hong, G.; Robinson, J. T.; Zhang, Y.; Diao, S.; Antaris, A. L.; Wang, Q.; Dai, H. In Vivo Fluorescence Imaging with Ag₂S Quantum Dots in the Second Near-Infrared Region. *Angewandte Chemie* **2012**, *124*, 9956-9959.

30. Jiang, P.; Zhu, C.-N.; Zhang, Z.-L.; Tian, Z.-Q.; Pang, D.-W. Water-soluble Ag₂S quantum dots for near-infrared fluorescence imaging in vivo. *Biomaterials* **2012**, *33*, 5130-5135.

31. Sun, L.; Choi, J. J.; Stachnik, D.; Bartnik, A. C.; Hyun, B.-R.; Malliaras, G. G.; Hanrath, T.; Wise, F. W. Bright infrared quantum-dot light-emitting diodes through inter-dot spacing control. *Nature Nanotechnology* **2012**, *7*, 369-373.

32. Zhao, N.; Osedach, T. P.; Chang, L.-Y.; Geyer, S. M.; Wanger, D.; Binda, M. T.; Arango, A. C.; Bawendi, M. G.; Bulovic, V. Colloidal PbS quantum dot solar cells with high fill factor. *Acs Nano* **2010**, *4*, 3743-3752.

33. Hu, R.; Law, W.-C.; Lin, G.; Ye, L.; Liu, J.; Liu, J.; Reynolds, J. L.; Yong, K.-T. PEGylated phospholipid micelle-encapsulated near-infrared PbS quantum dots for in vitro and in vivo bioimaging. *Theranostics* **2012**, *2*, 723.

34. Tan, T. T.; Selvan, S. T.; Zhao, L.; Gao, S.; Ying, J. Y. Size control, shape evolution, and silica coating of near-infrared-emitting PbSe quantum dots. *Chemistry of Materials* **2007**, *19*, 3112-3117.

35. Pichaandi, J.; Abel, K. A.; Johnson, N. J.; van Veggel, F. C. Long-Term Colloidal Stability and Photoluminescence Retention of Lead-Based Quantum Dots in Saline Buffers and Biological Media through Surface Modification. *Chemistry of Materials* **2013**, *25*, 2035-2044.

36. Bagalkot, V.; Zhang, L.; Levy-Nissenbaum, E.; Jon, S.; Kantoff, P. W.; Langer, R.; Farokhzad, O. C. Quantum dot-aptamer conjugates for synchronous cancer imaging, therapy, and sensing of drug delivery based on bi-fluorescence resonance energy transfer. *Nano Letters* **2007**, *7*, 3065-3070.

37. Yu, W. W.; Falkner, J. C.; Shih, B. S.; Colvin, V. L. Preparation and characterization of monodisperse PbSe semiconductor nanocrystals in a noncoordinating solvent. *Chemistry of Materials* **2004**, *16*, 3318-3322.
38. Hinds, S.; Myrskog, S.; Levina, L.; Koleilat, G.; Yang, J.; Kelley, S. O.; Sargent, E. H. NIR-emitting colloidal quantum dots having 26% luminescence quantum yield in buffer solution. *Journal of the American Chemical Society* **2007**, *129*, 7218-7219.
39. Chen, G.; Desinan, S.; Nechache, R.; Rosei, R.; Rosei, F.; Ma, D. Bifunctional catalytic/magnetic Ni@Ru core-shell nanoparticles. *Chem Commun* **2011**, *47*, 6308-6310.
40. Derfus, A. M.; Chan, W. C.; Bhatia, S. N. Probing the cytotoxicity of semiconductor quantum dots. *Nano Letters* **2004**, *4*, 11-18.
41. Kirchner, C.; Liedl, T.; Kudera, S.; Pellegrino, T.; Muñoz Javier, A.; Gaub, H. E.; Stölzle, S.; Fertig, N.; Parak, W. J. Cytotoxicity of colloidal CdSe and CdSe/ZnS nanoparticles. *Nano letters* **2005**, *5*, 331-338.
42. Ye, L.; Yong, K.-T.; Liu, L.; Roy, I.; Hu, R.; Zhu, J.; Cai, H.; Law, W.-C.; Liu, J.; Wang, K. A pilot study in non-human primates shows no adverse response to intravenous injection of quantum dots. *Nature Nanotechnology* **2012**, *7*, 453-458.
43. Ren, F.; Zhao, H.; Vetrone, F.; Ma, D. Microwave-assisted cation exchange toward synthesis of near-infrared emitting PbS/CdS core/shell quantum dots with significantly improved quantum yields through a uniform growth path. *Nanoscale* **2013**, *5*, 7800-7804.
44. Zhao, H.; Chaker, M.; Ma, D. Effect of CdS shell thickness on the optical properties of water-soluble, amphiphilic polymer-encapsulated PbS/CdS core/shell quantum dots. *Journal of Materials Chemistry* **2011**, *21*, 17483-17491.
45. Zhao, H.; Wang, D.; Zhang, T.; Chaker, M.; Ma, D. Two-step synthesis of high-quality water-soluble near-infrared emitting quantum dots via amphiphilic polymers. *Chem Commun* **2010**, *46*, 5301-5303.
46. Benayas, A.; Ren, F.; Carrasco, E.; Marzal, V.; del Rosal, B.; Gonfa, B. A.; Juarranz, Á.; Sanz - Rodríguez, F.; Jaque, D.; García-Solé J. PbS/CdS/ZnS Quantum Dots: A Multifunctional Platform for In Vivo Near-Infrared Low-Dose Fluorescence Imaging. *Advanced Functional Materials* **2015**, *25*, 6650-6659.
47. Hines, M. A.; Scholes, G. D. Colloidal PbS nanocrystals with size-tunable near-infrared emission: observation of post-synthesis self-narrowing of the particle size distribution. *Advanced Materials* **2003**, *15*, 1844-1849.
48. Zhang, T.; Zhao, H.; Riabinina, D.; Chaker, M.; Ma, D. Concentration-dependent photoinduced photoluminescence enhancement in colloidal PbS quantum dot solution. *The Journal of Physical Chemistry C* **2010**, *114*, 10153-10159.
49. Moreels, I.; Lambert, K.; Smeets, D.; De Muynck, D.; Nollet, T.; Martins, J. C.; Vanhaecke, F.; Vantomme, A.; Delerue, C.; Allan, G. Size-dependent optical properties of colloidal PbS quantum dots. *ACS Nano* **2009**, *3*, 3023-3030.
50. Moreels, I.; Justo, Y.; De Geyter, B.; Hastraete, K.; Martins, J. C.; Hens, Z. Size-tunable, bright, and stable PbS quantum dots: a surface chemistry study. *Acs Nano* **2011**, *5*, 2004-2012.
51. Uyeda, H. T.; Medintz, I. L.; Jaiswal, J. K.; Simon, S. M.; Mattoussi, H. Synthesis of compact multidentate ligands to prepare stable hydrophilic quantum dot fluorophores. *Journal of the American Chemical Society* **2005**, *127*, 3870-3878.
52. Dubois, F.; Mahler, B.; Dubertret, B.; Doris, E.; Mioskowski, C. A versatile strategy for quantum

- dot ligand exchange. *Journal of the American Chemical Society* **2007**, 129, 482-483.
53. Zhao, H.; Wang, D.; Chaker, M.; Ma, D. Effect of different types of surface ligands on the structure and optical property of water-soluble PbS quantum dots encapsulated by amphiphilic polymers. *The Journal of Physical Chemistry C* **2011**, 115, 1620-1626.
54. Kovalenko, M. V.; Schaller, R. D.; Jarzab, D.; Loi, M. A.; Talapin, D. V. Inorganically Functionalized PbS-CdS Colloidal Nanocrystals: Integration into Amorphous Chalcogenide Glass and Luminescent Properties. *Journal of the American Chemical Society* **2012**, 134, 2457-2460.
55. Zhao, H.; Chaker, M.; Wu, N.; Ma, D. Towards controlled synthesis and better understanding of highly luminescent PbS/CdS core/shell quantum dots. *J. Mater. Chem.* **2011**, 21, 8898-8904.
56. Zhao, H.; Wang, D.; Zhang, T.; Chaker, M.; Ma, D. Two-step synthesis of high-quality water-soluble near-infrared emitting quantum dots via amphiphilic polymers. *Chem. Commun.* **2010**, 46, 5301-5303.
57. Smith, A. M.; Duan, H.; Rhyner, M. N.; Ruan, G.; Nie, S. A systematic examination of surface coatings on the optical and chemical properties of semiconductor quantum dots. *Physical Chemistry Chemical Physics* **2006**, 8, 3895-3903.
58. Zhang, Y.; Hong, G.; Zhang, Y.; Chen, G.; Li, F.; Dai, H.; Wang, Q. Ag₂S quantum dot: a bright and biocompatible fluorescent nanoprobe in the second near-infrared window. *ACS Nano* **2012**, 6, 3695-3702.
59. Gerion, D.; Pinaud, F.; Williams, S. C.; Parak, W. J.; Zanchet, D.; Weiss, S.; Alivisatos, A. P. Synthesis and properties of biocompatible water-soluble silica-coated CdSe/ZnS semiconductor quantum dots. *The Journal of Physical Chemistry B* **2001**, 105, 8861-8871.
60. Bruchez, M.; Moronne, M.; Gin, P.; Weiss, S.; Alivisatos, A. P. Semiconductor nanocrystals as fluorescent biological labels. *Science* **1998**, 281, 2013-2016.
61. Qadri, S.; Skelton, E.; Hsu, D.; Dinsmore, A.; Yang, J.; Gray, H.; Ratna, B. Size-induced transition-temperature reduction in nanoparticles of ZnS. *Physical Review B* **1999**, 60, 9191.
62. Talapin, D. V.; Mekis, I.; Götzinger, S.; Kornowski, A.; Benson, O.; Weller, H. CdSe/CdS/ZnS and CdSe/ZnSe/ZnS core-shell-shell nanocrystals. *The Journal of Physical Chemistry B* **2004**, 108, 18826-18831.
63. Dubertret, B.; Skourides, P.; Norris, D. J.; Noireaux, V.; Brivanlou, A. H.; Libchaber, A. In vivo imaging of quantum dots encapsulated in phospholipid micelles. *Science* **2002**, 298, 1759-1762.
64. Moghimi, S. M.; Hunter, A. C.; Murray, J. C. Nanomedicine: current status and future prospects. *The FASEB Journal* **2005**, 19, 311-330.
65. Gao, X.; Cui, Y.; Levenson, R. M.; Chung, L. W.; Nie, S. In vivo cancer targeting and imaging with semiconductor quantum dots. *Nature Biotechnology* **2004**, 22, 969-976.
66. Choi, H.; Ko, J.-H.; Kim, Y.-H.; Jeong, S. Steric-hindrance-driven shape transition in PbS quantum dots: understanding size-dependent stability. *Journal of the American Chemical Society* **2013**, 135, 5278-5281.
67. Ma, J.; Chen, J.-Y.; Zhang, Y.; Wang, P.-N.; Guo, J.; Yang, W.-L.; Wang, C.-C. Photochemical instability of thiol-capped CdTe quantum dots in aqueous solution and living cells: process and mechanism. *The Journal of Physical Chemistry B* **2007**, 111, 12012-12016.
68. He, Y.; Lu, H.-T.; Sai, L.-M.; Su, Y.-Y.; Hu, M.; Fan, C.-H.; Huang, W.; Wang, L.-H. Microwave synthesis of water-dispersed CdTe/CdS/ZnS core-shell-shell quantum dots with excellent photostability and biocompatibility. *Advanced Materials* **2008**, 20, 3416-3421.
69. Biju, V.; Kanemoto, R.; Matsumoto, Y.; Ishii, S.; Nakanishi, S.; Itoh, T.; Baba, Y.; Ishikawa, M.

Photoinduced photoluminescence variations of CdSe quantum dots in polymer solutions. *The Journal of Physical Chemistry C* **2007**, 111, 7924-7932.

70. Tang, J.; Brzozowski, L.; Barkhouse, D. A. R.; Wang, X.; Debnath, R.; Wolowiec, R.; Palmiano, E.; Levina, L.; Pattantyus-Abraham, A. G.; Jamakosmanovic, D. Quantum dot photovoltaics in the extreme quantum confinement regime: the surface-chemical origins of exceptional air-and light-stability. *ACS Nano* **2010**, 4, 869-878.

71. Eadington, P. The oxidation of lead sulphide in aqueous suspension. University of London, 1966.

72. Duan, H.; Nie, S. Cell-penetrating quantum dots based on multivalent and endosome-disrupting surface coatings. *Journal of the American Chemical Society* **2007**, 129, 3333-3338.

73. Ryman-Rasmussen, J. P.; Riviere, J. E.; Monteiro-Riviere, N. A. Surface coatings determine cytotoxicity and irritation potential of quantum dot nanoparticles in epidermal keratinocytes. *Journal of Investigative Dermatology* **2007**, 127, 143-153.

74. Fischer, D.; Li, Y.; Ahlemeyer, B.; Krieglstein, J.; Kissel, T. In vitro cytotoxicity testing of polycations: influence of polymer structure on cell viability and hemolysis. *Biomaterials* **2003**, 24, 1121-1131.

75. Benayas, A.; Ren, F.; Carrasco, E.; Marzal, V.; del Rosal, B.; Gonfa, B. A.; Juarranz, Á.; Sanz - Rodríguez, F.; Jaque, D.; Garc á - Sol é J. PbS/CdS/ZnS Quantum Dots: A Multifunctional Platform for In Vivo Near-Infrared Low-Dose Fluorescence Imaging. *Advanced Functional Materials* **2015**, 25, 6650-6659.

76. Tang, Y.; Han, S.; Liu, H.; Chen, X.; Huang, L.; Li, X.; Zhang, J. The role of surface chemistry in determining in vivo biodistribution and toxicity of CdSe/ZnS core-shell quantum dots. *Biomaterials* **2013**, 34, 8741-8755.

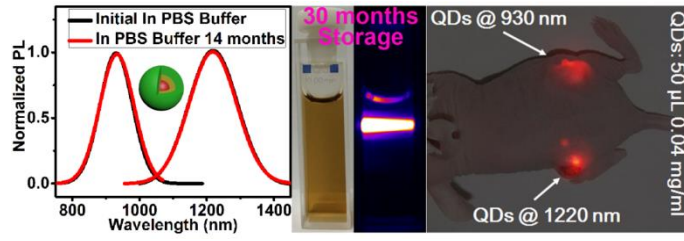
77. Mortensen, L. J.; Oberdörster, G.; Pentland, A. P.; DeLouise, L. A. In vivo skin penetration of quantum dot nanoparticles in the murine model: the effect of UVR. *Nano letters* **2008**, 8, 2779-2787.

78. Maestro, L.; Ramirez-Hernandez, J.; Bogdan, N.; Capobianco, J.; Vetrone, F.; Sol é J. G.; Jaque, D. Deep tissue bio-imaging using two-photon excited CdTe fluorescent quantum dots working within the biological window. *Nanoscale* **2012**, 4, 298-302.

79. Welsher, K.; Sherlock, S. P.; Dai, H. Deep-tissue anatomical imaging of mice using carbon nanotube fluorophores in the second near-infrared window. *Proceedings of the National Academy of Sciences* **2011**, 108, 8943-8948.

80. Naczynski, D.; Tan, M.; Zevon, M.; Wall, B.; Kohl, J.; Kulesa, A.; Chen, S.; Roth, C.; Riman, R.; Moghe, P. Rare-earth-doped biological composites as in vivo shortwave infrared reporters. *Nature Communications* **2013**, 4.

TOC



Supporting information for

Development and Investigation of Ultrastable PbS/CdS/ZnS Quantum Dots for Near-Infrared Tumor Imaging

Fuqiang Ren,[†] Blanca del Rosal,[‡] So Young An,[§] Fan Yang,[†] Elisa Carrasco,[‡] Antonio Benayas,[†] Jung Kwon Oh,[§] Daniel Jaque,^{*,‡} Ángeles Juarranz de la Fuente,[‡] Fiorenzo Vetrone,^{*,†,∇} Dongling Ma^{*,†}

[†] Institut National de la Recherche Scientifique - Énergie, Matériaux et Télécommunications, Université du Québec, 1650 Boul. Lionel-Boulet, Varennes, Québec J3X 1S2, Canada

[‡] Fluorescence Imaging Group, Departamento de Física de Materiales, Facultad de Ciencias, Universidad Autónoma de Madrid, Madrid 28049, Spain.

[§] Department of Chemistry and Biochemistry, Concordia University, Montreal, Quebec H4B 1R6, Canada

[∇] Centre for Self-Assembled Chemical Structures, McGill University, Montreal, Quebec H3A 2K6, Canada

[‡] Grupo de Dermatología Experimental, Instituto Ramón y Cajal de Investigación Sanitaria, IRYCIS, Madrid 28034, Spain

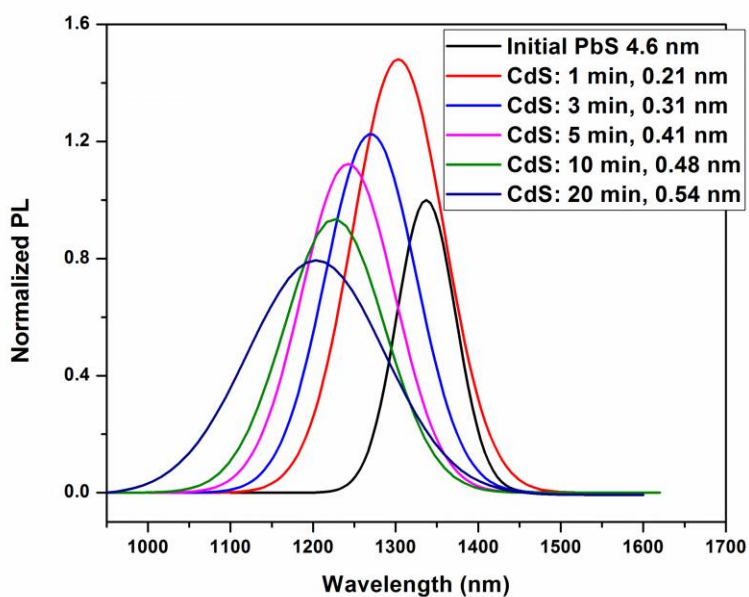


Figure S1. PL spectra of initial PbS QDs (emitting at 1340 nm) and PbS/CdS core/shell QDs in toluene with different CdS shell thicknesses.

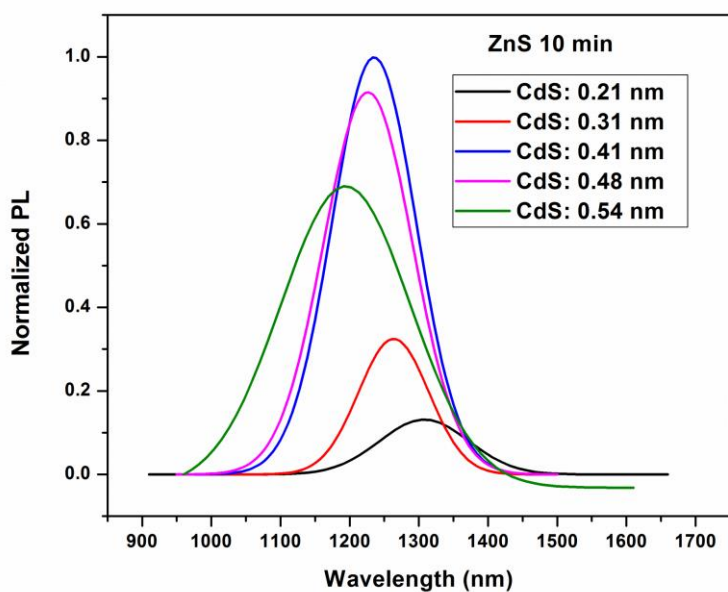


Figure S2. PL spectra of PbS/CdS/ZnS core/shell/shell QDs in PBS buffer with different CdS shell thicknesses (Initial PbS: emitting at 1340 nm).

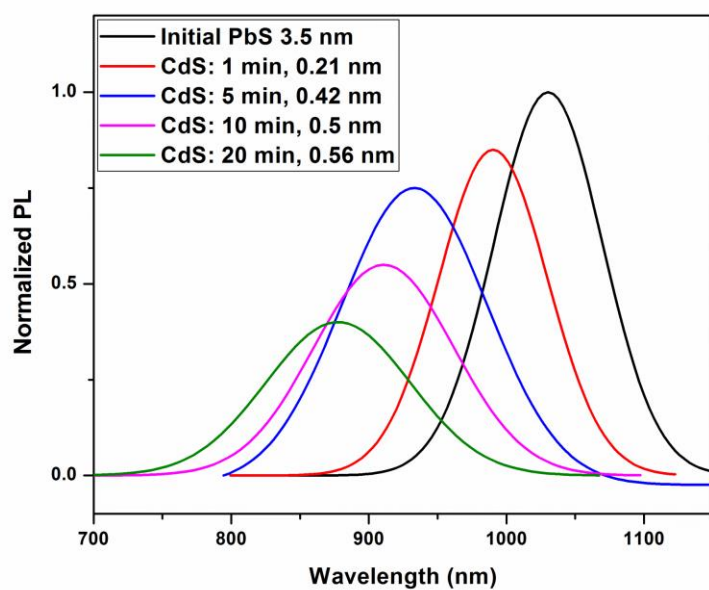


Figure S3. PL spectra of initial PbS QDs (emitting at 1030 nm) and PbS/CdS core/shell QDs in toluene with different CdS shell thicknesses.

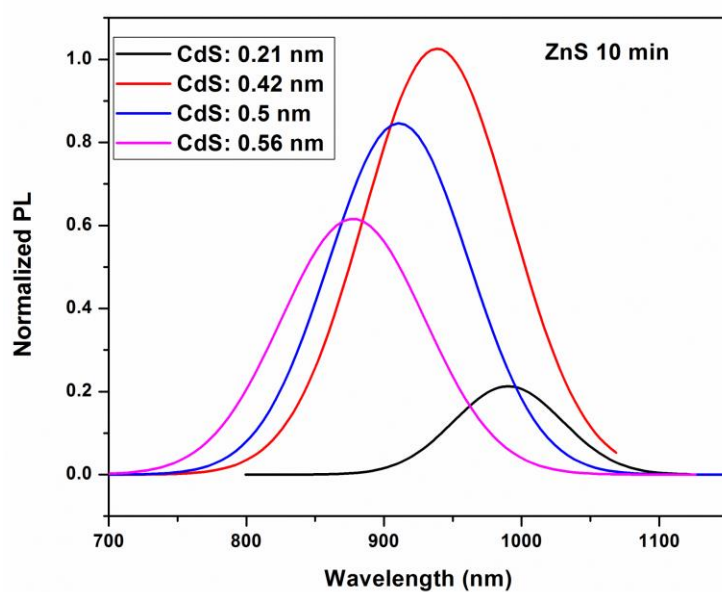


Figure S4. PL spectra of PbS/CdS/ZnS core/shell/shell QDs in PBS buffer with different CdS shell thicknesses (Initial PbS: emitting at 1030 nm).

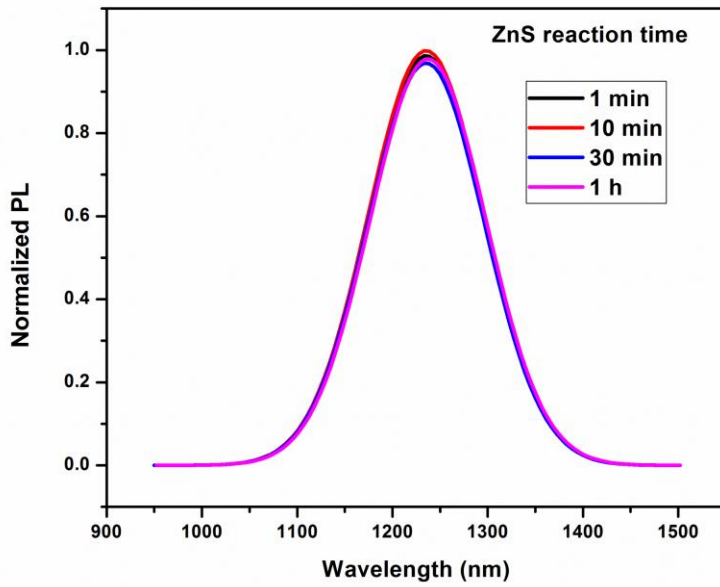


Figure S5. PL spectra of PbS/CdS/ZnS core/shell/shell QDs with different ZnS reaction times (Initial PbS: emitting at 1340 nm; CdS thickness: 0.41 nm).

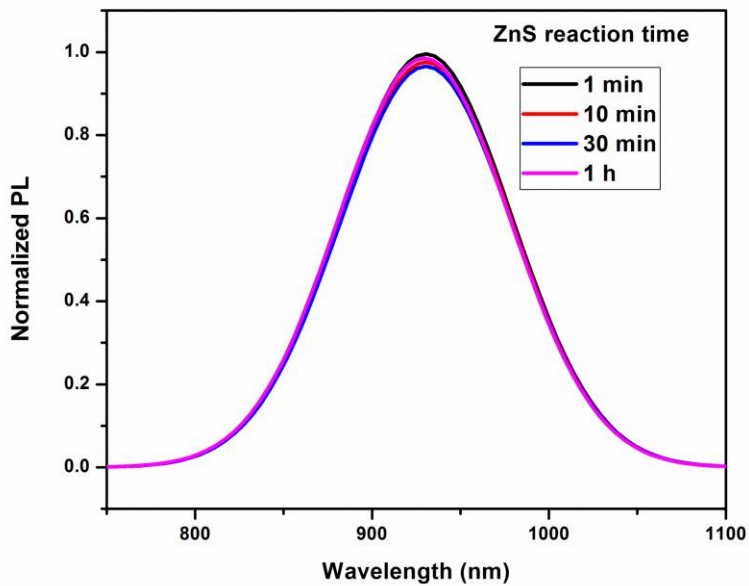


Figure S6. PL spectra of PbS/CdS/ZnS core/shell/shell QDs in PBS buffer with different ZnS reaction times (Initial PbS: emitting at 1030 nm; CdS thickness: 0.42 nm).

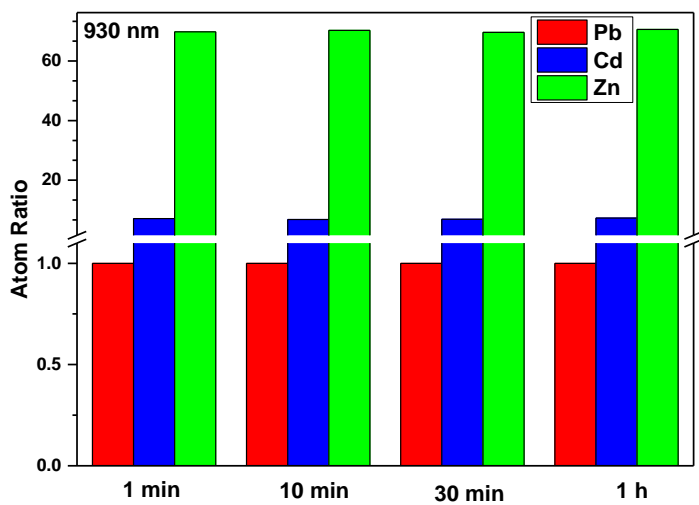


Figure S7. Detailed Pb, Cd and Zn elements atom ratio of 930 nm emitting PbS/CdS/ZnS core/shell/shell QDs obtained by ICP-OES.

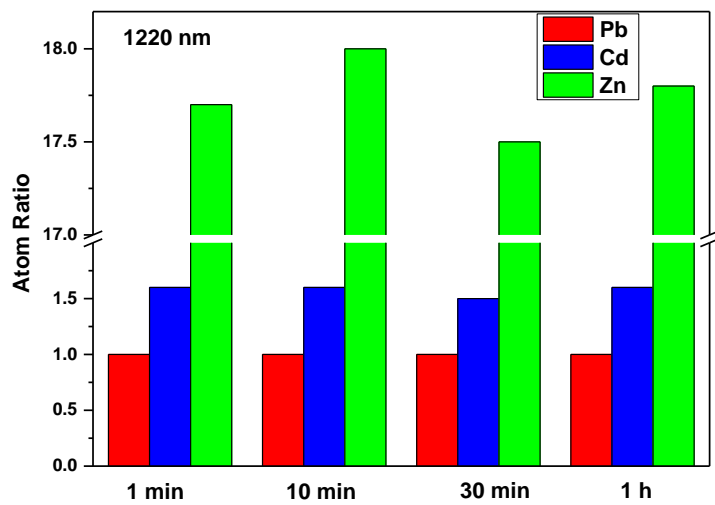


Figure S8. Detailed Pb, Cd and Zn elements atom ratio of 1220 nm emitting PbS/CdS/ZnS core/shell/shell QDs obtained by ICP-OES.

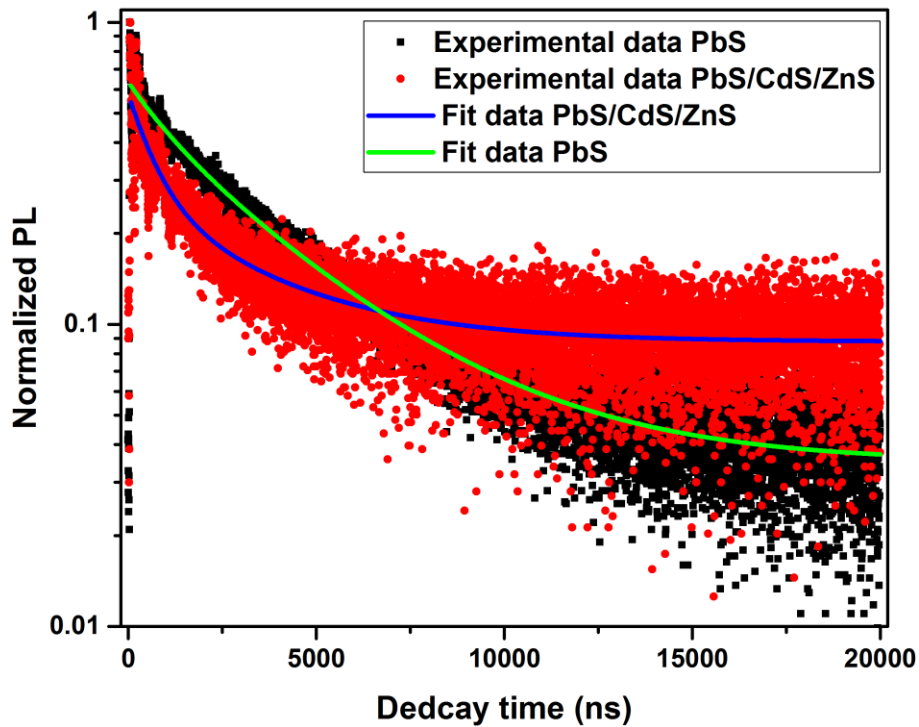


Figure S9. Typical room-temperature PL decay curves of 1030 nm emitting PbS and 930 nm emitting PbS/CdS/ZnS QDs.

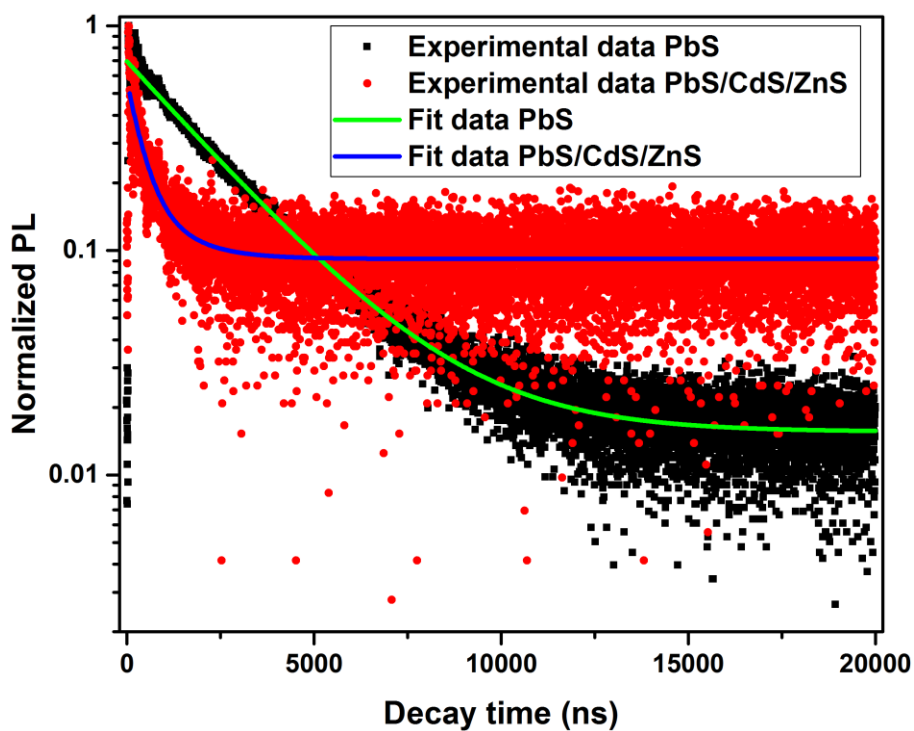


Figure S10. Typical room-temperature PL decay curves of 1340 nm emitting PbS and 1220 nm emitting PbS/CdS/ZnS QDs.

Section IV PbS/CdS/ZnS Quantum Dots: A Multifunctional Platform for In Vivo Near-Infrared Low-Dose Fluorescence Imaging

In this section, we used the PbS/CdS/ZnS core/shell shell QDs as NIR imaging probes to develop a QD-based imaging system. The emission wavelength of the QDs probe lying within the second biological window leads to higher penetration depths because of the low extinction coefficient of biological tissues in this spectral range. Their intense fluorescence emission enables to follow the real-time evolution of QD biodistribution, after low-dose intravenous administration. The system is also capable of acting as a biological nanothermometer, based on the reliable thermal-dependent behavior of the fluorescence signal. The PbS/CdS/ZnS QDs studied here can easily be exploited to obtain thermal mapping of subskin areas in live specimens, an accomplishment of great relevance for early disease detection and also for real-time therapy monitoring.

Advanced Functional Materials 25 (2015) 6650–6659

Cet article a dû être retiré de la version électronique en raison de restrictions liées au droit d'auteur.
Vous pouvez le consulter à l'adresse suivante :
DOI : [10.1002/adfm.201502632](https://doi.org/10.1002/adfm.201502632)

CHAPTER 4 CONCLUSIONS AND PERSPECTIVES

4.1 Conclusions

NIR PbS based QDs have attracted considerable attention due to their unique properties and are currently exploited for various applications in NIR photodetectors, light-emitting diodes, solar cells and biological sensors. Due to the quantum confinement effects, the QDs show a size-dependent bandgap. As a result, the optical properties of QDs can be tuned over a wide spectral region in the NIR range. The synthesis of PbS QDs was advanced largely over the last decade and now QDs with uniform and narrow size distribution can be achieved routinely in many laboratories. However, the quantum efficiency and stability of these QDs need to be further studied and improved. In particular, for QDs that are required to be dispersed in aqueous system, there remain great challenges to overcome.

Due to the large surface-to-volume ratio, the properties of QDs become extremely sensitive to surface characteristics. In order to improve the optical properties of these QDs, great efforts have been undertaken in the past few decades on the surface engineering of QDs. A passivation shell is normally grown over the QDs to form a core/shell structure which in turn improves the optical properties and stability.

Part I is mainly focused on the investigation of the synthesis and optical properties of PbS/CdS core/shell QDs. It is divided into two sections according to different research objects. In Section I, I firstly synthesized a series of different sized PbS QDs by using the traditional hot inject method, then these PbS QDs were coated with a thin

CdS shell to form PbS/CdS core/shell structure by a new microwave-assisted cation exchange approach. The synthesized QDs show a QY as high as 57%, ~1.4 times higher than that of QDs achieved by conventional heating in oil bath. The reaction was successfully scaled up by several times by increasing the initial PbS concentration or by amplifying reaction volume and the as-synthesized core/shell QDs show similarly high QY. In Section II, I report the anomalous size-dependent PL intensity variation of PbS QDs with the formation of a thin CdS shell via the same microwave-assisted cation exchange approach. I attempted to understand this abnormal phenomenon from the perspective of trap density variation and the probability of electrons and holes reaching surface defects. Systematic optical characterizations, including QY measurements as well as dynamic PL and absorption measurements, provided fundamental insights into the exciton dynamics on the relevant time scales from fs to μ s. Ultimately, a model was constructed to show the energy levels and trap states for various sizes.

Part II focuses on the development of water dispersible PbS/CdS/ZnS core/shell/shell QDs and their potential bio-applications. It is divided into two sections, corresponding to the synthesis, optical property and stability of these newly developed core/shell/shell QDs (Section III) and their potential bio-applications (Section IV), respectively. In section III, we report for the first time detailed investigations of the synthesis of NIR, water dispersible, strongly luminescent and highly stable PbS/CdS/ZnS core/shell/shell quantum dots (QDs), their properties in different buffers, their cytotoxicity and further their applications in tumor imaging. In

particular, we focus on the QDs emitting at 930 and 1220 nm, within the first and second biological windows, respectively. These QDs were synthesized via our recently developed microwave-assisted approach to grow a ZnS shell and to simultaneous exchange initial ligand with mercaptopropyl acid on the PbS/CdS core/shell QDs dispersed in an organic phase. These QDs were extremely stable in commonly used biological buffers and remarkably, they could keep their initial morphology, dispersion status and PL in PBS buffer for as long as 14 months, which was the longest time point we investigated with both transmission electron microscopy and PL spectroscopy herein. PL image taken on the 930 nm emitting PbS/CdS/ZnS core/shell/shell QDs revealed that they could still emit strongly after 30-month storage in PBS. Such long term stability of water dispersible QDs is rarely reported in the literature. Their colloidal stability was further investigated by keeping them in high ionic concentration conditions. Their PL intensity didn't show any change for at least 3 weeks at high NaCl concentration up to 400 mM. The QDs also showed excellent photostability and could keep about 80% of their initial PL intensity after 1 h continuous, strong UV illumination. More interestingly, they showed negligible toxicity to cultured cells even at high QDs concentration (50 nM). Given these outstanding properties, the ultrastable and biocompatible QDs were explored for the first time for in vivo, tumor imaging in mice. With one order of magnitude lower QD concentration (0.04 mg/mL), significantly weaker laser intensity (0.04 W/cm² vs ~1 W/cm²) and considerably shorter signal integration time (\leq 1 ms vs several hundreds of ms) as compared to the best reported rare earth doped nanoparticles, the

QDs showed high emission intensity even at injection depth of ~ 2.5 mm, hard to achieve with visible QDs and other NIR PL probes. In Section IV, we have developed a QD-based imaging system based on NIR PbS/CdS/ZnS QDs with minimal noticeable toxicity that, through careful engineering of their emission wavelength, allowed us to obtain fluorescence imaging nanoprobe with optimal penetration depths in biological tissue. Additionally, this new platform exhibited multifunctionality beyond their use as pure imaging nanoprobe. The system is capable of acting as a biological nanothermometer, based on the reliable thermal-dependent behavior of the fluorescence signal. The PbS/CdS/ZnS QDs studied here can easily be exploited to obtain thermal mapping of subskin areas in live specimens, an accomplishment of great relevance for early disease detection and also for real-time therapy monitoring. Moreover, as a result of the intense signal provided by the NIR-emitting QDs, we are able to elucidate the real-time biodistribution of the QDs by means of *in vivo* experiments in live mice.

4.2 Perspectives

I developed a reproducible and controllable microwave-assisted cation exchange approach, for the first time, to quickly synthesize high-quality, NIR emitting PbS/CdS core/shell QDs. These monodisperse QDs show a QY as high as 57%. Meanwhile, the reaction has been successfully scaled up by several times and the as-synthesized core/shell QDs show similarly high QY and uniform size distribution. The stable and optical properties of the PbS/CdS core/shell QDs are largely improved, it is interesting to explore the use of the PbS/CdS QDs in the LED devices.

In the past few decades, the development of low-cost, solution-based synthesis of colloidal QDs have promoted the research of QDs based LEDs. These LEDs exhibit pure and saturated colours with a narrow bandwidth of the electroluminescence peak of 30 nm [97-103]. Emission from the QD-LEDs can easily be tuned by varying the size or the composition of the QDs without changing their processing properties. However, most of the research focused on Cd- or GaN based LEDs [97-103], which emit in the visible emission range. The NIR QD-LEDs which will further progress in applications such as night vision, optical communications and sensing are rarely reported. The seminal work on the fabrication of PbS based LEDs was first reported by Curry's group [104]. The use of PbS nanocrystals within a hybrid device that emits 1200 nm electroluminescence with an external quantum efficiency of 1.15%. They also claim that the emission wavelength can be tuned to cover a wide range of wavelengths including the 1300-1500 nm region without significant change of the efficiency. Another breakthrough on PbS based LEDs fabrication was later on achieved by Wise's group [45], who fabricated thin-film QD-LEDs with radiances ($6.4 \text{ W sr}^{-1} \text{ m}^{-2}$) eight times higher and external quantum efficiencies (2.0%) two times higher than the previously reported by tuning the distance between adjacent PbS QDs. As elaborated in our previous work, the quality of PbS/CdS core/shell QDs emitting in the 1300-1600 nm range, in terms of both QY and photo- and thermal stability, is much higher than that of shell-free QDs [82, 92, 96]. Therefore, these PbS/CdS core/shell QDs are more promising in fabricating higher quantum efficiency LEDs.

These synthesized core/shell/shell QDs are very stable in biological buffers and cytotoxicity studies show that they exhibit negligible toxicity to cultured cells. The ultrastable and biocompatible QDs were successfully used as NIR imaging probes and biological nanothermometers in mice. However, further systematic and thorough investigations on the toxic effects of PbS/CdS/ZnS core/shell/shell QDs are still necessary. It is very important to investigate the biocompatibility and toxicity of these QDs in small animals before further exploring their bio-applications such as human cancer imaging agents. Many factors such as composition, size and dose could affect the toxicity, however, such information is lacking. Therefore, it is essential to further assess and investigate the toxicity of PbS/CdS/ZnS core/shell/shell QDs in animals.

On the other hand, after injecting these PbS/CdS/ZnS core/shell/shell QDs into the mouse from the tail, the real-time biodistribution results show that QDs were present in the lungs in the first 30 s, and at longer times (1-2 min), accumulation in the liver happened. The detected biodistribution in the early stages after QDs injection is fairly consistent with the reports previously published concerning the biodistribution of NIR-emitting QDs and carbon nanotubes [42, 105, 106]. The phenomenon of accumulation in the liver and spleen is possible due to the negative surface charge of the QDs. Future work may focus on the surface engineering of the QDs to avoid the accumulation in the liver, opening the door for long circulation times that could lead, for instance, to tumor targeting.

Superparamagnetic NPs can serve both as magnetic resonance imaging (MRI) agents for the diagnosis of malignant tissues as well as vehicles for carrying therapeutic payloads (anticancer drugs, small inhibitory RNA, etc.) and efficiently delivering them to cancer sites in a target-specific manner [107]. They can also be used to magnetically confine cancer cells, allowing for ultra-sensitive cancer cell detection. In view of all these advantages of NIR fluorescent and superparamagnetic NPs, combining these two components into a single nanoarchitecture will undoubtedly lead to a new range of potential applications in biological systems. Basically, such multifunctional NPs bear at least two attractive features, the fluorescence properties (with both absorption and emission in the NIR) and superparamagnetism, which allows them to act as multi-dimensional (targeting, imaging and treatment) tools in biomedical applications. The combination of NIR QDs and superparamagnetic NPs into a single nanoarchitecture will undoubtedly lead to a new range of potential applications in biological systems. We propose to rationally design and synthesize novel multifunctional NPs with controlled morphology for specific applications related to cancers that are of high health concern in our society. Nonetheless, the development of such fluorescent-superparamagnetic multifunctional NPs can lead to a wealth of other applications, by, for example, loading antiviral drugs or targeting bacteria, and therefore the actual interest of this work is much wider than cancer diagnostics and therapy.

REFERENCES

- [1] S.V. Gaponenko, *Optical properties of semiconductor nanocrystals*, Cambridge University press, 1998.
- [2] A.M. Smith, S. Nie, *Accounts of Chemical Research*, 43 (2009) 190-200.
- [3] C. de Mello Donega, *Chemical Society Reviews*, 40 (2011) 1512-1546.
- [4] C. Burda, X. Chen, R. Narayanan, M.A. El-Sayed, *Chemical Reviews*, 105 (2005) 1025-1102.
- [5] L. Ye, K.-T. Yong, L. Liu, I. Roy, R. Hu, J. Zhu, H. Cai, W.-C. Law, J. Liu, K. Wang, *Nature Nanotechnology*, 7 (2012) 453-458.
- [6] T.J. Fountaine, S.M. Wincovitch, D.H. Geho, S.H. Garfield, S. Pittaluga, *Modern Pathology*, 19 (2006) 1181-1191.
- [7] K.-S. Cho, E.K. Lee, W.-J. Joo, E. Jang, T.-H. Kim, S.J. Lee, S.-J. Kwon, J.Y. Han, B.-K. Kim, B.L. Choi, *Nature Photonics*, 3 (2009) 341-345.
- [8] Q. Sun, Y.A. Wang, L.S. Li, D. Wang, T. Zhu, J. Xu, C. Yang, Y. Li, *Nature Photonics*, 1 (2007) 717-722.
- [9] X. Lan, S. Masala, E.H. Sargent, *Nature Materials*, 13 (2014) 233-240.
- [10] C.-H.M. Chuang, P.R. Brown, V. Bulović, M.G. Bawendi, *Nature Materials*, 13 (2014) 796-801.
- [11] L.V. Wang, H.-i. Wu, *Biomedical optics: principles and imaging*, John Wiley & Sons, 2012.
- [12] L.V. Wang, S. Hu, *Science*, 335 (2012) 1458-1462.
- [13] V.J. Pansare, S. Hejazi, W.J. Faenza, R.K. Prud'homme, *Chemistry of Materials*, 24 (2012) 812-827.
- [14] J. Bartelmeß, S. Quinn, S. Giordani, *Chemical Society Reviews*, (2015).
- [15] G. Hong, S.M. Tabakman, K. Welsher, Z. Chen, J.T. Robinson, H. Wang, B. Zhang, H. Dai, *Angewandte Chemie International Edition*, 50 (2011) 4644-4648.
- [16] B. del Rosal, I. Villa, D. Jaque, F. Sanz - Rodríguez, *Journal of Biophotonics*, (2015).
- [17] A.M. Smith, M.C. Mancini, S. Nie, *Nature Nanotechnology*, 4 (2009) 710-711.
- [18] U. Resch-Genger, M. Grabolle, S. Cavaliere-Jaricot, R. Nitschke, T. Nann, *Nature Methods*, 5 (2008) 763-775.
- [19] L.-M. Lacroix, F. Delpech, C. Nayral, S. Lachaize, B. Chaudret, *Interface Focus*, 3 (2013) 20120103.
- [20] K. Welsher, Z. Liu, D. Daranciang, H. Dai, *Nano Letters*, 8 (2008) 586-590.
- [21] Z. Liu, S. Tabakman, K. Welsher, H. Dai, *Nano Research*, 2 (2009) 85-120.
- [22] I. Villa, A. Vedda, I.X. Cantarelli, M. Pedroni, F. Piccinelli, M. Bettinelli, A. Speghini, M. Quintanilla, F. Vetrone, U. Rocha, *Nano Research*, 8 (2015) 649-665.
- [23] Y.-F. Wang, G.-Y. Liu, L.-D. Sun, J.-W. Xiao, J.-C. Zhou, C.-H. Yan, *ACS Nano*, 7 (2013) 7200-7206.
- [24] Q. Zhan, J. Qian, H. Liang, G. Somesfalean, D. Wang, S. He, Z. Zhang, S. Andersson-Engels, *ACS Nano*, 5 (2011) 3744-3757.
- [25] E. Hemmer, A. Benayas, F. L égar é F. Vetrone, *Nanoscale Horizons*, (2016).
- [26] Y. Du, B. Xu, T. Fu, M. Cai, F. Li, Y. Zhang, Q. Wang, *Journal of the American Chemical Society*, 132 (2010) 1470-1471.

- [27] S. Shen, Y. Zhang, L. Peng, Y. Du, Q. Wang, *Angewandte Chemie International Edition*, 50 (2011) 7115-7118.
- [28] L. Bakueva, I. Gorelikov, S. Musikhin, X.S. Zhao, E.H. Sargent, E. Kumacheva, *Advanced Materials*, 16 (2004) 926-929.
- [29] X. Peng, H. Chen, D.R. Draney, W. Volcheck, A. Schutz-Geschwender, D.M. Olive, *Analytical Biochemistry*, 388 (2009) 220-228.
- [30] K. Licha, B. Riefke, V. Ntziachristos, A. Becker, B. Chance, W. Semmler, *Photochemistry and Photobiology*, 72 (2000) 392-398.
- [31] K. Welsher, Z. Liu, S.P. Sherlock, J.T. Robinson, Z. Chen, D. Daranciang, H. Dai, *Nature Nanotechnology*, 4 (2009) 773-780.
- [32] D.B. Warheit, B.R. Laurence, K.L. Reed, D.H. Roach, G.A. Reynolds, T.R. Webb, *Toxicological Sciences*, 77 (2004) 117-125.
- [33] C.-W. Lam, J.T. James, R. McCluskey, R.L. Hunter, *Toxicological Sciences*, 77 (2004) 126-134.
- [34] J. Pichaandi, F.C. van Veggel, *Coordination Chemistry Reviews*, 263 (2014) 138-150.
- [35] E.N. Cerón, D.H. Ortgies, B. del Rosal, F. Ren, A. Benayas, F. Vetrone, D. Ma, F. Sanz-Rodríguez, J.G. Solé D. Jaque, E.M. Rodríguez, *Advanced Materials*, 27 (2015) 4781-4787.
- [36] A. Benayas, F. Ren, E. Carrasco, V. Marzal, B.R. del B. Gonfa, A. Juarranz, F. Sanz-Rodríguez, D. Jaque, J.G. Solé D. Ma, F. Vetrone, *Advanced Functional Materials*, 25 (2015) 6650-6659.
- [37] P.M. Allen, W. Liu, V.P. Chauhan, J. Lee, A.Y. Ting, D. Fukumura, R.K. Jain, M.G. Bawendi, *Journal of the American Chemical Society*, 132 (2009) 470-471.
- [38] D.J. Bharali, D.W. Lucey, H. Jayakumar, H.E. Pudavar, P.N. Prasad, *Journal of the American Chemical Society*, 127 (2005) 11364-11371.
- [39] J.M. Pietryga, R.D. Schaller, D. Werder, M.H. Stewart, V.I. Klimov, J.A. Hollingsworth, *Journal of the American Chemical Society*, 126 (2004) 11752-11753.
- [40] L. Cademartiri, E. Montanari, G. Calestani, A. Migliori, A. Guagliardi, G.A. Ozin, *Journal of the American Chemical Society*, 128 (2006) 10337-10346.
- [41] Y.-P. Gu, R. Cui, Z.-L. Zhang, Z.-X. Xie, D.-W. Pang, *Journal of the American Chemical Society*, 134 (2011) 79-82.
- [42] G. Hong, J.T. Robinson, Y. Zhang, S. Diao, A.L. Antaris, Q. Wang, H. Dai, *Angewandte Chemie*, 124 (2012) 9956-9959.
- [43] P. Jiang, C.-N. Zhu, Z.-L. Zhang, Z.-Q. Tian, D.-W. Pang, *Biomaterials*, 33 (2012) 5130-5135.
- [44] A.L. Rogach, A. Eychmüller, S.G. Hickey, S.V. Kershaw, *Small*, 3 (2007) 536-557.
- [45] L. Sun, J.J. Choi, D. Stachnik, A.C. Bartnik, B.-R. Hyun, G.G. Malliaras, T. Hanrath, F.W. Wise, *Nature Nanotechnology*, 7 (2012) 369-373.
- [46] N. Zhao, T.P. Osedach, L.-Y. Chang, S.M. Geyer, D. Wanger, M.T. Binda, A.C. Arango, M.G. Bawendi, V. Bulovic, *Acs Nano*, 4 (2010) 3743-3752.
- [47] R. Hu, W.-C. Law, G. Lin, L. Ye, J. Liu, J. Liu, J.L. Reynolds, K.-T. Yong, *Theranostics*, 2 (2012) 723.
- [48] Y.L. Z. Xu, F. Ren, F. Yang, D. Ma, *Coordination Chemistry Reviews*, (2016).
- [49] M.A. Hines, G.D. Scholes, *Advanced Materials*, 15 (2003) 1844-1849.

- [50] L. Cademartiri, J. Bertolotti, R. Sapienza, D.S. Wiersma, G. von Freymann, G.A. Ozin, *The Journal of Physical Chemistry B*, 110 (2006) 671-673.
- [51] H. Zhao, M. Chaker, D. Ma, *The Journal of Physical Chemistry C*, 113 (2009) 6497-6504.
- [52] W.W. Yu, J.C. Falkner, B.S. Shih, V.L. Colvin, *Chemistry of Materials*, 16 (2004) 3318-3322.
- [53] S. Hinds, S. Myrskog, L. Levina, G. Koleilat, J. Yang, S.O. Kelley, E.H. Sargent, *Journal of the American Chemical Society*, 129 (2007) 7218-7219.
- [54] J. Pichaandi, K.A. Abel, N.J. Johnson, F.C. van Veggel, *Chemistry of Materials*, 25 (2013) 2035-2044.
- [55] G. Chen, S. Desinan, R. Nechache, R. Rosei, F. Rosei, D. Ma, *Chemical Communications*, 47 (2011) 6308-6310.
- [56] C.B. Murray, D.J. Norris, M.G. Bawendi, *Journal of the American Chemical Society*, 115 (1993) 8706-8715.
- [57] M.R. Kim, D. Ma, *The Journal of Physical Chemistry Letters*, 6 (2014) 85-99.
- [58] X. Peng, M.C. Schlamp, A.V. Kadavanich, A. Alivisatos, *Journal of the American Chemical Society*, 119 (1997) 7019-7029.
- [59] A. Aharoni, T. Mokari, I. Popov, U. Banin, *Journal of the American Chemical Society*, 128 (2006) 257-264.
- [60] J. McBride, J. Treadway, L. Feldman, S.J. Pennycook, S.J. Rosenthal, *Nano Letters*, 6 (2006) 1496-1501.
- [61] R. Xie, U. Kolb, J. Li, T. Basch & A. Mews, *Journal of the American Chemical Society*, 127 (2005) 7480-7488.
- [62] C. de Mello Donega, *Chemical Society Reviews*, 40 (2011) 1512-1546.
- [63] A. Aharoni, T. Mokari, I. Popov, U. Banin, *Journal of the American Chemical Society*, 128 (2006) 257-264.
- [64] A.M. Smith, S. Nie, *Accounts of Chemical Research*, 43 (2010) 190-200.
- [65] M.R. Kim, Z. Xu, G. Chen, D. Ma, *Chemistry-A European Journal*, 20 (2014) 11256-11275.
- [66] B. Dabbousi, J. Rodriguez-Viejo, F.V. Mikulec, J. Heine, H. Mattoussi, R. Ober, K. Jensen, M. Bawendi, *The Journal of Physical Chemistry B*, 101 (1997) 9463-9475.
- [67] J.M. Pietryga, D.J. Werder, D.J. Williams, J.L. Casson, R.D. Schaller, V.I. Klimov, J.A. Hollingsworth, *Journal of the American Chemical Society*, 130 (2008) 4879-4885.
- [68] N. Won, S. Jeong, K. Kim, J. Kwag, J. Park, S.G. Kim, S. Kim, *Molecular Imaging*, 11 (2012) 338.
- [69] E.J. Henderson, A.J. Shuhendler, P. Prasad, V. Baumann, F. Maier - Flaig, D.O. Faulkner, U. Lemmer, X.Y. Wu, G.A. Ozin, *Small*, 7 (2011) 2507-2516.
- [70] J.-C. Boyer, M.-P. Manseau, J.I. Murray, F.C. van Veggel, *Langmuir*, 26 (2009) 1157-1164.
- [71] Y.T. Lim, S. Kim, A. Nakayama, N.E. Stott, M.G. Bawendi, J.V. Frangioni, *Molecular Imaging*, 2 (2003) 50-64.
- [72] Y. Zhang, G. Hong, Y. Zhang, G. Chen, F. Li, H. Dai, Q. Wang, *ACS Nano*, 6 (2012) 3695-3702.

- [73] N. Venkatachalam, T. Yamano, E. Hemmer, H. Hyodo, H. Kishimoto, K. Soga, *Journal of the American Ceramic Society*, 96 (2013) 2759-2765.
- [74] E. Hemmer, N. Venkatachalam, H. Hyodo, A. Hattori, Y. Ebina, H. Kishimoto, K. Soga, *Nanoscale*, 5 (2013) 11339-11361.
- [75] B.-R. Hyun, H. Chen, D.A. Rey, F.W. Wise, C.A. Batt, *The Journal of Physical Chemistry B*, 111 (2007) 5726-5730.
- [76] Y. Nakane, Y. Tsukasaki, T. Sakata, H. Yasuda, T. Jin, *Chemical Communications*, 49 (2013) 7584-7586.
- [77] A.M. Derfus, W.C. Chan, S.N. Bhatia, *Nano letters*, 4 (2004) 11-18.
- [78] C. Kirchner, T. Liedl, S. Kudera, T. Pellegrino, A. Muñoz Javier, H.E. Gaub, S. Stölzle, N. Fertig, W.J. Parak, *Nano letters*, 5 (2005) 331-338.
- [79] K.A. Abel, J. Shan, J.-C. Boyer, F. Harris, F.C. van Veggel, *Chemistry of Materials*, 20 (2008) 3794-3796.
- [80] I. Moreels, Y. Justo, B. De Geyter, K. Haestraete, J.C. Martins, Z. Hens, *Acs Nano*, 5 (2011) 2004-2012.
- [81] O.E. Semonin, J.C. Johnson, J.M. Luther, A.G. Midgett, A.J. Nozik, M.C. Beard, *The Journal of Physical Chemistry Letters*, 1 (2010) 2445-2450.
- [82] F. Ren, H. Zhao, F. Vetrone, D. Ma, *Nanoscale*, 5 (2013) 7800-7804.
- [83] T. Zhang, H. Zhao, D. Riabinina, M. Chaker, D. Ma, *The Journal of Physical Chemistry C*, 114 (2010) 10153-10159.
- [84] G. Hornyak, T. Sawitowski, G. Schmid, *Micron*, 29 (1998) 183-190.
- [85] K.D. Harris, M. Tremayne, B.M. Kariuki, *Angewandte Chemie International Edition*, 40 (2001) 1626-1651.
- [86] C.B. Boss, K.J. Fredeen, *Concepts, instrumentation and techniques in inductively coupled plasma optical emission spectrometry*, Perkin Elmer Norwalk, 1999.
- [87] H.J. Yvon, HORIBA, Jobin Yvon Ltd., Stanmore, Middlesex, UK, (2012).
- [88] C. Würth, M. Grabolle, J. Pauli, M. Spieles, U. Resch-Genger, *Nature Protocols*, 8 (2013) 1535-1550.
- [89] J.R. Lakowicz, *Principles of fluorescence spectroscopy*, Springer Science & Business Media, 2013.
- [90] I. Moreels, K. Lambert, D. Smeets, D. De Muynck, T. Nollet, J.C. Martins, F. Vanhaecke, A. Vantomme, C. Delerue, G. Allan, *ACS Nano*, 3 (2009) 3023-3030.
- [91] E.V. Ushakova, A.P. Litvin, P.S. Parfenov, A.V. Fedorov, M. Artemyev, A.V. Prudnikau, I.D. Rukhlenko, A.V. Baranov, *ACS Nano*, 6 (2012) 8913-8921.
- [92] H. Zhao, M. Chaker, D. Ma, *Journal of Materials Chemistry*, 21 (2011) 17483-17491.
- [93] K. Gopidas, M. Bohorquez, P.V. Kamat, *Journal of Physical Chemistry*, 94 (1990) 6435-6440.
- [94] B. De Geyter, Y. Justo, I. Moreels, K. Lambert, P.F. Smet, D. Van Thourhout, A.J. Houtepen, D. Grodzinska, C. de Mello Donega, A. Meijerink, *ACS nano*, 5 (2010) 58-66.
- [95] A. Benayas, F. Ren, E. Carrasco, V. Marzal, B. del Rosal, B.A. Gonfa, Á. Juarranz, F. Sanz - Rodríguez, D. Jaque, J. García - Solé *Advanced Functional Materials*, 25 (2015) 6650-6659.
- [96] H. Zhao, M. Chaker, N. Wu, D. Ma, *Journal of Materials Chemistry*, 21 (2011) 8898-8904.

- [97] V. Colvin, M. Schlamp, A. Alivisatos, *Nature*, 370 (1994) 354-357.
- [98] B. Dabbousi, M. Bawendi, O. Onitsuka, M. Rubner, *Applied Physics Letters*, 66 (1995) 1316-1318.
- [99] J. Zhao, J.A. Bardecker, A.M. Munro, M.S. Liu, Y. Niu, I.-K. Ding, J. Luo, B. Chen, A.K.-Y. Jen, D.S. Ginger, *Nano letters*, 6 (2006) 463-467.
- [100] S. Coe - Sullivan, J.S. Steckel, W.K. Woo, M.G. Bawendi, V. Bulović, *Advanced Functional Materials*, 15 (2005) 1117-1124.
- [101] J.S. Steckel, P. Snee, S. Coe - Sullivan, J.P. Zimmer, J.E. Halpert, P. Anikeeva, L.A. Kim, V. Bulovic, M.G. Bawendi, *Angewandte Chemie International Edition*, 45 (2006) 5796-5799.
- [102] A.H. Mueller, M.A. Petruska, M. Achermann, D.J. Werder, E.A. Akhador, D.D. Koleske, M.A. Hoffbauer, V.I. Klimov, *Nano Letters*, 5 (2005) 1039-1044.
- [103] M. Gao, C. Lesser, S. Kirstein, H. M \ddot{u} hwald, A.L. Rogach, H. Weller, *Journal of Applied Physics*, 87 (2000) 2297-2302.
- [104] K. Bourdakos, D. Dissanayake, T. Lutz, S. Silva, R. Curry, *Applied Physics Letters*, 92 (2008).
- [105] K. Welsher, S.P. Sherlock, H. Dai, *Proceedings of the National Academy of Sciences*, 108 (2011) 8943-8948.
- [106] Y. Zhang, Y. Zhang, G. Hong, W. He, K. Zhou, K. Yang, F. Li, G. Chen, Z. Liu, H. Dai, *Biomaterials*, 34 (2013) 3639-3646.
- [107] P. Tartaj, M. del Puerto Morales, S. Veintemillas-Verdaguer, T. Gonz \acute{a} lez-Carre \tilde{n} o, C.J. Serna, *Journal of Physics D: Applied Physics*, 36 (2003) R182.

Résumé

L'introduction

Un point quantique (en anglais: Quantum Dot (QD)), est un nanocristal (NC) semiconducteur, qui est composé de II-VI, IV - VI ou III-V. Typiquement, les points quantiques (QDs) sont inférieures à 100 nm en dimension et montrent de nouvelles propriétés différentes de leurs matériaux massifs, comme l'absorption optique et des spectres d'émission dépendant de la taille [1]. Ces caractéristiques uniques proviennent de l'effet de confinement quantique qui est observé aussi longtemps que la taille du matériau est plus petite que le rayon de l'exciton de Bohr définissant la taille d'un exciton (la paire électron-trou). Le confinement quantique affecte la fonction d'onde d'exciton, et induit des modifications de la densité d'états électroniques et à la séparation des niveaux d'énergie. Cela se manifeste par l'augmentation de la largeur de bande interdite avec une taille décroissante et l'apparition des niveaux d'énergie discrets à proximité des bords de la bande [2, 3].

L'imagerie optique à base de fluorescence dans le domaine visible (400-700 nm) avec la réponse rapide a été montrée des utilisations sur l'imagerie in-vitro et in-vivo [11], mais elle est limitée par la pénétration tissulaire d'environ 1 mm [12]. Pour l'imagerie tissulaire profonde, dans le proche infrarouge (en anglais: near infrared (NIR)), des sondes de fluorescence permettant de l'absorption tissulaire et de la dispersion beaucoup plus faible, l'élimination de l'autofluorescence indésirable et de la pénétration plus profonde sont plus souhaitables [15, 16]. En particulier, les longueurs

d'onde entre 650-950 nm et 1000-1350 nm, comme les premières et les deuxièmes fenêtres biologiques (I-BW et II-BW), respectivement, ont été identifiées [17]. Généralement, un fluorochrome NIR approprié, qui permet d'être utilisé pour l'application biologique, doit satisfaire les conditions suivantes [18, 19]: (a) dispersible et stable dans des tampons appropriés, des milieux de culture cellulaire ou fluides corporels, (b) la luminosité élevée et disponible dans une qualité reproductible, (c) absence de la toxicité ou de l'interférence avec la physiologie cellulaire. Cependant, il n'y a que des choix limités de fluorochromes NIR émettrices, comme les nanotubes de carbone à paroi simple (SWCNTs) [20, 21], nanoparticules dopées à Nd^{3+} et Er^{3+} [22-25], certains types de QDs [26-28], et quelques colorants organiques [29, 30]. Les relativement faibles rendements quantiques (en anglais: quantum yields (QYs)) de fluorescence et/ou une mauvaise biocompatibilité des SWCNTs, des colorants et des nanoparticules de terres rares dopées ont limité leur utilisation pour l'imagerie in-vivo [18, 31]. Il a également rapporté que les nanotubes de carbone peuvent empaler les cellules pulmonaires comme des aiguilles [32, 33]. QDs NIR en raison de leur photostabilité remarquable, la luminosité et la photoluminescence (PL) dépendant de la taille ont été explorés, de nouvelles sondes d'imagerie biomédicale [34]. Il existe plusieurs types de QDs comme InAs et InP (III-V) [35, 36], PbSe et PbS (IV-VI) [37, 38], Ag_2S et Ag_2Se (I-VI) [26, 39], qui permettent de régler de l'émission dans le rang NIR. Parmi eux, QDs de Ag_2S avec fluorescence relativement élevée dans la deuxième fenêtre biologique ont été utilisés pour l'imagerie in-vivo NIR [40, 41]. L'imagerie avec ces QDs Ag_2S a permis de donner l'enregistrement intérieur d'organes, le contraste

de la tumeur dynamique, et la détection de la tumeur rapide. Cependant, leur faible photostabilité peut être un problème majeur pour certaines applications. Il a rapporté que l'intensité de PL a diminué de la moitié dans les premières 200 secondes sous une illumination continue avec une diode laser à 808 nm [40]. Par conséquent, il est urgent d'exploiter d'autres fluorescentes vives et des sondes fluorescentes NIR-II biocompatibles pour l'imagerie biologique dans *in vitro* et *in vivo*.

QDs de PbS s'ont attiré l'attention considérable pendant la dernière décennie grâce aux caractéristiques uniques, par exemple, les band-gaps étroites (0,41 eV à température ambiante), des grands rayons Bohr (18 nm), des grandes absorptions optiques et émissions des spectres dépendant de la taille (Figure 1.7) [44]. Grâce aux caractéristiques uniques, les QDs de PbS ont montré des applications potentielles, par exemple, dans les cellules solaires, des bio-imageries, des télécommunications et des diodes électroluminescentes [7, 45, 46]. La synthèse de QDs de PbS colloïdales est normalement effectuée par la méthode d'injection chaude, qui permet d'injecter la source de soufre aux précurseurs organométalliques de plomb chauds. Étant donné que cette méthode peut séparer les étapes de nucléation et de croissance par la température contrôlable précisément, il donne habituellement la meilleure qualité jugée par la distribution de la taille et la forme ainsi que des propriétés optiques. Les travaux fondamentaux sur la synthèse de monodispersés de QDs de PbS par la voie organométallique utilisant l'injection chaude été premièrement rapporté par Hines et Scholes [47]. Les QDs montrent une dispersion de taille étroite (15-20%) avec une largeur à mi-hauteur (en anglais : full width at half maximum (FWHM)) du pic de PL

d'environ 100 meV sans aucun processus de sélection de la taille. Cependant, leur synthèse implique l'utilisation du produit chimique dangereux et nauséabond de bis(triméthylsilyl) sulfure (TMS) comme source de soufre. Récemment, notre groupe a développé une approche simple, verte et facilement reproductible pour synthétiser QDs de PbS. Nous avons fait l'effort de faire la synthèse dans un système "non visqueux" sans solvant oléamine (OLA) en utilisant une température de réaction constante [49].

QDs de PbS synthétisés par la méthode d'injection à chaud sont normalement dispersés dans une phase organique. Pour les applications biomédicales, QDs doivent non seulement être soluble dans l'eau, mais aussi montrent une grande QY (en anglais : quantum yield) et bonne stabilité de PL dans un tampon. Dans ce cas, la modification de surface de QDs est indispensable, qui est habituellement réalisé par échange de ligand, revêtement de silice ou d'un procédé d'intercalation. Le premier rapport sur la modification de surface de QDs à base de Pb a été publié par le groupe de Colvin, où l'acide 11-mercaptoundécanoïque a été utilisé pour remplacer le ligand oléate sur la surface de QDs de PbSe [50]. Ces QDs solubles dans l'eau préparés ont été constatés la stabilité dans l'eau, mais pas dans des tampons physiologiques. Hinds *et al.* ont transféré ultérieurement QDs de PbS du solvant organique à la solution aqueuse en remplaçant le ligand de l'oléate de (1-mercaptoundec-11-yl) tétra (éthylène glycol) [51]. Ces QDs de PbS présentaient une meilleure stabilité colloïdale dans un tampon pendant environ 5 jours. De nos jours, le groupe de van Veggel a utilisé une approche de

polymère modifié pour fonctionnaliser QDs en forme de noyau / coquille (en anglais : *core/shell*) de PbS/CdS et les transférer dans l'eau [52] en montrant dans la Figure 1.8. Ces QDs ont montré une stabilité colloïdale à long terme renforcée et excellente dans des tampons, cependant, aucune information n'a été fournie sur la photostabilité de ces QDs sous illumination continue dans des tampons, ce qui est une condition importante pour des applications biomédicales lorsque des processus biologiques du suivi à long terme sont nécessaires [53].

Comme le cristal devient plus petit, le taux de surface-volume devient plus grand, et donc les propriétés des nanomatériaux qui ne sont limitées par des ligands organiques deviennent extrêmement sensibles aux caractéristiques de surface. En particulier, les atomes de surface ont moins de voisins que leurs homologues de l'intérieur, il est difficile de passiver simultanément les deux sites de surface anioniques et cationiques par un ligand organique. Par conséquent, les atomes de surface possèdent des liaisons chimiques insatisfaites (liaisons pendantes), qui peut piéger les porteurs de charges et peut augmenter la probabilité d'événements de désintégration non radiatifs [54]. Pour ces raisons, les propriétés optiques peuvent être largement affectées. Il est donc essentiel de contrôler la qualité de surface et d'éliminer les liaisons pendantes. À la fin, les chercheurs ont fait de grands efforts sur l'ingénierie de surface de QDs pendant les dernières décennies. Une meilleure passivation de surface a été réalisée par l'ajout d'une coquille inorganique d'un plus large semiconducteur de bande interdite pour former la structure "*core/shell*" [55]. En conséquence, l'impact des états de défauts de surface, des sites piégés et des facteurs environnementaux sur les QDs sera diminué [2, 56-59].

1.5 Les objectifs de la thèse

Cette thèse comprend deux parties: la première partie est essentiellement concernée sur l'étude des QDs *core/shell* de PbS / CdS.

À ce jour, il y a plusieurs approches pour produire QDs de PbS dans la phase organique, cependant, le QY est seulement entre 20-40% pour les QDs de plus grande taille, dont les pics d'émission sont dans un domaine de 1300-1600 nm [49, 50, 68, 69]. C'est parce que l'émission de grandes QDs peut être facilement trempée par les états piégés localisés [70] comparé avec des plus petites QDs émettant dans un domaine de 1100-1300 nm, qui possèdent généralement QY entre 60% - 90% [49, 50, 68, 69]. Par conséquent, c'est très souhaitable, mais aussi difficile d'élaborer une approche réalisable pour la synthèse de QDs à base de PbS de haute qualité avec une grande QY dans la gamme de longueur d'onde plus longue. L'objectif de cette section est:

1. Développer une approche reproductible et contrôlable pour la synthèse rapide avec haute qualité émettant de NIR de QDs de *core/shell* de PbS/CdS à longueurs d'ondes longues (1300-1600 nm).
2. Étudier le mécanisme d'échange de cations de la formation de QDs de *core/shell* de PbS / CdS sous différente source de chauffage. Par la compréhension du mécanisme d'échange, l'optimisation des paramètres de réaction pour synthétiser QDs de *core/shell* avec haute qualité et grandes quantités.

3. Synthétiser les QDs de *core/shell* de PbS / CdS avec une série de taille différente en changeant la taille initiale du PbS.

4. Étudier et comprendre la variation de l'intensité de PL de QDs de PbS colloïdales avec la formation de coquille mince de CdS d'après perspectives de la variation de densité piégée et la probabilité d'électrons et des trous atteignant les défauts de surface.

La deuxième partie se concentre principalement sur la photo-stabilité et la stabilité colloïdale de QDs de *core/shell/shell* PbS/CdS/ZnS et leurs applications potentielles dans le domaine biologique. Comme il est mentionné ci-dessus, les QDs de PbS synthétisés par l'injection chaude sont normalement dispersés dans une phase organique. Pour les applications biomédicales, QDs doivent non seulement être solubles dans l'eau, mais aussi montrent une grande stabilité de PL et QY dans un tampon. Bien que les QDs émettrices visibles et solubles d'eau ont été synthétisés par l'échange de ligand, le revêtement de silice ou processus d'intercalation, les rapports sur QDs de PbS de émettrices NIR encore manque. Il est très souhaitable, mais aussi au défi de développer une approche possible de synthétiser QDs à base de PbS d'émettrice NIR et solubles dans l'eau avec haute qualité Par conséquent, l'objectif de cette section est suivant:

1. Synthétiser des QDs de *core/shell/shell* PbS/CdS/ZnS en croissant un *shell* biocompatible ZnS sur la surface de QDs de *core/shell* PbS/CdS. En réglant et en optimisant les épaisseurs de CdS et de ZnS pour synthétiser des QDs solubles dans l'eau avec haute qualité

2. Étudier la photo-stabilité et la stabilité colloïdale ainsi que leurs effets sur la cytotoxicité, de manière à utiliser ces QDs de l'eau pour servir comme d'agents d'imagerie.

3. Étudier leur comportement dépendant thermal du signal de fluorescence. Les QDs de PbS/CdS/ZnS sont exploités pour obtenir la cartographie thermique des zones de sous-peau dans des spécimens vivants.

Dans la première section, je développe une approche reproductible, contrôlable et d'échange de cations assisté par micro-ondes, pour la première fois, synthèse rapide des QDs de core/shell PbS/CdS émettrices NIR avec haute qualité. Ces QDs monodispersés émettant à l'échelle de 1300-1600 nm, montrent un rendement quantique plus élevé que 57% qui est d'environ 1,4 fois comparé avec les mêmes QDs préparés en utilisant un chauffage classique dans un bain d'huile. Au meilleur de notre connaissance, il est la valeur reproductible la plus élevée rapportée à ce jour pour QDs à base de PbS dans cette échelle d'émission. Plus important, les QDs de PbS/CdS peuvent auto-assembler presque parfaitement et facilement à l'échelle du micromètre en raison de leur forme uniforme et la distribution de taille étroite (Figure R1).

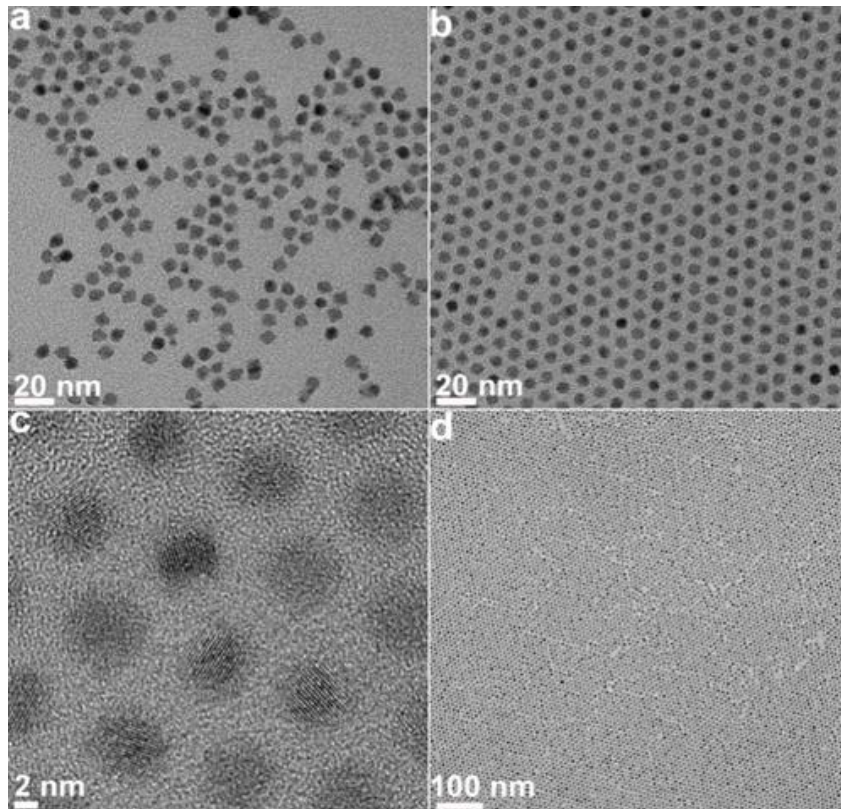


Figure R1. (a) image de MEB de QDs PbS parents; (b) image de MEB de QDs PbS/CdS *core /shell* synthétisés par un chauffage par micro-ondes avec le temps de réaction de 30 s à 100 °C; (c) image de MEB haute résolution de (b); (d) image de MEB avec basse de grossissement de (b).

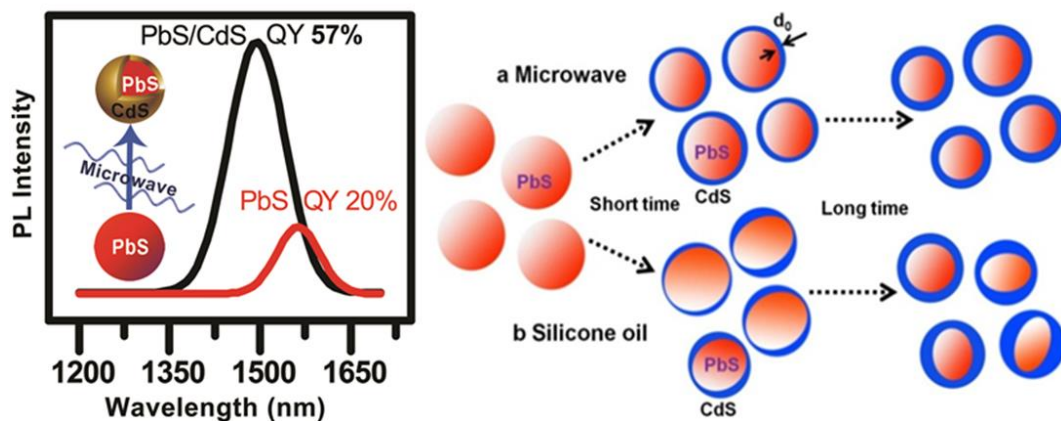


Figure R2. (À gauche) spectres PL des QDs de PbS parents et échange de cations échantillons de QDs de PbS/CdS. (À droite) Le chemin de croissance proposé de QDs

PbS/CdS lors de l'échange de cations : (a) chauffage par micro-ondes, (b) chauffage par huile avec différents temps de réaction. d_0 est l'épaisseur "critique" de la *shell* en dessous de laquelle aucun des défauts évidents sont induits et dans l'ensemble les QDs sont en grande partie bénéficiant d'une meilleure passivation des *shell* CdS.

Les résultats correspondants dans cette section sont publiés dans la publication [69]:

F. Ren, H. Zhao, F. Vetrone, D. Ma, *nanoscale*, 5 (2013) 7800-7804.

Nous avons proposé un mécanisme pour expliquer ce phénomène (Figure R2). En général, au cours du processus de formation échange de cations de *core/shell*, il y a deux facteurs qui déterminent le QY final des QDs. La passivation de surface améliorée du noyau de semi-conducteur se conduira par l'augmentation de QY, tandis que, simultanément à la création de nouveaux défauts d'interface en raison du *mismatch* réticulaire ou la tension interfaciale entre le noyau et la coquille des matériaux diminuant du noyau de QY. Ces deux facteurs sont en compétition au cours du processus de formation de la structure *core/shell* et QY globale dépendant de l'interaction entre ces deux facteurs.

Dans la deuxième partie, je concerne la variation de l'intensité anormale de PL dépendant de la taille de QDs PbS avec la formation d'un *shell* mince de CdS par la même approche d'échange de cations assistée par micro-ondes. La stratégie de *core/shell* a été largement utilisée comme un moyen utile pour améliorer les propriétés photophysiques de QDs. Normalement, la structure *core/shell* peut améliorer QY et la stabilité par rapport à QDs initiales et non-*shell*. Cependant, une épaisseur de *shell*

optimale existe dans le système *core/shell*, au-delà de certaines épaisseurs de *shell*, l'intensité de PL diminue par rapport à celle des QDs initiales en raison de l'introduction de nouveaux défauts. Cela a été prouvé par nos précédents travaux publiés [79, 83]. Dans la dernière section, nous avons constaté que QY de QDs PbS avec pic de PL de 1340 nm à 1560 nm (diamètre de 4,5 à 5,9 nm) a été largement amélioré après le revêtement avec un *shell* de CdS avec une épaisseur optimale, en raison de l'amélioration de passivation de surface du noyau PbS. Dans cette section, nous avons utilisé l'approche de cation d'échange assistée par micro-ondes pour revêtir les QDs PbS de tailles différentes avec CdS d'épaisseur variable (Figure R3) et trouvé un phénomène anormal. Contrairement à grandes QDs, QDs ultra petites ont représenté la diminution immédiate de l'intensité de PL lors de la formation de la *shell*, contrairement à la compréhension commune que la stratégie *core/shell* peut améliorer PL (Figure R4 a). Nous avons essayé de comprendre ce phénomène anormal du point de vue de la variation de densité de pièges et la probabilité d'électrons et des trous atteignant les défauts de surface. À cette fin, la durée de vie de QY et PL (sur l'échelle de temps ns- μ s) de QDs PbS primitives et QDs de *core/shell* PbS / CdS ont été mesurées et les taux de recombinaison radiative et non radiative ont été dérivés et comparés. De plus, l'analyse d'absorption transitoire (sur l'échelle de temps fs-ns) a été réalisée pour mieux comprendre la dynamique d'excitons sur des échelles de temps ultrarapides. Un modèle a été proposé pour expliquer les propriétés optiques et dynamiques observées (Figure R4 b et c).

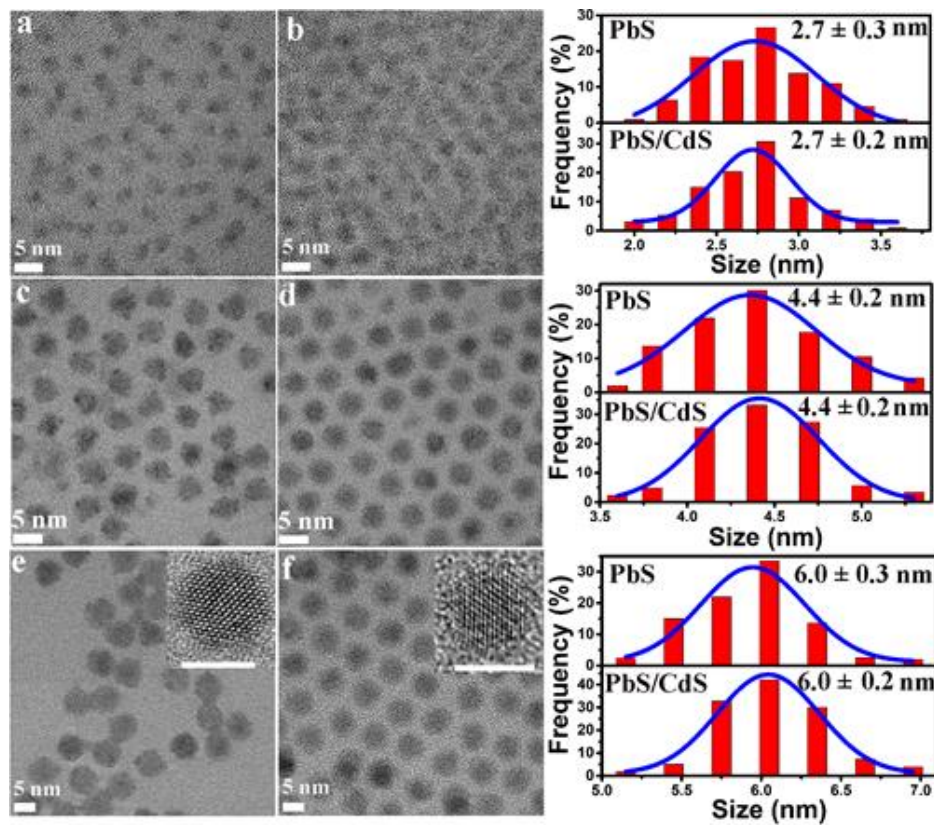


Figure R3. Image de MEB de QDs de taille différente de PbS (a: $2,7 \pm 0,3$ nm ; c: $4,4 \pm 0,2$ nm ; e: $6,0 \pm 0,3$ nm) et de PbS/CdS (b: $2,7 \pm 0,2$ nm ; d: $4,4 \pm 0,2$ nm ; f: $6,0 \pm 0,2$ nm) et leurs histogrammes correspondants (à droite). L'encart de e et f montrent des images de MEB avec haute résolution de QDs PbS et PbS / CdS, respectivement. La barre d'échelle est de 5 nm.

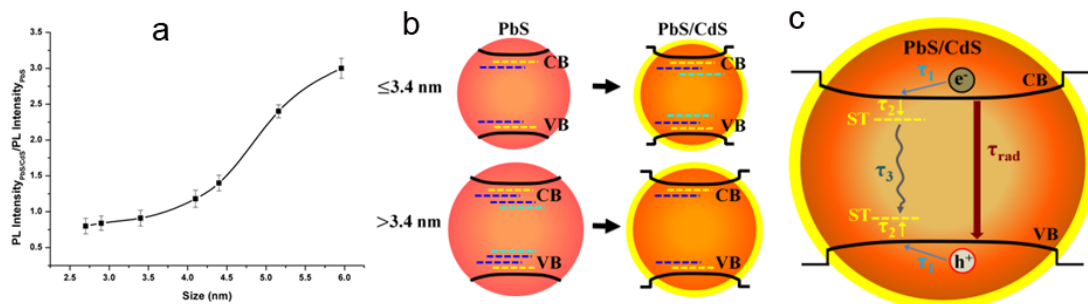


Figure R4. (a) L'intensité relative de PL, i.e. le rapport entre l'intensité de PL intégrée de QDs PbS/CdS à celle de QDs PbS en fonction de la taille de QD. L'illustration de schéma de la (b) addition d'état de piège et de réduction lors de la formation de la *shell* pour QDs PbS/CdS des régimes ultrapetits et plus grande, respectivement, et (c) des processus de relaxation des excitons proposés dans QDs PbS / CdS.

Les résultats correspondants dans cette section ont été soumis pour publication :

Fuqiang Ren, Sarah A. Lindley, Haiguang Zhao, Long Tan, Belete Atomsa Gonfa, Ying-Chih Pu, Fan Yang, Xinyu Liu, François Vidal, Jin Z. Zhang, Fiorenzo Vetrone, Dongling Ma. *Towards Understanding Unusual Photoluminescence Intensity Variation of Ultrasmall Colloidal PbS Quantum Dots with the Formation of Thin CdS Shell*. Soumettre au journal Chemistry of Materials.

Partie II La deuxième partie comprend deux sections, ce qui correspond à la synthèse (partie III) et les applications potentielles biologiques (partie IV), respectivement. Il concentre la photostabilité et la stabilité colloïdale de l'eau solubles de QDs *core/shell/shell* de PbS/CdS/ZnS et leurs applications dans le domaine biologique. Dans la partie III, des QDs *core/shell/shell* PbS/CdS/ZnS, solubles dans l'eau et NIR ont été premièrement synthétisés par la croissance d'un *shell* de ZnS biocompatible sur la surface de QDs de *core/shell* PbS/CdS et simultanément fonctionnaliser la surface avec des ligands d'acide mercaptopropionique. Ces QDs *core/shell/shell* synthétisés sont très stables dans trois tampons biologiques utilisés et montrent longtemps stable

jusqu'à au moins 14 mois dans un tampon PBS. Comme les figures 5R a et c montrent, leurs pics de PL ont montré un changement non sensible pendant 14 mois qu'ils ont été gardés dans un tampon PBS, ce qui était le point de plus long du temps que nous avons étudié par la MEB et la spectroscopie PL pour les deux tailles de QDs présentes. Figure 5R b (à gauche) montre la photo optique d'une dispersion aqueuse de 930 nm d'émission de QDs *core/shell/shell* de PbS/CdS/ZnS après un stockage de 30 mois dans du PBS et leur photo de luminescence NIR (Figure 5R b, à droite). La haute transparence optique, absence de précipités et une forte émission de NIR soutient fortement une fois de plus la qualité supérieure, une excellente stabilité et une durée de vie très longue de ces QDs dans le tampon. Leur excellente stabilité a été confirmée par des observations MEB montrant les figures 3d et e, les deux QDs 930 nm et 1220 nm étaient encore homogènes, non agglomérés et montraient les mêmes distributions de tailles uniformes que les QDs fraîchement préparés. La raison principale de cette stabilité à long terme est que le ligand MPA dotait la stabilité de dispersion excellente des QDs, tandis que les doubles shells CdS et ZnS interdisaient l'attaque des molécules d'eau, de sels ou d'autres ions au noyau PbS, qui a dominé les caractéristiques optiques globales des QDs.

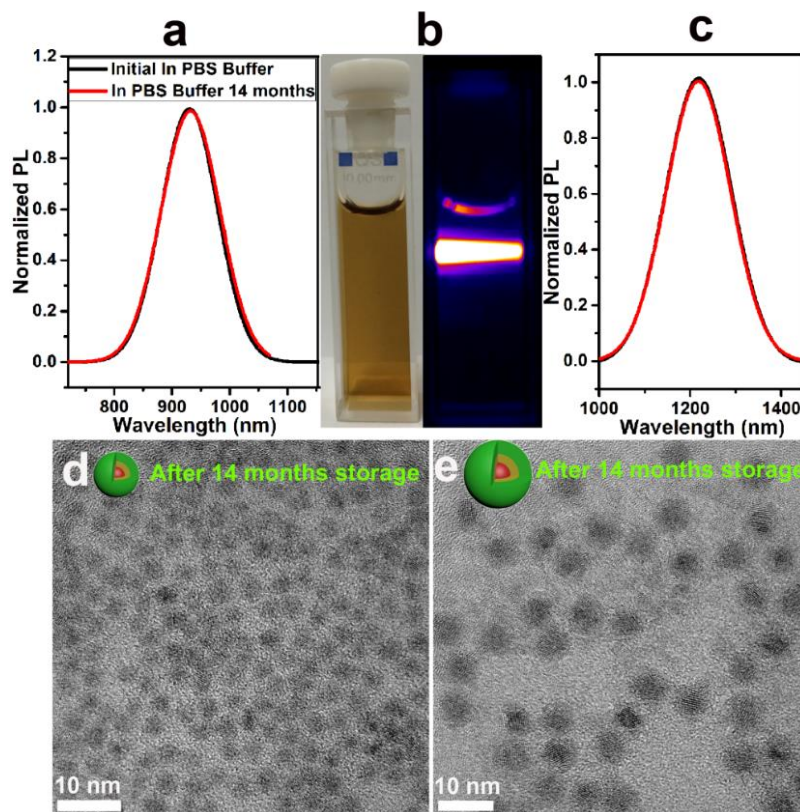


Figure 5R. Spectres PL de (a) 930 nm et (c) 1220 nm émettant QDs *core/shell/shell* de PbS/CdS/ZnS fraîchement préparés et dispersés dans du tampon PBS et après stockage de 14 mois dans le tampon PBS. Photos optique (à gauche) et la luminescence (à droite) de (b) 930 nm émettant QDs de *core/shell/shell* PbS/CdS/ZnS stockés dans un tampon PBS pendant 30 mois. Images MEB de (d) 930 nm et (e) QDs *core/shell/shell* de PbS/CdS/ZnS de 1220 nm stockés dans un tampon PBS pendant 14 mois.

La stabilité colloïdale de QDs *core/shell/shell* PbS/CdS/ZnS de 930 nm et 1220 nm a été étudiée en les gardant dans des conditions de concentration ionique élevée. Les résultats montrent que l'intensité de PL de QDs de *core/shell/shell* PbS/CdS/ZnS n'a pas changé pendant au moins 3 semaines à forte concentration de NaCl à 400 mM. Les QDs présentent également une excellente photostabilité, l'intensité de PL garde encore

d'environ 80% de l'intensité de PL initiale après 1 heure de l'illumination UV continue. Les résultats des effets de QDs de cytotoxicité montrent que ces QDs core/shell/shell sont une toxicité négligeable pour des cellules culturels, même avec la concentration des QDs élevée (50 nM). Les QDs ultrastables et biocompatibles ont été utilisés pour le test d'imagerie de la tumeur dans la souris (Figure R6). Avec des concentrations faibles et faible intensité du laser, les QDs montrent une luminosité élevée même avec l'injection de profondeur d'environ 2,5 mm, ce qui est beaucoup plus profond que QDs visibles.

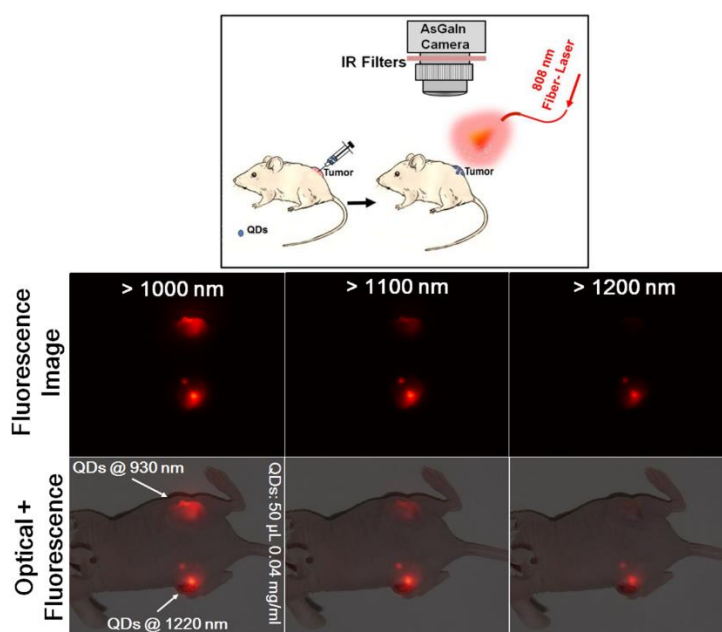


Figure R6. Dessus: Schéma de la procédure expérimentale pour l'imagerie de la tumeur. 50 µl de solutions de tampon PBS contenant QDs ont été injecté directement dans les tumeurs et la profondeur de l'injection estimée était d'environ 2,5 mm. Un laser à diode de 808 nm (L 'intensité $0,04 \text{ W/cm}^2$) a été utilisé pour exciter les QDs. La fluorescence NIR générée par les QDs a été enregistrée avec une caméra d'InGaAs refroidie par

l'effet Peltier, capable de traitement d'imageries en temps réel dans le domaine spectral entre 900-1700 nm. Des expériences *in vivo*: la souris de la fluorescence (au milieu) et des optiques + la fluorescence d'imageries (en bas) d'après l'injection avec les deux solutions de QDs avec différentes tailles en émettant dans les première et deuxième fenêtres biologiques, respectivement.

Dans la partie IV, nous avons développé un système d'imagerie à base de QD basé sur QDs PbS/CdS/ZnS et NIR-émettrice avec une toxicité très faible. Grâce à l'ingénierie de leur longueur d'onde d'émission, nous avons obtenu des nanosondes d'imagerie de la fluorescence avec des profondeurs de pénétration optimale dans le tissu biologique. De plus, cette nouvelle plate-forme a montré la multifonctionnalité au-delà de leur utilisation telle que nanosondes d'imagerie pures. Le système est capable d'agir comme un nanothermomètre biologique, basé sur du comportement dépendant thermique fiable du signal de fluorescence. Les QDs PbS/CdS/ZnS étudiés ici peuvent facilement être exploités pour obtenir la cartographie thermique des zones de sous-peau de spécimens vivants, une réalisation d'une grande importance pour la détection de maladies et aussi pour la surveillance de la thérapie en temps réel (Figure R7). En outre, le signal intense fourni par les QDs de NIR-émettrice, nous pouvons élucider la biodistribution de QDs en temps réel par des expériences *in vivo* dans la souris (Figure R8). Nous avons déterminé l'absence de toxicité chimique détectable attribuée aux QDs basés sur des essais culturels de cellules, ainsi que l'absence d'effets négatifs sur la santé sur (pas de changements des poids ou des anomalies de comportement ont été trouvés plus de 4 semaines) pour les souris injectées avec une faible concentration de QDs, associée à

l'absence de tout signal de fluorescence détecté dans les organes du corps à la fin de l'expérience. Nous pouvons constater que la coquille (en anglais: *shell*) extérieure de ZnS donne beaucoup de biocompatibilités et la stabilité des QDs PbS/CdS/ZnS. Aussi, l'émission de fluorescence intense de ce matériau permet d'utiliser des faibles doses s'améliorant de l'état actuel de la technique. Cela diminue la probabilité d'avoir des effets négatifs sur la santé sur les spécimens vivants lorsqu'ils sont utilisés comme des sondes de bioimagerie optiques.

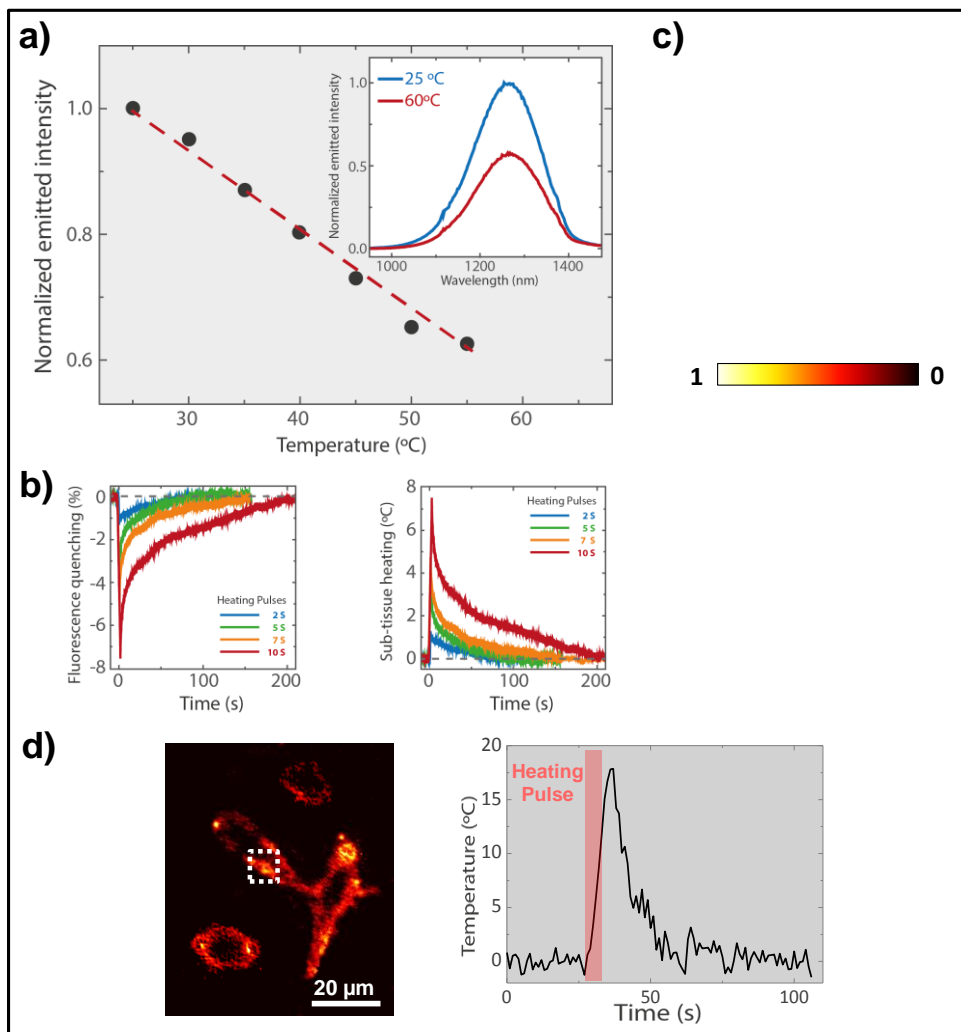


Figure R7 Nanothermométrie. **a)** l'intensité d'émission (normalisée par valeurs mesurées à la température ambiante) ont été recueillies à partir des QDs émettant à 1270 nm en fonction de la température induite de la solution. L'encart montre deux spectres enregistrés sur les deux valeurs extrêmes (25 °C et 60 °C) de la plage de température étudiée. **b)** L'intensité enregistrée en fonction du temps des QDs après d'être le chauffage de la poitrine de poulet en utilisant des impulsions à air chaud courtes. La trempe de la fluorescence d'évolution temporelle (gauche) peut être traduite le processus de chauffage sous-tissu dans le temps l'évolution correspondante (droite), grâce à la calibration montré dans la figure 5a. **c)** des images de fluorescence sous-tissulaire ont pris à deux températures différentes de la poitrine de poulet injecté avec des QDs émettant à 1270 nm.

d) l'image de fluorescence de quatre cellules He La, lors de leur excitation par une diode laser à 808 nm. Les cellules ont été incubées avec une solution de 1270 nm émettant des QDs (gauche). Avant la surveillance continue de température de cellules He La, duré et après une impulsion de 10s de chauffage, en fonction du temps (à droite); carré pointillé blanche dans la figure à gauche montre la zone sous surveillance de la température.

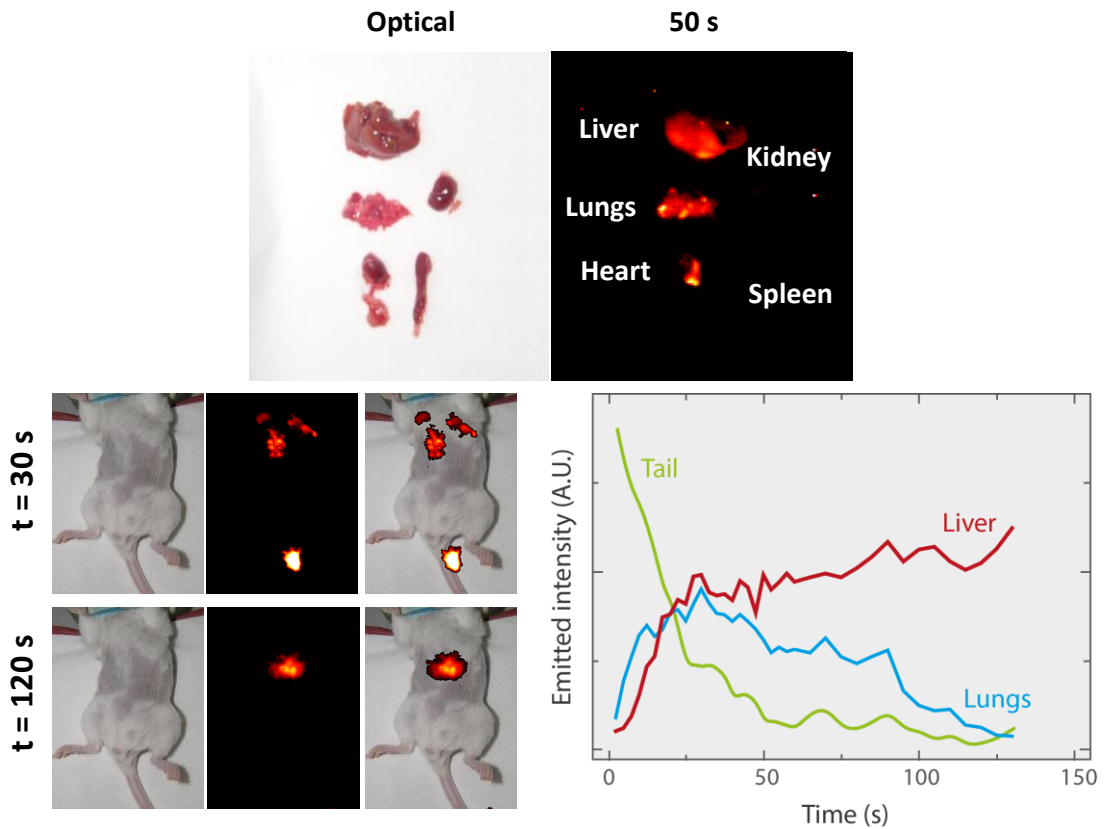


Figure R8 La durée courte des expériences *ex vivo* et *in vivo*. **En haut**: des images optiques des cinq organes sélectionnés à partir de la souris injectée, et des images de fluorescence *ex vivo* sous excitation de 808 nm des mêmes organes prélevés sur des souris sacrifiées de 50 secondes après l'injection de la solution de QDs à une concentration de 0,2 mg/ml. **En bas-gauche** : Optique (à gauche), la fluorescence (au centre) et des images combinées (à droite) de la souris fait des 30 s (rangée supérieure) et 120 s (rangée en bas) après l'injection de la solution de QDs à une concentration de 0,04 mg/ml. **En bas-droite**: le graphique montrant l'évolution de l'intensité émise par trois différentes parties du corps de la souris (arrière/vert, foie/rouge et poumons/bleu) en fonction du temps après l'injection.

Les résultats correspondants dans cette partie sont montrés dans la publication

[82] A. Benayas,¹ F. Ren,¹ E. Carrasco,¹ V. Marzal , B. del Rosal , B.A. Gonfa, Á. Juarranz, F. Sanz - Rodríguez, D. Jaque, J. Garc á- Solé Advanced Functional Materials, 25 (2015) 6650-6659 . (1: Contribution également à ce travail).

LIST OF PUBLICATIONS AND CONFERENCE CONTRIBUTIONS

Journal Publications

1. **Fuqiang Ren**, Haiguang Zhao, Fiorenzo Vetrone and Dongling Ma. Microwave-assisted Cation Exchange Toward Synthesis of Near-infrared Emitting PbS/CdS Core/shell Quantum Dots with Significantly Improved Quantum Yields Through a Uniform Growth Path. *Nanoscale* 5 (2013) 7800–7804.
2. **Fuqiang Ren**, Sarah A. Lindley, Haiguang Zhao, Long Tan, Belete Atomsa Gonfa, Ying-Chih Pu, Fan Yang, Xinyu Liu, François Vidal, Jin Z. Zhang, Fiorenzo Vetrone and Dongling Ma. Towards Understanding Unusual Photoluminescence Intensity Variation of Ultrasmall Colloidal PbS Quantum Dots with the Formation of Thin CdS Shell. Submitted.
3. **Fuqiang Ren**, Blanca del Rosal, So Young An, Fan Yang, Antonio Benayas, Jung Kwon Oh, Daniel Jaque, Fiorenzo Vetrone, Dongling Ma, Development and Investigation of Ultrastable PbS/CdS/ZnS Quantum Dots for Near-Infrared Tumor Imaging. Submitted.
4. Antonio Benayas¹, **Fuqiang Ren**¹, Elisa Carrasco¹, Vicente Marzal, Blanca del Rosal, Belete A. Gonfa, Ángeles Juarranz, Francisco Sanz-Rodríguez, Daniel Jaque, José García-Solé, Dongling Ma, and Fiorenzo Vetrone. PbS/CdS/ZnS Quantum Dots: A Multifunctional Platform for In Vivo Near-Infrared Low-Dose Fluorescence Imaging. *Advanced Functional Materials* 25 (2015) 6650–6659 (1: Contributed equally to this work).

5. Marta Quintanilla¹, **Fuqiang Ren**¹, Dongling Ma, Fiorenzo Vetrone. Light Management in Upconverting Nanoparticles: Ultrasmall Core/Shell Architectures to Tune the Emission Color. *ACS Photonics* 1 (2014) 662–669 (1: Contributed equally to this work).
6. Zhenhe Xu¹, Yanlong Liu¹, **Fuqiang Ren**¹, Fan Yang, Dongling Ma. Development of Functional Nanostructures and their Applications in Catalysis and Solar Cells. *Coordination Chemistry*. In press (1: Contributed equally to this work).
7. Elizabeth Navarro Cerón, Dirk H. Ortgies, Blanca del Rosal, **Fuqiang Ren**, Antonio Benayas, Fiorenzo Vetrone, Dongling Ma, Francisco Sanz-Rodríguez, José García Solé, Daniel Jaque, and Emma Martín Rodríguez. Hybrid Nanostructures for High-Sensitivity Luminescence Nanothermometry in the Second Biological Window. *Advanced Materials* 27 (2015) 4781–4787.
8. Blanca del Rosal, Elisa Carrasco, **Fuqiang Ren**, Antonio Benayas, Fiorenzo Vetrone, Dongling Ma, Ángeles Juarranz de la Fuente, and Daniel Jaque. Near-infrared-emitting QDs as self-controlled thermal therapeutic agents. *Advanced Functional Materials*. Accepted.
9. Xuyong Yang, **Fuqiang Ren**, Yue Wang, Tao Ding, Linyi Bai, Cuong Dang, Hilmi Volkan Demir¹, Dongling Ma, and Xiao Wei Sun. High-performance near-infrared quantum dot light-emitting diodes employing iodide passivated PbS/CdS core-shell nanocrystals. Submitted.

Conference Presentations

1. **Fuqiang Ren**, Haiguang Zhao, Fiorenzo Vetrone and Dongling Ma.

Microwave-assisted synthesis of high quality near-infrared emitting PbS/CdS Core/Shell Quantum Dots. Colloque *annuel du CQMF*, Auberge Gouverneur, Shawinigan, November 7 and 8, 2013 (*Poster presentation*)

2. **Fuqiang Ren**, Haiguang Zhao, Fiorenzo Vetrone and Dongling Ma. Microwave-assisted cation exchange toward synthesis of near-infrared emitting PbS/CdS core/shell quantum dots with significantly improved quantum yields through a uniform growth path. *Materials Science & Technology*, October 27-31, 2013 Montreal, Quebec Canada (*Oral presentation*)
3. Long Tan, **Fuqiang Ren**, Mohamed Chaker and Dongling Ma. A facile route towards synthesizing ultra-small near infrared quantum dots (QDs). Colloque annuel du CQMF, École de technologie supérieure, Montreal, May 3 and 4, 2016 (*Poster presentation*)